SCUOLA DI DOTTORATO
UNIVERSITÀ DEGLI STUDI DI MILANO - BICOCCA

School of Medicine and Surgery

PhD program in Translational and Molecular Medicine (DIMET)
XXXI Cycle

Characterization of the role of mutated *ETNK1* in the onset of atypical Chronic Myeloid Leukemia

Surname: FONTANA

Name: DILETTA

Registration number: 760552

Tutor: Prof. CARLO GAMBACORTI-PASSERINI

Co-tutor: Dott. ROCCO PIAZZA

Coordinator: Prof: ANDREA BIONDI

ACADEMIC YEAR 2017/2018

TABLE OF CONTENTS

CHAPTER I

Introduction

1. LEUKEMIA: HISTORICAL BACKGROUND

"The longer you can look back, the farther you can look forward"

Winston Churchill

The Royal College of Physicians

London, March 2nd 1944

The early history of leukemia is a gradual process, which has its roots back in the nineteenth century, when the first cases of patients affected by uncommon or distinctive alterations of the blood were published (Figure 1). Different physicians contributed to the identification of leukemia and they should be considered pioneers in the discovery and early understanding of blood cancer (1, 2). Noteworthy are the observations made by Velpeau, Donné, Bennett, and Virchow (3-9), even if the first reports connected the accumulation of white blood cells to infections.

In 1811, Cullen published a case of "*splenitis acutus*", an acute hyperplasia of the spleen, in which the blood serum appeared like milk in color and consistence (10). This report is the first description of a

patient affected by leukemia. However, the author did not explain his finding in relation to the acute hyperplasia of the spleen.

The earliest accurate description of leukemia was provided by Velpeau, back in 1827 (11). Velpeau reported a case of a 63 years old patient with swollen abdomen, fever, and weakness. At autopsy, Velpeau observed hepatosplenomegaly and an altered blood composition, described “thick like gruel” (12). The author believed that the disease was associated with the increased white blood cells, rather than an inflammation.

In 1839, Donné examined the blood of a patient with splenomegaly and observed an altered blood composition, since half of the corpuscles in the blood appeared like “mucous/purulent globules” (13-15). Observing these cells under the microscope, he said that these purulent cells looked microscopically identical to the normal leucocytes, and he stated that the excess of the globules was caused by a differentiation arrest of the white blood cells (16), which is still one of the main feature of leukemia. However, he did not explain the associated symptoms of the leukemic patient he examined.

The first physician who gave leukemia its early published recognition as a clinical entity and as a blood-related disease was Bennett in 1845 (17-19). Bennett described the serum of the blood of a patient with hepatosplenomegaly as composed of coagulated fibrin filaments, mixed with numerous colorless corpuscles, the white blood cells (17). These cells were round shaped, and granular. He described and named this disease “leucocythemia” (20), and stated that, in case of leucocythemia, the accumulation of leucocytes was a primary systemic blood disorder.

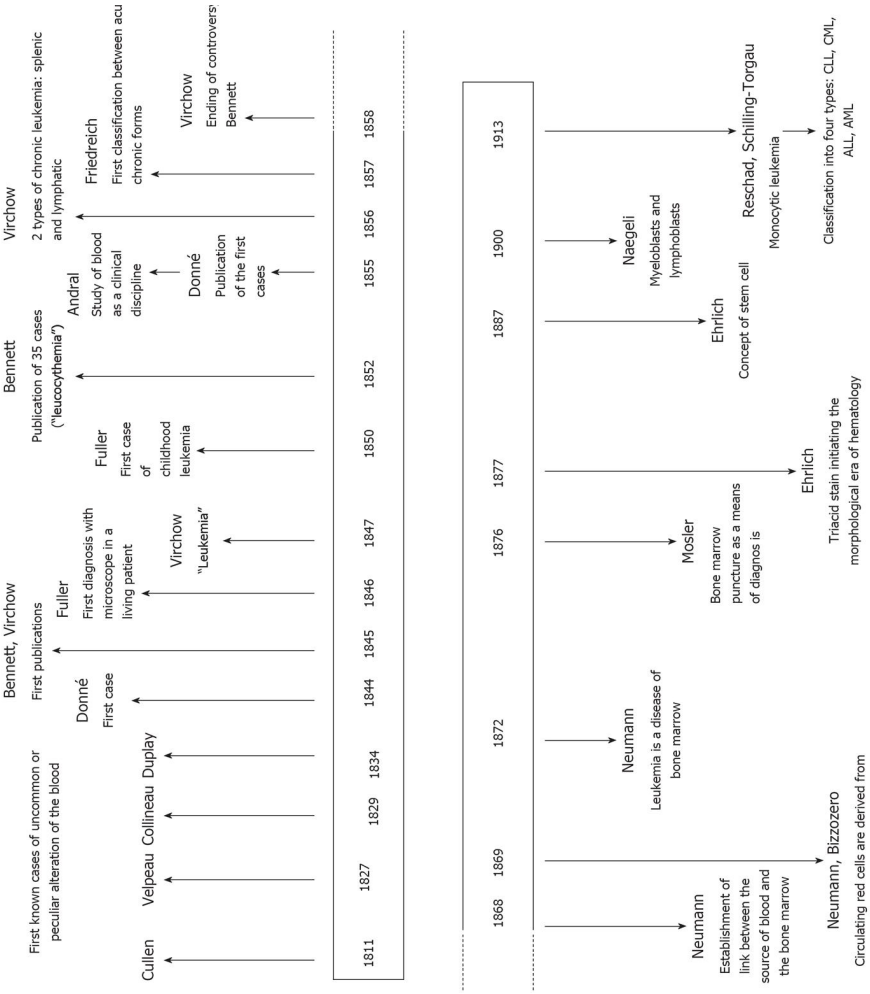

Figure 1. Historical overview. Early reports associated to leukemia, representing the first contributors in the history of leukemia are reported.

(from Thomas X. First contributors in the history of leukemia. *World J Hematol* 2013 Aug 6; **2**(3): 62-70)

The second case of leukemia, published six weeks later, was reported by Virchow (21), who described a case of a patient suffering from splenomegaly, with an excess of white cells in the blood, even if these cells were not completely regular granular cells. Virchow did not call this disorder leucocythemia, as Bennet did, instead he focused on the inequality between white and red blood cells. In 1847, Virchow described this disease as "*weisses blut*" (21), and termed it as "*leukämie*" (22, 23), from the Greek words "*leukós*" (*λευκός*), and "*haîma*" (*αιμία*), that mean "white" and "blood", respectively. In 1856, Virchow concluded that the disease was not the result of an infectious process, but rather it was caused by the tissue that produced the white blood cells (24).

Leukemia is known to be a heterogeneous disease (25), and this characteristic might explain why it was so difficult back then to understand this type of disorder. In 1856, Virchow, basing on the starting site of the disease, firstly classified leukemia into two different types of disorder, the splenic and the lymphatic forms, which we now know as leukemia and lymphoma, respectively (24). In 1843, Andral proposed the study of blood as a clinical discipline, and became the founder of the science of hematology (26). As from that moment, gradually, leukemia started to be accepted as a separate disease, and clinical and pathological description got more detailed.

The first classification of leukemia was introduced in 1857 by Friedreich (27), making a distinction between acute and chronic forms of leukemia, while Mosler added the classification of myelogenous leukemia to the splenic and lymphatic types of the disease (28). It was only in 1877, thanks to a triacid stain, that Ehrlich simplified the

classification of leukemia into the myeloid group and the lymphoid one (29), initiating the morphological era of hematology. In 1869, an important breakthrough in the understanding of leukemia took place, thanks to the finding of Neumann (30), who reported changes in the leukemic bone marrow, and established the link between the source of blood and the bone marrow. He also described the cells in the bone marrow (30), and stated that the circulating red cells were derived from an ancestral cell (31). In the same period, Bizzozero confirmed that circulating red blood cells derived from nucleated red cells present in the bone marrow (32), and asserted that the formation of white blood cells started in the bone marrow (33). In the 1872, Neumann stated that leukemia was a bone marrow disease (34), and few years later, Mosler introduced bone marrow puncture as a technique for the diagnosis of leukemia (35). Finally, in 1913, leukemia was classified into four types: chronic myelogenous leukemia, chronic lymphocytic leukemia, acute myelogenous leukemia, and acute lymphocytic leukemia (1), but these scientific advancements were not followed by any form of effective treatment of the disease (36). Indeed, since 1878, when Cutler and Bradford published the results of their study regarding the arsenic effects on blood cells, arsenic became the first agent in the treatment of leukemia inducing, in some cases, a short remission due to a reduction in both white and red cells count (37). After that, the discovery of X-rays by Röntgen in 1895 (38) brought a new treatment for leukemia, but, despite an initial response, this therapy did not cure the disease (39). Basing on these disastrous results, in 1938, Forkner wrote that “acute leukemia is rarely benefited by treatment of any sort” (40); while in

1945 Wintrobe stated that “there is no specific treatment for leukemia” (41). However, in 1947, Bessis and Bernard carried out the first complete exchange blood transfusion, achieving a few months of remission (42). Meanwhile, in 1940s, the advent of chemotherapy occurred. Gilman and Philips made the first clinical observations on nitrogen mustard (43), reporting its effect on the hematopoietic system. From now on, several efforts were made in order to seek more effective and less toxic compounds, resulting in the development of different drugs, some of those still in use, such as cyclophosphamide (44), methotrexate (45), prednisone (46), and 6-mercaptopurine (47, 48). However, the treatment of leukemia did not have major improvements up to 1960.

Indeed, as time went on, the development of cytogenetic, immunologic and molecular techniques let us to better understand the neoplastic origin of leukemia, though already proposed by Boveri in 1914, when he suggested that leukemia arose from a single cell through chromosomal changes (49). The improvements in technology allowed us to identify new molecular markers, which helped clinicians in the diagnosis and classification of different types of this disease, as well as in the choice of the best therapy to apply. The turning point was represented by the discovery of the Philadelphia (Ph) chromosome as a hallmark of chronic myelogenous leukemia (CML) in 1960 by Nowell and Hungerford (50). This finding marked the starting point of a new era in cancer research, leading toward the identification of a new molecule able to inhibit the BCR-ABL1 fusion protein, imatinib mesylate (51), completely revolutionizing the treatment and the prognosis of classical CML (52-55). This event

started the so-called personalized medicine (56). Nowadays, the application of next-generation sequencing techniques allows researchers to explore genomic, transcriptomic and epigenetic landscapes in a high-throughput approach unthinkable until few years ago, directing toward the targeted therapy.

2. ATYPICAL CHRONIC MYELOID LEUKEMIA

Atypical chronic myeloid leukemia (aCML) is a rare clonal hematopoietic stem cell disorder, which shows both myelodysplastic and myeloproliferative features (57).

As the name suggests, this disease is an atypical variant of CML, which lacks the pathognomonic Ph chromosome or the *BCR-ABL1* fusion gene that are both considered the hallmarks of classical CML (58). Since BCR-ABL1 fusion protein is not present, this disease cannot benefit from tyrosine kinase inhibitors treatment, such as imatinib or other second-generation drugs. Therefore, the prognosis remains fatal and poor, with a median overall survival of 37 months after the diagnosis (59).

2.1. aCML: from the beginning to the 2010s

In the past, the term aCML was used for various Ph chromosome negative myeloproliferative neoplasms closely mimicking CML; reports on aCML included patients with a broad range of clinical and laboratory features, with heterogeneous ones accounting for chronic myelomonocytic leukemia (CMML) or other myelodysplastic syndromes (60-62). In particular, there have been several controversies about whether this disorder should be regarded as distinct from CML (at the time still called chronic granulocytic leukemia, CGL) and from CMML (63). In their work, a morphological study of the Ph negative cases in a Medical Research Council trial, Shepherd and colleagues, basing on dysgranulopoiesis features, proposed the use of morphological criteria, such us morphology of granulocytes, monocytosis, absolute basophil count, and the number of mature and immature granulocytes in peripheral blood, to define CML, aCML and CMML (63). Therefore, for the first time, the aCML subgroup, with distinct features from CMML and CML, was recognized (63), and further studies confirmed the existence of aCML (64-66). Four years later, Martiat and collaborators added the percentage of erythroblasts in bone marrow to Shepherd criteria, and speculated that CMML and aCML might be two aspects of the same disorder (67). Moreover, two other studies supported the hypothesis that aCML could be regarded as a subgroup of CMML (68, 69).

2.1.1. aCML according to the FAB classification

Since there were overlapping quantitative and qualitative features between aCML and CMML, in October 1991, April 1992, and April 1993 respectively, the French – American – British (FAB) Cooperative Leukemia group held three workshops with the aim of assessing the hematological features of CML, aCML and CMML in order to determine whether there was a case for a formal subclassification (70). All the following information were taken in account:

- Peripheral blood
    - Complete blood count
    - Differential count
    - Description of the granulocytes with special attention to dysplastic features
    - Cytochemistry including leucocyte alkaline phosphatase and non-specific esterase
- Bone marrow biopsy
    - Assessment of cellularity
    - Degree of myelofibrosis
    - Commentary on the number and special features of megakaryocytes, erythroid and granulocytic precursors
- Bone marrow aspirates
    - Cellularity
    - Number of megakaryocytes (presence of dysplasia)
    - Myeloid: Erythroid (M:E) ratio
    - Percentage of blasts (types I and II)

- Percentage and distribution of the granulocytes, eosinophils and basophils
- Percentage of monocytes (as defined by the non-specific esterase stain)
- Dysplasia of granulocytes and erythroblasts

Basing on all these information and on the observations made by Galton (66), they agreed on the guidelines reported in the Table 1, to assist investigators in assigning a given patient to one of the three categories.

	CML	**aCML**	**CMML**
Basophils	≥2%	<2%	<2%
Monocytes	<3%	≥3-10%	≥3-10% (usually >10%)
Granulocytic dysplasia	–	++	+
Immature granulocytes	>20%	10-20%	≤10%
Blasts	≤2%	>2%	<2%
Marrow erythroid cells	–	–	+

Table 1. Criteria for morphological diagnosis of CML, aCML, and CMML proposed by the FAB group in 1994.

(adapted from Bennett JM *et al*. The chronic myeloid leukaemias: guidelines for distinguishing chronic granulocytic, atypical chronic

myeloid, and chronic myelomonocytic leukaemia. Proposals by the French-American-British Cooperative Leukaemia Group. *Br J Haematol* 1994 Aug; **87**(4):746-54 and from Oscier DG. Atypical chronic myeloid leukaemia, a distinct clinical entity related to the myelodysplastic syndrome? *Br J Haematol* 1996 Mar; **92**(3):582-6)

So, aCML delineated a group of patients who were morphologically and clinically distinct from both CML and CMML, but the FAB group acknowledged that there was frequently an overlap between aCML and CMML, and they recognized that further studied would have been required to "decide whether aCML is a quantitative and/or qualitative variant of CMML" (70). In 1996, Oscier and colleagues described 10 cases of aCML, diagnosed following the latest FAB criteria (71). All of them presented with features of typical refractory anemia and were only diagnosed as aCML once the disease had evolved, mostly from previous myelodysplastic syndrome (MDS). Basing on their findings, the authors suggested that aCML should be considered as a distinct clinical entity more closely related to myelodysplastic syndrome than to myeloproliferative disorders (71). In 2000, Hernández and collaborators published an article reporting clinical, hematological and cytogenetic characteristics of 11 cases of aCML, diagnosed according the FAB criteria (72). Differently from Oscier, in all their cases but one, the diagnosis of aCML was made at presentation. Moreover, their data supported the idea that aCML was a distinct entity with intermediate features of both myelodysplastic and

myeloproliferative diseases (72). Therefore, despite the presence of the FAB classification, it was clear that further and up-to-date criteria would be needed.

2.1.2. aCML according to the 2001 WHO classification

In 2001, the situation changed again thanks to the introduction of the World Health Organization (WHO) classification system. The classification of Tumors of the Hematopoietic and Lymphoid Tissues was part of the 3rd edition of the WHO Classification of Tumors series (73); it was the effort made for the WHO by several experts belonging to the Society for Hematopathology and to the European Association of Hematopathologists, who have agreed on using a combination of morphology, immunophenotype, genetic features, and clinical syndromes in order to attempt a classification of hematological diseases. This classification of myeloid and lymphoid neoplasms provided for the first time a description jointed with a set of precise criteria for the diagnosis of hematological disorders, stratified according to their lineage in myeloid neoplasms, lymphoid neoplasms, mast cell disorders, and histiocytic neoplasms (73). Many controversial issues were discussed, in particular the clinicians were asked to decide what should be the nomenclature and category for aCML. As reported in Table 2, aCML entered the myelodysplastic/myeloproliferative diseases group, within chronic myelomonocytic leukemia and juvenile myelomonocytic leukemia. This new overlap category, not present in the FAB classification, was

introduced to include myeloid neoplasms with clinical, laboratory, and morphologic features that were in common between MDS and myeloproliferative diseases (MPN). The following paragraph reports the description of aCML, according to the aforementioned 2001 WHO.

"Atypical CML was first recognized as a disease involving predominantly the neutrophil series and lacking Philadelphia chromosome or the BRC/ABL translocation. It has dysplastic as well as proliferative features and often occurs with multilineage dysplasia. The prognosis is significantly worse than that for Philadelphia-positive CML. It is clear that it is clinically, genetically, and morphologically distinct from Ph-positive CML; therefore, the term aCML is suboptimal, implying both a relationship to Ph-positive CML and a chronic process. The clinical advisory committee was unable to agree on another name, and thought the term aCML could be retained, provided the disease was clearly defined to prevent confusion. The pathologists recommended placing aCML with JMML and CMML in a category of myelodysplastic/myeloproliferative diseases" (74).

Myeloproliferative diseases
Chronic myelogenous leukemia, Philadelphia chromosome positive (t(9;22)(q34;q11), *BCR/ABL*)
Chronic neutrophilic leukemia
Chronic eosinophilic leukemia/hypereosinophilic syndrome
Chronic idiopathic myelofibrosis
Polycythemia vera
Essential thrombocythemia
Myeloproliferative disease, unclassifiable
Myelodysplastic/myeloproliferative diseases
Chronic myelomonocytic leukemia

- Atypical chronic myelogenous leukemia
- Juvenile myelomonocytic leukemia

Myelodysplastic syndromes

- Refractory anemia
  - With ringed sideroblasts
  - Without ringed sideroblasts
- Refractory cytopenia (myelodysplastic syndrome) with multilineage dysplasia
- Refractory anemia (myelodysplastic syndrome) with excess blasts
- 5q- syndrome
- Myelodysplastic syndrome, unclassifiable

Acute myeloid leukemias

- AMLs with recurrent cytogenetic translocations
  - AMLs with t(8;21)(q22;q22), AML1 (CBF-alpha)/ETO
  - Acute promyelocytic leukemia (AML with t(15;17)(q22;q11-12) and variants, PML/RAR-alpha
  - AML with abnormal bone marrow eosinophils (inv(16)(p13q22) or t(16;16)(p13;q11), CBFβ/MYH11X)
  - AML with 11q23 (MLL) abnormalities
- AML with multilineage dysplasia
  - With prior myelodysplastic syndrome
  - Without prior myelodysplastic syndrome
- AML and myelodysplastic syndromes, therapy-related
  - Alkylating agent-related
  - Epipodophyllotoxin-related (some may be lymphoid)
  - Other types
- AML not otherwise categorized
  - AML minimally differentiated
  - AML without maturation
  - AML with maturation
  - Acute myelomonocytic leukemia
  - Acute monocytic leukemia
  - Acute erythroid leukemia
  - Acute megakaryocytic leukemia
  - Acute basophilic leukemia
  - Acute panmyelosis with myelofibrosis

Acute biphenotypic leukemias

Table 2. Proposed WHO Classification of Myeloid Neoplasms in 2001.

(from Harris NL *et al.* World Health Organization classification of neoplastic diseases of the hematopoietic and lymphoid tissues: report of the Clinical Advisory Committee meeting-Airlie House, Virginia, November 1997. *Journal of clinical oncology: official journal of the American Society of Clinical Oncology* 1999 Dec; **17**(12): 3835-3849)

In order to identify aCML, in addition to the absence of Ph chromosome or the *BCR-ABL1* fusion gene, these new criteria included (75):

- the presence of persistent unexplained leukocytosis with severe dysgranulopoiesis
- no or minimal absolute monocytosis (monocytes <10% of white blood cells [WBC]) and no or minimal basophilia (basophils <2%)
- presence of neutrophil precursors (≥10%), and a peripheral blood and bone marrow blast count of less than 20%
- absence of *PDGFRA* and *PDGFRB* rearrangements.

Besides these myeloproliferative features, aCML was characterized by the presence of dysplasia, and this further hallmark let it to be considered a myelodysplastic/myeloproliferative neoplasm. As defined by these criteria, aCML was a rare disorder with a relatively poor diagnosis, with a median survival ranging from 14 to 25 months, and in which the transformation to acute myeloid leukemia (AML)

occurred in 25-40% of patients (59, 76). Again, the molecular pathogenesis of aCML was unknown, and no recurrent cytogenetic abnormalities had been identified (62).

2.1.3. aCML according to the 2008 WHO classification

In 2008, in order to incorporate new laboratorial as well as clinical information to refine diagnostic criteria for previously described neoplasms and to introduce newly recognized disease entities, the WHO classification was revised and updated, and published as part of the 4th edition of the WHO monograph series (77, 78). In Table 3 the major subgroup of myeloid neoplasms are listed. The following main changes are noteworthy:

- the nomenclature for the myeloproliferative entities was changed from 'chronic myeloproliferative disease' to 'myeloproliferative neoplasms' to reflect their neoplastic nature in a more accurate way
- for the same reason, the subgroup formerly designated as 'myelodysplastic/myeloproliferative disease' was renamed 'myelodysplastic/myeloproliferative neoplasms'
- in addition, a new subgroup named 'myeloid and lymphoid neoplasms with eosinophilia and abnormalities of *PDGFRA, PDGFRB,* and *FGFR1*' was added.

Regarding the aCML category, its name 'atypical chronic myelogenous leukemia' has been renamed 'atypical CML, *BCR-*

ABL1-negative' to emphasize that it was not merely a variant of CML, *BCR-ABL1*-positive (79).

Myeloproliferative neoplasms (MPN)
- Chronic myelogenous leukemia, *BCR/ABL1*-positive
- Chronic neutrophilic leukemia
- Polycythemia vera
- Primary myelofibrosis
- Essential thrombocythemia
- Chronic eosinophilic leukemia, not otherwise specified
- Mastocytosis
- Myeloproliferative neoplasms, unclassifiable

Myeloid and lymphoid neoplasms associated with eosinophilia and abnormalities of *PDGFRA*, *PDGFRB*, or *FGFR1*
- Myeloid and lymphoid neoplasms associated with *PDGFRA* rearrangement
- Myeloid neoplasms associated with *PDGFRB* rearrangement
- Myeloid and lymphoid neoplasms associated with *FGFR1* abnormalities

Myelodysplastic/myeloproliferative neoplasms (MDS/MPN)
- Chronic myelomonocytic leukemia
- Atypical chronic myeloid leukemia, *BCR-ABL1*-negative
- Juvenile myelomonocytic leukemia
- Myelodysplastic/myeloproliferative neoplasm, unclassifiable
  - *Provisional entity: refractory anemia with ring sideroblasts and thrombocytosis*

Myelodysplastic syndrome (MDS)
- Refractory cytopenia with unilineage dysplasia
  - Refractory anemia
  - Refractory neutropenia
  - Refractory thrombocytopenia
- Refractory anemia with ring sideroblasts
- Refractory cytopenia with multilineage dysplasia
- Refractory anemia with excess blasts
- Myelodysplastic syndrome with isolated del(5q)
- Myelodysplastic syndrome, unclassifiable
- Childhood myelodysplastic syndrome
  - *Provisional entity: refractory cytopenia of childhood*

Table 3. WHO classification of myeloid neoplasms in 2008.
(adapted from Vardiman JW *et al.* The 2008 revision of the World Health Organization (WHO) classification of myeloid neoplasms and acute leukemia: rationale and important changes. *Blood* 2009 Jul 30; **114**(5): 937-951)

aCML is a rare MDS/MPN neoplasm which affected elderly patients with a median age ranging between 60 and 76 years, and with an apparent male predominance. Its estimated incidence is 1 case for every 100 cases of t(9;22), *BCR/ABL1*-positive chronic myelogenous leukemia, meaning 1 case per 1000000 persons per year or less (75, 80-82). Patients presented some features of *BCR/ABL1*-positive CML including bone marrow failure, systemic symptoms, splenomegaly, an elevated WBC count with a predominance of granulocytic cells (basically a neutrophilic leukocytosis with dysgranulopoiesis and circulating immature granulocytes), and moderate anemia (Figure 2). The major characteristic that distinguishes aCML from *BCR/ABL1*-positive CML was dysgranulopoiesis, often in its severe form.

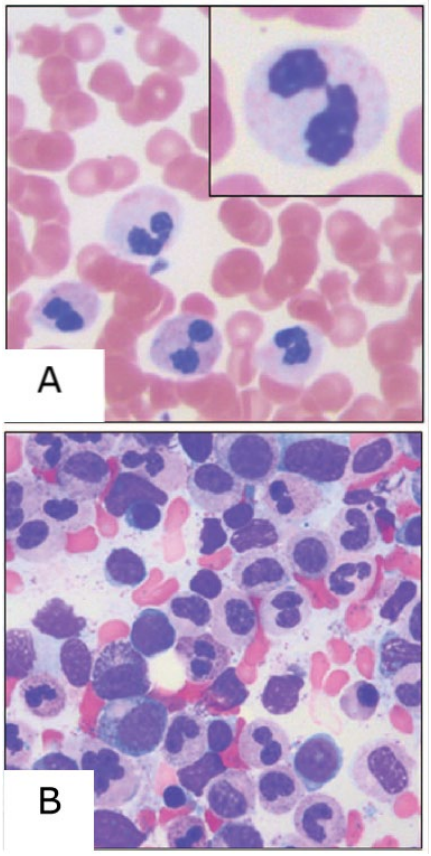

Figure 2. (A) aCML typical peripheral blood smear: frequent dysplastic neutrophils are present; the dysplastic morphologic features including hypogranularity and hypolobation (pseudo-Pelger–Huët anomaly, inset) are shown. (B) aCML typical bone marrow aspirate smear: myeloid hyperplasia with prominent dysplasia and without basophilia/eosinophilia are present.

(from Dao KH *et al*. What's different about atypical CML and chronic neutrophilic leukemia? *Hematology Am Soc Hematol Educ Program*. 2015;**2015**:264-71)

Diagnosis

The diagnosis required the presence of several findings, which are listed below (83):

- increased WBC count, and shift to the left with immature granulocytes (including blast cells, promyelocytes and myelocytes) representing 10-20% of peripheral blood white cells
- presence of dysplastic neutrophils
- granulocytes may show typical pseudo-Pelger-Huët changes, nuclear hypolobation and/or abnormal chromatin condensation, and cytoplasmic hypogranularity
- monocytes relative number is less than 10%
- basophils represent <2% of peripheral blood white cells
- bone marrow presents hypercellularity, with an elevated myeloid-to-erythroid ratio, due to granulocytic hyperplasia
- trilineage dysplasia can be present

Differential diagnosis

The differential diagnosis between aCML and chronic neutrophilic leukemia (CNL) is difficult since the proportion of immature neutrophils is the only distinctive feature (≥10% in aCML and <10% in CNL) (82). On the other hand, CMML can be excluded by the lack of monocytosis (83). In Table 4, the diagnostic criteria for myelodysplastic/myeloproliferative neoplasms are listed (84).

Genetics

In up to 80% of patients with aCML, karyotypic abnormalities such us +8 and del(20q) were reported (75, 81, 85). Moreover, the absence of rearrangements involving *PDGFRA* or *PDGFRB* (83), and the negativity for JAK2 V617F mutation (62) supported a diagnosis of exclusion for aCML. Regarding somatic mutations, *TET2* (86), *CBL* (87), and *EZH2* (88) mutations had been found, confirming a possible overlap between aCML and CMML at the molecular level.

Prognostic considerations

aCML is an aggressive disease generally associated with poor outcome, with an overall median survival ranging 11-25 months. Patients might develop acute leukemia or complications related to bone marrow failure. No drug had so far proved to be effective. Hydroxyurea could be used for controlling excessive leukocytosis and splenomegaly, and patients who were eligible could be considered for allogeneic stem cell transplantation (75, 76, 80, 81).

CMML[a]	aCML	MDS/MPN-U and RARS-T	JMML
Persistent PB monocytosis ($>1 \times 10^9$/l) No Philadelphia chromosome, *BCR-ABL1* fusion gene, *PDGFRA*, or *PDGFRB* rearrangement PB or BM blasts <20% (blasts in the context includes myeloblasts, monoblasts, and promonocytes) Presence of dysplasia in ≥1 hematopoietic lineages If the fourth criteria is not satisfied, the diagnosis can still be made if the first three criteria are met AND Presence of an acquired clonal cytogenetic or molecular genetic abnormality OR Persistent monocytosis of ≥3 months unexplained by other causes	PB leukocytosis (WBC $\geq 13 \times 10^9$/l) from increased neutrophilic precursors and mature neutrophils with prominent dysgranulopoiesis PB or BM blasts <20% No Philadelphia chromosome, *BCR-ABL1* fusion gene, *PDGFRA*, or *PDGFRB* rearrangement Neutrophil precursors (promyelocytes, myelocytes, metamyelocytes) ≥10% of leukocytes Mild absolute basophilia (<2% of leukocytes) No or minimal absolute monocytosis (<10% of WBC) Presence of a hypercellular BM with granulocytic proliferation and dysplasia; ±an accompanying dysplasia of the erythroid and megakaryocytic lineages	The case has clinical, laboratory, and morphological features of one of the categories of MDS and PB and BM blast percentages do not fulfill the criteria for AML, AND Prominent myeloproliferative features exemplified by thrombocytosis ($\geq 450 \times 10^9$/l) associated with megakaryocytic proliferation or PB leukocytosis (WBC $\geq 13 \times 10^9$/l) with or without splenomegaly, AND No prior MPN or MDS diagnosis, no history of recent cytotoxic or growth factor therapy that could explain the MDS or MPN features, no Philadelphia chromosome, *BCR-ABL1* fusion gene, *PDGFRA*, or *PDGFRB* rearrangement, and absence of isolated del(5q), t(3;3)(q21;q26) or inv(3)(q21q26), *OR* The patient has de-novo disease with mixed myeloproliferative and myelodysplastic features and cannot be assigned to any other category of MDS, MPN, or of MDS/MPN RARS-T: Platelet count of $\geq 450 \times 10^9$/l Presence of ≥15% ring sideroblast in the BM Presence of megakaryocytic atypia resembling those of ET or MF	Presence of PB monocytosis ($>1 \times 10^9$/l) Presence of blasts which includes promonocytes accounting for <20% of the total WBC count in the PB and BM Absence of the Philadelphia chromosome or *BCR-ABL1* fusion gene PLUS two or more of the following: Hemoglobin F increased for age Presence of PB immature granulocytes WBC count $>10 \times 10^9$/l Presence of the clonal cytogenetic abnormality (including −7), and/or In-vitro hypersensitivity of myeloid progenitors to GM-CSF

Table 4. Diagnostic criteria for MDS/MPN neoplasms in 2008.

(from Tiu RV *et al.* Making sense of the myelodysplastic/myeloproliferative neoplasms overlap syndromes. *Current opinion in hematology* 2014 Mar; **21**(2): 131-140)

2.2. aCML from the 2010s to nowadays: *SETBP1* and *ETNK1* discoveries

In the last decades, the application of next-generation sequencing techniques, has dramatically improved the biology, genetics, and medicine fields. As said before, many mutations in known oncogenes, such as *NRAS*, *KRAS*, *TET2*, *EZH2*, *ASXL1*, U*2AF1*, and *CBL* had been described, but also *IDH2* mutation can be detected, although with lower frequency (89-94).

However, the molecular lesions responsible for the onset and the progression of aCML remained unknown till 2012, when, by applying next-generation sequencing techniques, our group firstly described the presence of recurrent somatic mutations in *SETBP1* gene (89). These mutations cluster in the SKI homologous region of the protein, and confer a proliferative advantage to mutated cells. Moreover, they are associated with a worse prognosis in patients with aCML (Figure 3). Subsequently, *SETBP1* mutations were also confirmed by other independent studies (91, 95-101).

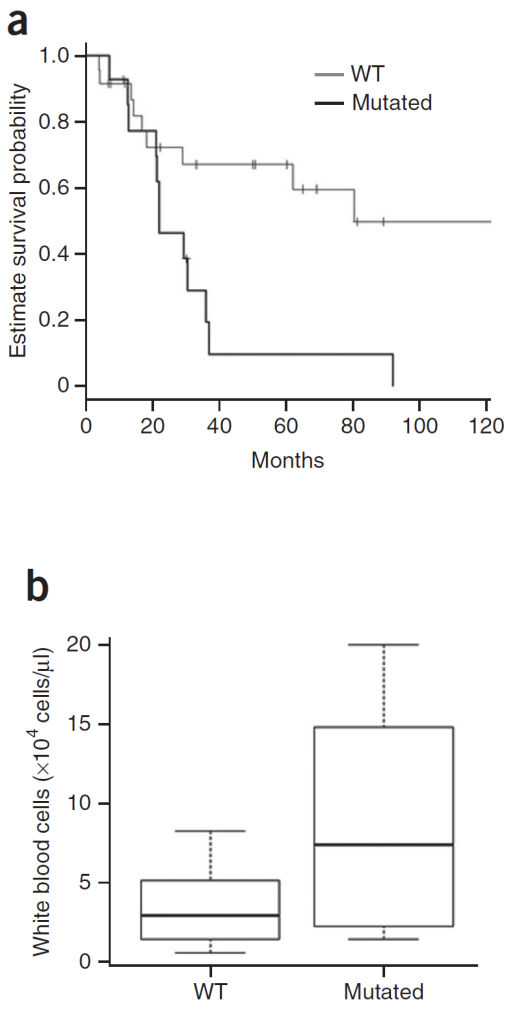

Figure 3: (A) overall survival: SETBP1-mutated cases showed worse prognosis (median survival of 22 vs 77 months, P=0.01, hazard ratio=2.27) compared to cases with wild-type SETBP1. (B) white blood cell count: SETBP1-mutated cases presented higher white blood cell counts at diagnosis (median of 81.0 × 10^9 cells/l vs 38.5 × 10^9 cells/l, P=0.008) compared to cases with wild-type SETBP1.

(from Piazza R *et al*. Recurrent SETBP1 mutations in atypical chronic myeloid leukemia. *Nat Genet*. 2013 Jan;**45**(1):18-24)

Later on, in 2015, extending our previous study, we identified the presence of recurrent somatic mutations in *ETNK1* gene (90), clustering in the kinase catalytic domain, and responsible for the inhibition of the activity of the enzyme. Subsequently, Lasho and collaborators found the same variants in CMML and systemic mastocytosis with eosinophilia (102).

SETPB1 and *ETNK1* genes will be described more in detail in paragraphs 3 and 4, respectively.

2.2.1. WHO classification: the 2016 revision

In 2016, after 8 years of information and experience in scientific and clinical studies, a revision of the 2008 WHO criteria for hematopoietic neoplasms was felt necessary. Indeed, the technology of genetic analysis was evolving rapidly, and the advances in the hematological field required an update of the diagnostic as well as prognostic criteria. However, the 2016 WHO is not a new edition of the classification of tumors of hematopoietic and lymphoid tissues, just a revision of the prior classification (57).

In Table 5 are listed the major subtypes of myeloid neoplasms and acute leukemias according to the updated 2016 WHO classification:

- acute myeloid leukemia (AML) and related neoplasms

- myeloid/lymphoid neoplasms with eosinophilia and rearrangement of *PDGFRA*, *PDGFRB*, or *FGFR1*, or with *PCM1-JAK2*
- myelodysplastic syndromes (MDS)
- myeloproliferative neoplasms (MPN)
- myelodysplastic/myeloproliferative neoplasms (MDS/MPN)

Since aCML belongs to the myelodysplastic/myeloproliferative group, in the next paragraphs more attention will be given to the MPN, MDS, and MDS/MPN categories.

Myeloproliferative neoplasms (MPN)
- Chronic myeloid leukemia (CML), *BCR/ABL1*$^{+}$
- Chronic neutrophilic leukemia (CNL)
- Polycythemia vera (PV)
- Primary myelofibrosis (PMF)
  - PMF, prefibrotic/early stage
  - PMF, overt fibrotic stage
- Essential thrombocythemia (ET)
- Chronic eosinophilic leukemia, not otherwise specified (NOS)
- MPN, unclassifiable

Mastocytosis

Myeloid/lymphoid neoplasms with eosinophilia and rearrangement of *PDGFRA*, *PDGFRB*, or *FGFR1*, or with *PCM1-JAK2*
- Myeloid/lymphoid neoplasms with *PDGFRA* rearrangement
- Myeloid/lymphoid neoplasms with *PDGFRB* rearrangement
- Myeloid/lymphoid neoplasms with *FGFR1* rearrangement
- *Provisional entity: Myeloid/lymphoid neoplasms with PCM1-JAK2*

Myelodysplastic/myeloproliferative neoplasms (MDS/MPN)
- Chronic myelomonocytic leukemia (CMML)
- Atypical chronic myeloid leukemia (aCML), *BCR-ABL1*$^{-}$
- Juvenile myelomonocytic leukemia (JMML)
- MDS/MPN with ring sideroblasts and thrombocytosis

(MDS/MPN-RS-T)
MDS/MPN, unclassifiable
Myelodysplastic syndromes (MDS)
MDS with single lineage dysplasia
MDS with ring sideroblasts (MDS-RS)
MDS-RS and single lineage dysplasia
MDS-RS and multilineage dysplasia
MDS with multilineage dysplasia
MDS with excess blasts
MDS with isolated del(5q)
MDS, unclassifiable
Provisional entity: refractory cytopenia of childhood
Myeloid neoplasms with germ line predisposition
Acute myeloid leukemia (AML) and related neoplasms
AML with recurrent genetic abnormalities
AML with t(8;21)(q22;q22.1);*RUNX1-RUNX1T1*
AML with inv(16)(p13.1q22) or t(16;16)(p13.1;q22);*CBFB-MYH11*
APL with *PML-RARA*
AML with t(9;11)(P21.3;q23.3);*MLL3-KMT2A*
AML with t(6;9)(p23;q34.1);*DEK-NUP214*
AML with inv(3)(q21.3q26.2) or t(3;3)(q21.3:q26.2);*GATA2, MECOM*
AML (megakaryoblastic) with t(1;22)(p13.3;q13.3);*RBM15-MKL1*
Provisional entity: AML with BCR-ABL1
AML with mutated *NPM1*
AML with biallelic mutations of *CEBPA*
Provisional entity: AML with mutated RUNX1
AML with myelodysplasia-related changes
Therapy-related myeloid neoplasms
AML, NOS
AML with minimal differentiation
AML without maturation
AML with maturation
Acute myelomonocytic leukemia
Acute monoblastic/monocytic leukemia
Pure erythroid leukemia
Acute megakaryoblastic leukemia
Acute basophilic leukemia
Acute panmyelosis with myelofibrosis

Myeloid sarcoma Myeloid proliferations related to Down syndrome Transient abnormal myelopoiesis (TAM) Myeloid leukemia associated with Down syndrome

Table 5. WHO classification of myeloid neoplasms and acute leukemia.

(adapted from Arber DA *et al.* The 2016 revision to the World Health Organization classification of myeloid neoplasms and acute leukemia. *Blood* 2016 May 19; **127**(20)**:** 2391-2405)

2.2.2. Myeloproliferative neoplasms

Myeloproliferative neoplasms (MPNs) are clonal bone marrow stem cell disorders involving a multipotent hematopoietic stem cell, characterized by an increased proliferation of one or more lineages of the myeloid, erythroid and megakaryocytic cell lines, which maintain all the maturation steps (103), and result in an increased number of granulocytes, erythrocytes and platelets in the peripheral blood. These disorders were classified for the first time by Dameshek in 1951 (104). According to the 2016 revision of WHO, chronic myeloid leukemia *BCR-ABL1*-positive, chronic neutrophilic leukemia, polycythemia vera, primary myelofibrosis, essential thrombocythemia, chronic eosinophilic leukemia not otherwise specified, and myeloproliferative neoplasms unclassifiable belong to this group (57). However,

mastocytosis, which in the 2008 WHO was listed in this category (79), is no longer classified as MPN since it presents unique clinical and pathologic features (57).

2.2.3. Myelodysplastic syndromes

Myelodysplastic syndromes (MDS) are hematopoietic stem cell disorders characterized by peripheral cytopenias and dysplasia of at least two of the three myeloid lineages, inefficient hemopoiesis, increased apoptosis and propensity to undergo transformation into AML (105). These disorders were probably first described in 1900 by Leube as "leukanamie" (106). According to the 2016 revision of WHO, MDS with single lineage dysplasia, MDS with ring sideroblasts, MDS with multilineage dysplasia, MDS with excess blasts, MDS with isolated del(5q), and MDS unclassifiable belong to this group (57). Regarding the cytopenia of childhood, it is still reported as a provisional entity, while the terminology "myelodysplastic syndrome" replaces the terms "refractory anemia" and "refractory cytopenia" of the 2008 WHO (79).

2.2.4. Myelodysplastic/myeloproliferative neoplasms

The myelodysplastic/myeloproliferative neoplasms category was introduced in the 3rd edition of the WHO Classification of Tumors (73), and includes myeloid neoplasms that exhibit, at presentation, laboratory, clinical, and morphologic features that overlap between

MDS and MPN (83). According to the 2016 revision of WHO, chronic myelomonocytic leukemia (CMML), atypical chronic myeloid leukemia (aCML) *BCR-ABL1*-negative, juvenile myelomonocytic leukemia (JMML), MDS/MPN with ring sideroblasts and thrombocytosis (MDS/MPN-RS-T), and MDS/MPN unclassifiable belong to this group (57). Based on accumulated scientific evidence, the provisional entity called "refractory anemia with ring sideroblasts associated with marked thrombocytosis", present in the 2008 WHO (79), is now accepted as a full entity and termed MDS/MPN with ring sideroblasts and thrombocytosis.

2.2.5. aCML according to the 2016 WHO revision

Regarding aCML, the recent discoveries of new molecular alterations occurring in *SETBP1* (89) and *ETNK1* (90) genes have impacted the diagnostic criteria for the disease. Indeed, this disorder is now better characterized from a molecular point of view, and can be more easily separated from CNL, since the latter disease is strongly associated with the presence of mutations occurring in *CSF3R* (107). On the other hand, *CSF3R* mutations are very rare in aCML (<10%), (108), while *JAK2*, *CALR*, and *MPL* mutations are absent (57). Moreover, aCML is associated with *SETBP1* and/or *ETNK1* mutations in up to a third of cases (89-91).

Diagnosis

In Table 6 the diagnostic criteria for aCML, *BCR-ABL1*-negative are reported. Summarizing, aCML is a pathology characterized by neutrophilic leukocytosis with the presence of immature myeloid precursor in the peripheral blood (≥10% of leukocytes), dysgranulopoiesis, low or absent basophils (<2% of leukocytes) and monocytes (<10% of leukocytes). In the blood and bone marrow there is less than 20% of blasts, there is hypercellular bone marrow with granulocytic proliferation and dysplasia, and absence of *PDGFRA*, *PDGFRB*, or *FGFR1* rearrangement, *or PCM1-JAK*. Moreover, aCML diagnosis must not meet the WHO criteria for *BCR-ABL1*-positive CML, primary myelofibrosis (PMF), polycythemia vera (PV) or essential thrombocythemia (ET).

aCML diagnostic criteria
• PB leukocytosis due to increased numbers of neutrophils and their precursors (promyelocytes, myelocytes, metamyelocytes) comprising ≥10% of leukocytes)
• Dysgranulopoiesis, which may include abnormal chromatin clumping
• No or minimal absolute basophilia; basophils usually <2% of leukocytes
• No or minimal absolute monocytosis; monocytes <10% of leukocytes
• Hypercellular BM with granulocytic proliferation and granulocytic dysplasia, with or without dysplasia in the erythroid and megakaryocytic lineages
• <20% blasts in the blood and BM
• No evidence of *PDGFRA*, *PDGFRB*, or *FGFR1* rearrangement, or *PCM1-JAK2*
• Not meeting WHO criteria for *BCR-ABL1*$^{+}$ CML, PMF, PV, or ET*

*Cases of MPN, particularly those in accelerated phase and/or in post-polycythemic or post-essential thrombocythemic myelofibrosis, if neutrophilic, may simulate aCML. A previous history of MPN, the presence of MPN features in the BM and/or MPN-associated mutations (in *JAK2*, *CALR*, or *MPL*) tend to exclude a diagnosis of aCML. Conversely, a diagnosis of aCML is supported by the presence of *SETBP1* and/or *ETNK1* mutations. The presence of a *CSF3R* mutation is uncommon in aCML and if detected should prompt a careful morphologic review to exclude an alternative diagnosis of CNL or other myeloid neoplasm.

Table 6. Diagnostic criteria for aCML, BCR-ABL1-negative.
(from Arber DA *et al.* The 2016 revision to the World Health Organization classification of myeloid neoplasms and acute leukemia. *Blood* 2016 May 19; **127**(20)**:** 2391-2405)

Differential diagnosis

The differential diagnosis still includes CML CMML, CNL and prefibrotic primary myelofibrosis (pre-PMF). The absence of *BCR-ABL1* rearrangement, and the absence or low basophils level (<2% of leukocytes) help in distinguishing aCML from *BCR-ABL1*-positive CML, while persistent peripheral blood monocytosis (<10% of leukocytes) is a marker for the differential diagnosis of CMML (57). The finding of ≥10% immature myeloid cells (promyelocytes,

myelocytes, and metamyelocytes) in peripheral blood and/or dysplasia are useful criteria in distinguishing aCML from CNL, which lacks these features (57). Moreover, in CNL white blood cell count in peripheral blood is higher than 25×10^9/l, while in aCML it is $\geq 13 \times 10^9$/l. Pre-PMF presents with megakaryocytic proliferation and atypia, and decreased erythropoiesis (57). In Figure 4, the algorithm for aCML diagnosis suggested by Gotlib is reported.

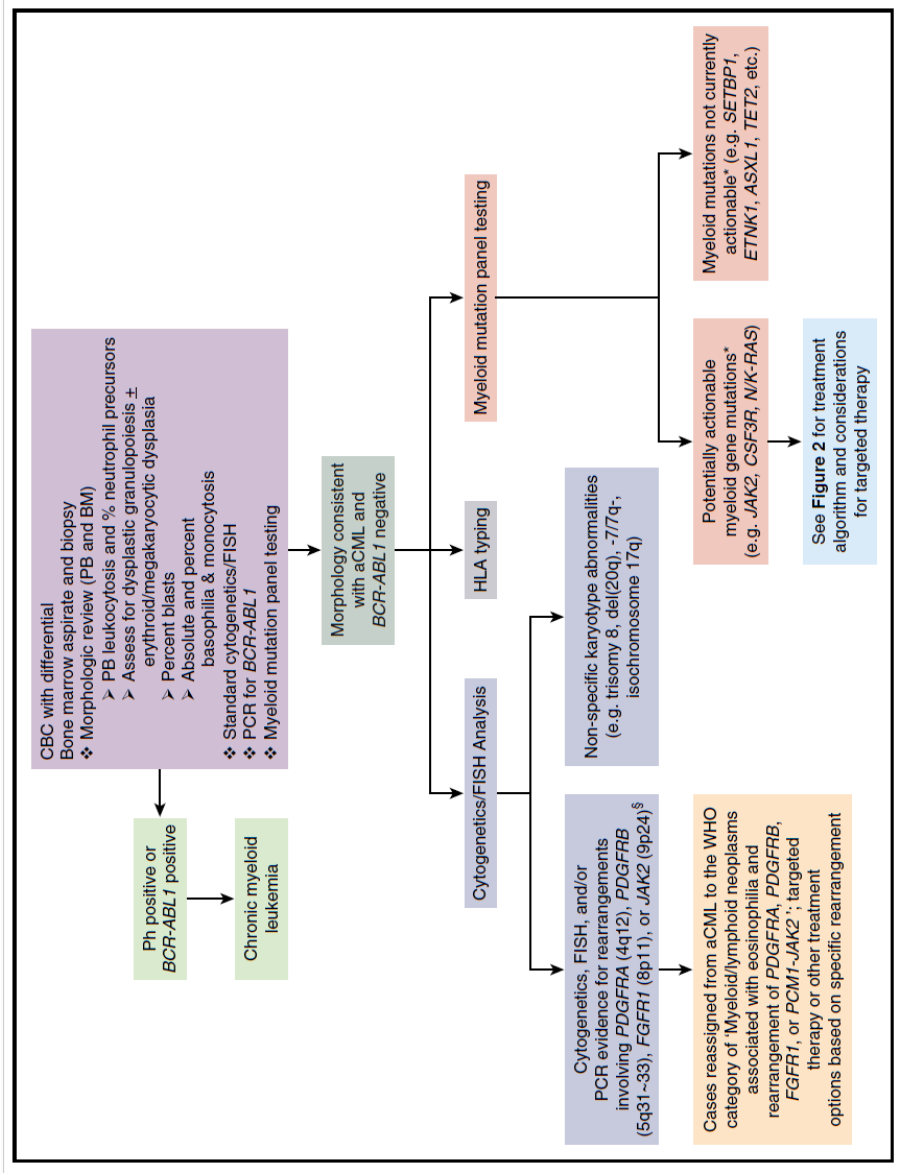

Figure 4. Diagnostic evaluation for aCML and identification of opportunities for targeted therapy.

(from Gotlib J. How I treat atypical chronic myeloid leukemia. *Blood*. 2017 Feb16;**129**(7):838-845).

Genetics

As previously said in the 2008 classification, there are several genetic alterations present in aCML. The most frequent mutations involve *SETPB1*, *ASXL1*, *NRAS*, *KRAS*, *SRSF2*, and *TET2*, while mutations in *CBL*, *CSF3R*, *JAK2*, and *ETNK1* are less frequent (109). The importance of these mutations is that they may signify the prognosis of the disease, and provide potential target for drug treatment. *SETBP1* and *ASXL1* are considered as high-risk mutations (108, 109).

Prognostic consideration

Nevertheless the last discoveries about aCML, it remains associated with a poor prognosis. The results of a study by the Surveillance, Epidemiology, and End Results (https://seer.cancer.gov/) reported a median overall survival (OS) of 15 months and a 5-years OS of 25%, with 15-40% of patients who evolves to AML. Moreover, in a US multicenter study, Wang observed an OS of 22 months with an AML-free survival of 19 months, and transformation to AML in 37% of cases (108), in line with what reported by other studies, where the median OS was 14-29 months (72, 75, 76, 81). In an Italian cohort of 55 aCML patients, the median OS was 25 months, and transformation to AML occurred in 40% of patients (81). On the other hand, some other papers describe a median OS of as high as 3 years (59, 67). The main adverse prognostic factors are female sex, age more than 65 years, hemoglobin

<10g/dl, leukocytes count ≥50 × 10^9/l, and immature circulating precursors (76, 81).

Therapy

No established standards of care exist for the treatment of aCML (109, 110). Moreover, no consensus recommendations such as risk-based treatments algorithms exist to help clinicians in choosing between a watch-and-wait approach and initiation of therapy.

During the last years, different therapeutic approaches were used, but at present, allogeneic hematopoietic stem cell transplantation (allo-HSCT) remains the only curative treatment option, even if only limited reports are available (111-115). However, it should be considered only for young eligible patients with a suitable donor, since the elderly age of patients makes difficult the transplant outcome. In older patients, especially with lower-risk disease, monitoring or palliative chemotherapy may be appropriate.

Regarding other medical therapies, hydroxyurea is used as a supportive care measure to control hyperleukocytosis or splenomegaly. Complete and partial hematological remissions have been reported in about 80% of patients, even if remissions are usually short lived (59, 67, 69, 72, 76, 81, 108, 116-119). Moreover, complete and partial hematological remissions have been reported also after treatment with interferon alfa, alone or in its PEGylate form, even if many patients were discontinued due to drug toxicity (59, 67, 69, 117, 118, 120, 121). However, both hydroxyurea and interferon alfa, despite being able to improve the white blood cell count, are unable to change the course of the disease.

Among other drugs that can be used in the treatment of aCML, especially in patients with high-risk disease, the hypomethylating agents, such as azacitidine or decitabine, are noteworthy (76, 116, 122-127). Indeed, basing on their established activity in MDS and CMML, in which the overall response rates range from 25% to 70% with overall survive ranging from 12 to 37 months (128), these drugs could be used also in aCML. Nevertheless, up to now, the experience with hypomethylating agents is still limited and the data available are not able to predict the response to these drugs. Therefore, hypomethylating agents cannot be considered a standard of care yet.

Other drugs that can be used for aCML treatment are tyrosine kinase inhibitors, in the field of personalized therapies. Indeed, as said before, thanks to new advances in the molecular pathogenesis of aCML, several mutations have been identified and could be targeted. For example, ruxolitinib, a JAK inhibitor approved by FDA in cases of intermediate- to high-risk myelofibrosis and polycythemia vera intolerant or resistant to hydroxyurea, can be used in cases of aCML carrying the *JAK2* V617F mutation, or harboring *JAK2* rearrangements, such as *PCM1-JAK2* (129-131). This inhibitor can be used in patients with *CSF3R* T618I mutation as well, since this mutation results in JAK-STAT pathway activation (132). An *in vivo* murine model predicted ruxolitinib activity on the rarely described *CSF3R* T640N mutation (109). However, the concomitant presence of additional mutations besides *CSF3R* may reduce responsiveness to JAK inhibition (133). A multicenter study (ClinicalTrials.gov Identifier: NCT02092324) is currently evaluating the safety and the efficacy of ruxolitinib in patients affected by CNL or aCML,

regardless their mutation status. In addition to ruxolitinib, other tyrosine kinase inhibitors currently available in clinical practice could be used. Wang and colleagues administrated RAS, FLT3, MAPK, MYC or AKT inhibitors to their patients (108), while Khanna and collaborators reported an aCML case with *NRAS* G12V mutation who experienced an exceptional response to the MEK1/2 inhibitor trametinib (134). Moreover, a phase I, open-label study is currently ongoing to evaluate safety and efficacy of TGR-1202, a PI3K-delta inhibitor, administered together with ruxolitinib in patients with MDS or MDS/MPN including aCML (ClinicalTrials.gov Identifier: NCT02493530).

Since the treatment of aCML remains a challenge, recently, Gotlib proposed his treatment algorithm (Figure 5), based on several decision nodes, including the potential candidacy for allogeneic hematopoietic stem cell transplantation, the results of myeloid mutation panel testing, the eligibility for enrollment in clinical trials, and the opportunities to adopt strategies used for MDS or MPN.

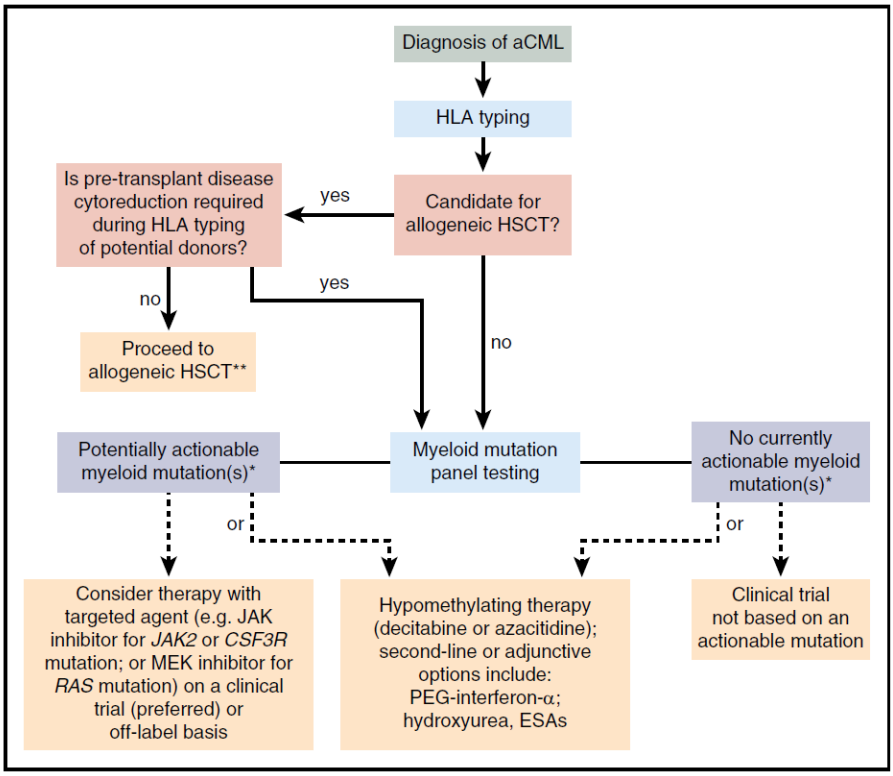

Figure 5. Treatment algorithm for aCML.

(from Gotlib J. How I treat atypical chronic myeloid leukemia. *Blood*. 2017 Feb16;**129**(7):838-845).

3. SETBP1

Recurrent somatic *SETBP1* mutations have been identified in about one-quarter of patients affected by aCML (89), but also in 10% of MDS/MPN unclassifiable cases (91), and in 6-15% of CMML

patients (96). Moreover, *SETBP1* mutations have been occasionally described in JMML, in about 1.7-7% of secondary AML arising from MPN or MDS (92). Several germline *SETBP1* mutations have been reported in the Schinzel-Giedion syndrome, a rare congenital malformation disorder defined by characteristic facial features, profound developmental delay, severe growth failure, and multiple congenital anomalies, many of which arise as a consequence of aberrant bone formation (135, 136).

SETBP1 is located at chromosome 18q21.1 and codes for SET binding protein 1a, a protein of 1596 residues (NM_015559.2, long isoform) with a predicted molecular weight of 170 kDa. The protein contains a SET-binding region, and a SKI homology region, in which the identified recurrent mutations occur. The latter is highly conserved among vertebrates, suggesting an important but still unknown biological function. Moreover, there are three AT hooks (Figure 6).

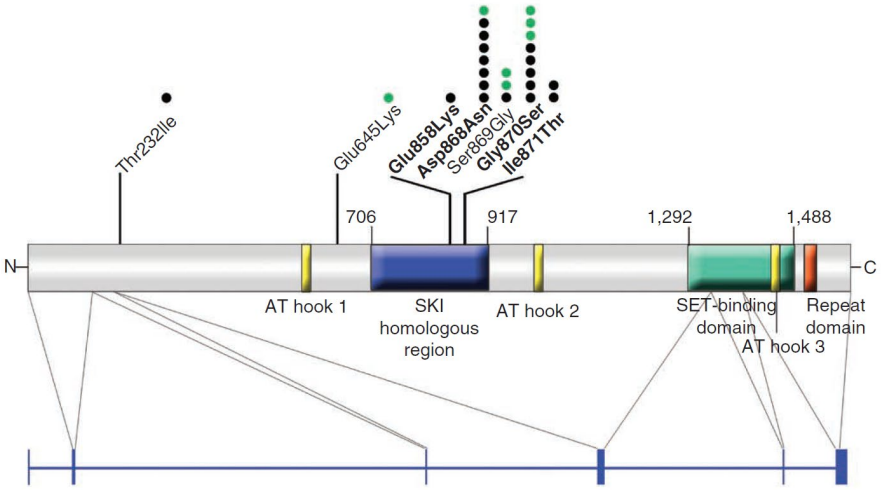

Figure 6. Distribution of alterations on the SETBP1 protein. The isoform A of the protein (1596 amino acids) is encoded by five exons

(blue bars). The SETBP1 sequence comprises three AT hook domains (amino acids 584-596, 1016-1028, and 1451-1463), a SKI homologous region (amino acids 706-917), a SET-binding domain (amino acids 1292-1488) and a repeat domain (amino acids 1520-1543). The black circles highlight the amino acids altered and represent the modifications found in aCML samples, whereas the green circles represent alterations found in other diseases. Variants confirmed as somatic are indicated in bold.
(from Piazza R *et al*. Recurrent SETBP1 mutations in atypical chronic myeloid leukemia. *Nat Genet*. 2013 Jan;**45**(1):18-24)

It is known that SETBP1 is a binding partner for the SET nuclear oncoprotein, and it plays a role in apoptosis, transcription and nucleosome assembly (137). On the other hand, SET binds and it is involved in negative regulation of phosphatase 2A (PP2A) (138), a major phosphatase implicated in many cellular processes, such as cellular proliferation (139-143). In particular, the loss of function of PP2A has been associated with cell transformation (144, 145). Indeed, PP2A is a tumor suppressor that inhibits cellular transformation by regulating several signaling pathways critical for malignant transformation, such as AKT and ERK1/2 (146-148). Once SETBP1 has bound SET, it protects SET from protease cleavage, increasing the amount of full-length SET protein, and leading to the formation of a SETBP1-SET-PP2A complex (Figure 7) resulting in PP2A inhibition. Therefore it guides the proliferation and expansion of leukemic cells (149).

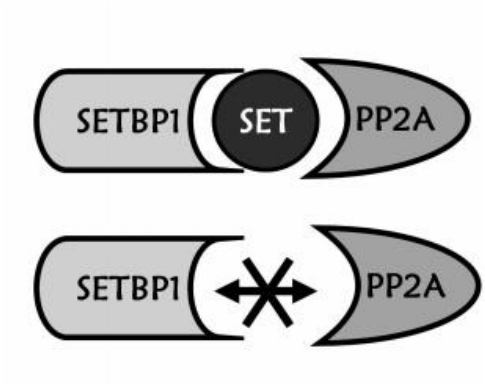

Figure 7. Complex SETBP1-SET-PP2A. The heterotrimeric complex SETBP1-SET-PP2A stabilizes SET and inhibits the phosphatase PP2A.
(from Cristobal I *et al.* SETBP1 overexpression is a novel leukemogenic mechanism that predicts adverse outcome in elderly patients with acute myeloid leukemia. *Blood* 2010 Jan 21; **115**(3)**:** 615-625)

In our previous work, we firstly demonstrated that the majority of SETBP1 somatic mutations occur in a mutational hotspot within the SKI-homologous region. This region is part of a degron motif (a specific sequence of amino acids in a protein that directs the initial step of degradation) recognized by the E3 ubiquitin ligase β-TrCP1 (Figure 8). SETBP1 mutations cause the reduction of the affinity of the E3 ubiquitin ligase to SETBP1, leading to the accumulation of SETBP1 protein, promoting its overexpression and triggering the stabilization of SET at the protein level. The consequence of these events is the inhibition of PP2A phosphatase oncosuppressor.

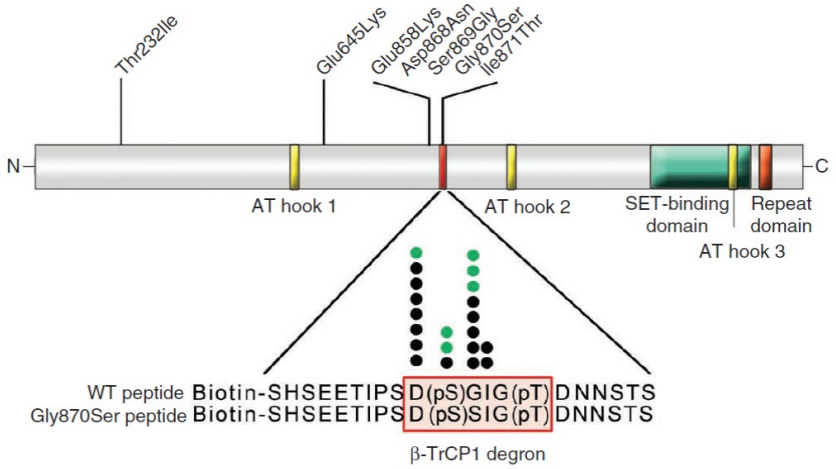

Figure 8. Interaction between β-TrCP1 and SETBP1. The β-TrCP1 degron motif (amino acids 868–873) is highlighted in red on the SETBP1 protein schematic. Black circles represent alterations found in aCML samples; green circles represent alterations found in other diseases.

(from Piazza R *et al*. Recurrent SETBP1 mutations in atypical chronic myeloid leukemia. *Nat Genet*. 2013 Jan;**45**(1):18-24)

Recently, our group demonstrated a new role for SETBP1, as DNA-binding protein, through its three conserved AT-hooks (150). In particular, SETBP1 interacts with gDNA thanks to the AT-hook domains, recruiting the transcriptional modulators such as HCF1, KMT2A, PHF8, and PHF6, which belong to the SET/KMT2A (MLL1) COMPASS-like complex, forming a multiprotein complex

that in turn causes the activation of gene expression (Figure 9). Notably, SETBP1 binds to the *MECOM* promoter, and it is known that *MECOM* modulates the expression of several genes involved in the proliferation of hematopoietic stem cells and in the myeloid differentiation (150, 151).

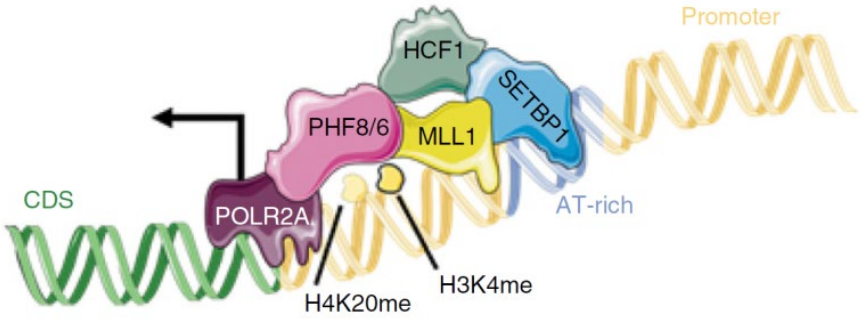

Figure 9. Proposed model of SETBP1-mediated epigentic regulation. SETBP1 recruits a HCF1/KMT2A/PHF8 complex to induce transcriptional activation. In the picture KMT2A is represented using its alternative name MLL1.
(from Piazza R *et al*. SETBP1 induces transcription of a network of development genes by acting as an epigenetic hub. *Nat Commun*. 2018 Jun 6;**9**(1):2192)

Moreover, *SETBP1* has been reported as involved in myeloid leukemia development. Indeed, SETBP1 overexpression confers self-renewal capability to myeloid progenitors *in vitro* by interacting with

the homeobox A9 (*HOXA9*) and homeobox A10 (*HOXA10*) promoters (152). In another study, Vishwakarma et al. demonstrated that SETBP1 is able to interact with the runt related transcription factor 1 (*Runx1*) promoter, resulting in Runx1 downregulation (153). RUNX1 is a well known negative regulator of the HSC self-renewal and its loss is known to be associated with a partial block of myeloid differentiation (154, 155).

4. ETNK1

ETNK1 gene (also known as *EKI1*) is located on chromosome 12p12.1. It spans 60.5 kb, and it consists of 8 exons and 7 introns. The exons size ranges between 77 and 828 bp, while the introns size ranges between 0.3 and 18.1 kb (156). *ETNK1* encodes for a protein of 452 residues (NM_018638), ethanolamine kinase, a cytoplasmic enzyme that catalyzes the first step of the *de novo* phosphatidylethanolamine (PE) biosynthesis through the Kennedy or cytidine diphosphate (CDP)-ethanolamine pathway (157). The Kennedy pathway is a series of biochemical reactions responsible for the *de novo* biosynthesis of the two major membrane phospholipids, phosphatidylcholine (PC) and PE. In particular, ETNK1 is responsible for the phosphorylation of ethanolamine to give phosphoethanolamine (P-Et) (157).

In our previous study, we firstly identified recurrent *ETNK1* mutations in aCML (90), generating whole-exome and transcriptome

sequencing data on a cohort of 15 matched case/control aCML samples. In 13.3% (2/15 samples) we identified the presence of missense, somatic, single-nucleotide variants occurring in *ETNK1*. Both *ETNK1* mutations were present as heterozygous variant in the dominant clone, and interestingly, the mutations affected two contiguous residues: H243Y and N244S. This finding prompted us to resequence *ETNK1* in samples from 515 clonal hematological disorders. As reported in Table 7, we found *ETNK1* mutations in 6 of 68 aCML samples (8.8%) and in 2 of 77 CMML samples (2.6%). In all the cases, *ETNK1* variants were heterozygous and clustered in the same, highly conserved region (158) within the kinase domain (Figure 10), encoding for H243Y (1/8) and N244S (7/8) substitutions.

Disease	Samples	Mutated samples	Mutated samples, %
AML	64	0	0.0
ALL	53	0	0.0
CLL	51	0	0.0
MDS	77	0	0.0
MPN			
CML	38	0	0.0
PV	18	0	0.0
ET	39	0	0.0
CNL	1	0	0.0
PMF	14	0	0.0
MDS/MPN			
aCML	68	6	8.8
CMML	77	2	2.6
JMML	5	0	0.0
MDS/MPN-u	10	0	0.0
Healthy donors	32	0	0.0

Table 7. Frequency of ETNK1 mutations in 515 patient samples and 32 healthy donors.

(from Gambacorti-Passerini CB *et al.* Recurrent ETNK1 mutations in atypical chronic myeloid leukemia. *Blood* 2015 Jan 15; **125**(3): 499-503)

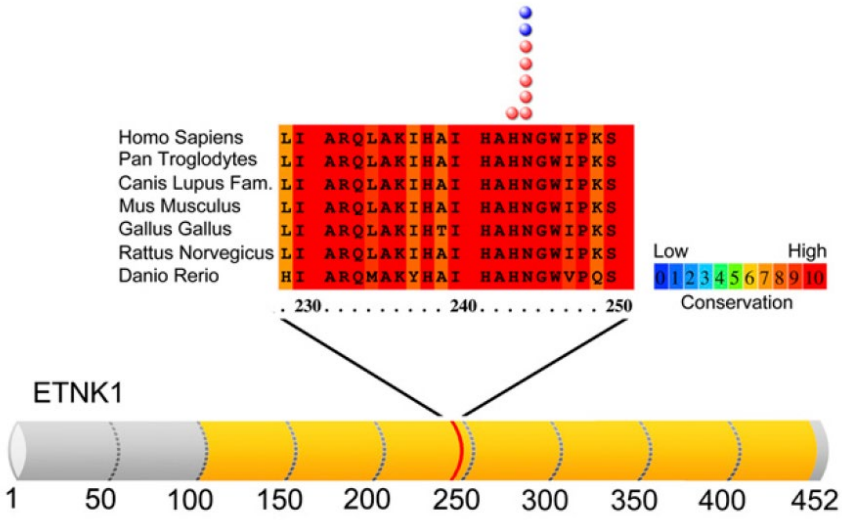

Figure 10. ETNK1 mutations in patients with aCML/chronic myelomonocytic leukemia. Outline of the ETNK1 protein. The yellow region highlights the catalytic domain of the protein. The red band corresponds to the mutational hotspot. In the upper part, a conservation analysis of the mutated locus is shown. The red and blue circles highlight the position of individual mutations identified in aCML and chronic myelomonocytic leukemia, respectively.

(from Gambacorti-Passerini CB *et al.* Recurrent ETNK1 mutations in atypical chronic myeloid leukemia. *Blood* 2015 Jan 15; **125**(3): 499-503)

To further characterize the pattern of *ETNK1* mutations in cancer, the presence of somatic *ETNK1* variants was tested in leukemias and solid tumors, in a total of 60 matched case/control whole-genome samples and more than 600 exomes making up 276 paired tumor/germline primary samples, and 344 cancer cell lines (159-165). No evidence of recurrent *ETNK1* mutations could be found, suggesting that *ETNK1* mutations are more frequent in aCML and closely related disorders.

Since *ETNK1* mutations cluster in a small region of the kinase domain (Figure 10), which is highly conserved across many species, we though that this locus could play a critical, but still unknown, functional role.

With the aim to assess the functional role of these mutations, we quantified the intracellular P-Et level on both ETNK1-positive and ETNK1-negative aCML primary samples, and on myeloid TF1 cell line transduced with ETNK-WT, ETNK1-H243Y, or ETNK1-N244S by using liquid chromatography-mass spectrometry techniques. As shown in Figure 11, the intracellular P-Et/phosphocholine (P-Ch) ratio was 5.2-fold lower in ETNK1-mutated samples than in wild-type ETNK1 ones, suggesting that the mutations could damage the catalytic activity of the enzyme. A similar pattern was seen on the transduced cell lines (Figure 12), where the P-Et/P-Ch ratio was significantly lower in ETNK-H243Y (0.37 ± 0.02; $P=0.0008$) and

ETNK1-N244S (0.76 ± 0.07; P=0.01) compared to ETNK1-WT (1.37 ± 0.32).

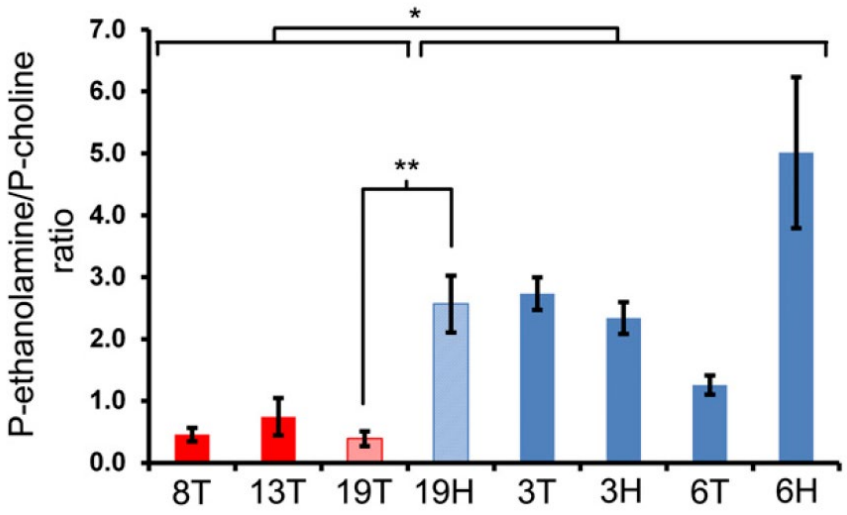

*Figure 11. ETNK1 mutations in patients with aCML/CMML. Intracellular phosphoethanolamine/phosphocholine ratio in patients with aCML. The red bars show the intracellular P-Et/P-Ch ratio of leukemic (myeloid) cells in 3 ETNK1 mutated patients (8T, 13T, and 19T, corresponding to patients CMLPh-008, CMLPh-013, and CMLPh-019). The blue bars show the intracellular P-Et/P-Ch ratio of myeloid (3T, 6T) or lymphoid (3H, 6H) cells negative for ETNK1 mutations (patients CMLPh-003 and CMLPh-006). The light red and light blue bars indicate the intracellular P-Et/P-Ch ratio of a matched myeloid/lymphoid sample whose leukemic (myeloid) cells are positive for ETNK1 mutation. The error bars represent the standard deviation of three experiments. The asterisks indicate the significance level: *P<0.05; **P<0.005.*

(from Gambacorti-Passerini CB *et al.* Recurrent ETNK1 mutations in atypical chronic myeloid leukemia. *Blood* 2015 Jan 15; **125**(3): 499-503)

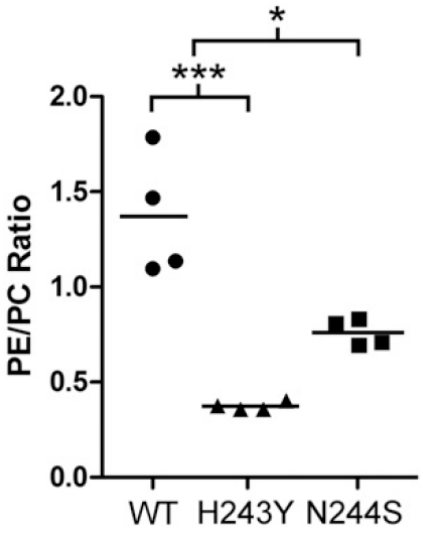

Figure 12. Phosphoethanolamine/phosphocholine ratio in a TF1-ETNK1 cellular model. Intracellular P-Et/P-Ch ratio as assessed by HPLC–mass Spectrometry in TF1 cells transduced with ETNK1-WT, N244S, and H243Y.
(from Gambacorti-Passerini CB *et al.* Recurrent ETNK1 mutations in atypical chronic myeloid leukemia. *Blood* 2015 Jan 15; **125**(3): 499-503)

In conclusion, it seems that *ETNK1* mutations impair the catalytic activity of the enzyme responsible for the first step of the *de*

novo PE biosynthesis pathway. The study of the biologic effect of these mutations in the onset of the aCML, and the mechanisms by which it occurs are the aim of this study.

The presence of *ETNK1* mutations was subsequently reported by Lasho and colleagues in a study carried on patients affected by aggressive systemic mastocytosis (SM) with associated eosinophilia and by CMML (102). In particular, they first identified a somatic missense mutation encoding for N244S in purified eosinophils derived from a patient with aggressive SM with eosinophilia, harboring the driver *KIT* D816V mutation, and later, they performed targeted resequencing on other MPN patients, for a total of 290 cases. They identified *ETNK1* mutations in 20% of patients affected by SM with associated eosinophilia, and in 14% of patients with CMML. Interestingly, these mutations were heterozygous, and clustered in the same locus within the kinase domain, where we found mutations in aCML (90). In particular, the novel *ETNK1* mutations encoded for N244S, N244T, N244K, and G245A substitutions. Notably, our group found the G245V variant in our patients' cohort, as well (data not published). In order to study the role of these mutations, Lasho and collaborators set up a Ba/F3 cell model overexpressing either wild-type or mutated *ETNK1*, but no effect on cell proliferation, survival or apoptosis was noted (102).

4.1. Phosphatidylethanolamine biosynthesis

In mammalian cells, the PE biosynthesis occurs through four different biochemical processes (Figure 13):

- the CDP-ethanolamine pathway (one branch of the Kennedy pathway (157), which allows the *de novo* PE synthesis from ethanolamine. This pathway occurs on the cytoplasmic side of the endoplasmic reticulum membrane, and consists of a sequence of reactions parallel to the CDP-choline pathway for PC synthesis (157). The first step of the CDP-ethanolamine pathway is catalyzed by an ethanolamine kinase, ETNK1, a cytosolic protein. In mammalian cells, two genes encoding ethanolamine kinase have been identified: *ETNK1* and *ETNK2* (166). *ETNK2* encodes a kinase that phosphorylates both ethanolamine and choline to form respectively phosphoethanolamine and phosphocholine. *ETNK1* encodes an enzyme that phosphorylates only ethanolamine, but not choline (156, 166). Subsequently, phosphoethanolamine reacts with cytidine triphosphate (CTP) to produce CDP-ethanolamine in a reaction catalyzed by the cytosolic enzyme CTP:phosphoethanolamine cytidylyltransferase. In the last step of PE synthesis, an integral endoplasmic reticulum (ER) membrane protein, CDP-ethanolamine:1,2-diacylglycerol ethanolaminephosphotransferase (EPT) combines CDP-ethanolamine and diacylglycerol to form PE (Figure 13) (167).
- the second major pathway for PE synthesis in mammalian cells utilizes phosphatidylserine, that, once have been synthetized in

the endoplasmic reticulum, is carried inside the mitochondria where it is decarboxylated to PE by the phosphatidylserine decarboxylase (PSD), an enzyme localized in the inner mitochondrial membrane (IMM) (168) (Figure 13).

- the third way is represented by exchange reactions occurring on the endoplasmic reticulum, by which PE is synthetized starting from PC or PS molecules (169, 170).
- moreover, PE can by synthesized by the acylation of liso-PE.

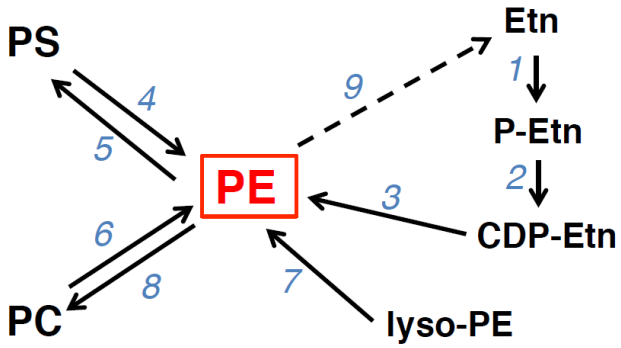

Figure 13. PE biosynthetic pathways in mammalian cells. The enzyme catalyzing each reaction is indicated by the number 1 to 9. #1: ethanolamine kinase; #2: CTP:phosphoethanolamine cytidylyltransferase; #3: CDP-ethanolamine:1,2-diacylglycerol ethanolaminephosphotransferase; #4: phosphatidylserine decarboxylase; #5: PS synthase-2; #6: PS synthase-1; #7: lyso-PE acyltransferase; #8: PE N-methyltransferase; #9: release of ethanolamine from PE. The abbreviation Etn denotes ethanolamine.

(from Vance JE. Historical perspective: phosphatidylserine and phosphatidylethanolamine from the 1800s to the present. *J Lipid Res*. 2018 Jun;**59**(6):923-944)

4.2. Phosphatidylethanolamine properties and functions

PE is the most abundant phospholipid in prokaryotic cells and the second most abundant phospholipid in mammalian cells after PC (Table 8). Its content is significantly higher in the mitochondrial inner membrane (~35-40% of total phospholipids) than in other organelles (~17-25%) (167).

	Percentage of total lipids[a]
Phosphatidylcholine	45–55
Phosphatidylethanolamine	15–25
Phosphatidylinositol	10–15
Phosphatidylserine	5–10
Phosphatidic acid	1–2
Sphingomyelin	5–10
Cardiolipin	2–5
Phosphatidylglycerol	<1
Glycosphingolipids	2–5
Cholesterol	10–20

[a]Data are averaged from several sources.

Table 8. Lipid composition of a typical nucleated mammalian cell.

(from Vance JE. Phospholipid synthesis and transport in mammalian cells. *Traffic* 2015 Jan; **16**(1)**:** 1-18)

From a functional point of view, PE is involved in several biochemical processes. In particular, PE plays a role in defining the membrane architecture (171) , it acts in the regulation of the topology of transmembrane domains of membrane proteins (172), in anchoring specific PE-binding proteins to the cell membrane, ensuring the proper progression of cytokinesis during cell division (173). Moreover, it is involved in assuring an optimal activity of the respiratory complexes in the inner membrane of mitochondria and a proper ubiquinone function (173).

Among the other zwitterionic phospholipids, PE plays a specific role in defining the membrane architecture because of its strong tendency to induce a curvature in the membranes due to its conical molecular structure (174, 175). Characteristically, PE forms inverted hexagonal phase structures triggering high tension within the membrane (176, 177). This effect seems to allow membrane fusion, vesicle formation and movement of proteins across membranes. Indeed, the amount of PE can influence these processes (178). Results obtained in *in vitro* experiments support the evidence of a role of PE in membrane fusion since PE has the tendency to form non-lamellar membrane structures and modulates membrane curvature (179, 180).

Consistent with these findings, PE plays an important role in contractile ring disassembly at the cleavage furrow during cytokinesis (181, 182). Studies in *E. coli* and in mammalian cells indicate that,

during cleavage, PE-rich domains become exposed on the surface of the cells to regulate and coordinate the interaction between the contractile ring and the plasma membrane (173). Besides, PE seems to be necessary for actin-filament disassembly at the end of cytokinesis in some cells, since PE-deficient cells are unable to complete cell division (173, 183).

PE also regulates the fusion of mitotic Golgi membranes (184), and, in mitochondrial membranes where PE is highly abundant, it is fundamental in the regulation of mitochondrial processes (185, 186). In particular, in the IMM, that presents a more pronounced curvature due to the presence of mitochondrial cristae compared to the outer mitochondrial membrane (OMM), the PE amount is higher compared to PC (187, 188). Many studies have highlighted the importance of PE on the MIM. Indeed, the amount of PE in mitochondrial membranes can widely alter the mitochondrial morphology and functions, such as energy production (189). In mice, the reduction of mitochondrial PE production and, as a consequence, the amount of PE, is responsible for mitochondrial abnormalities that in turn cause embryonic lethality (190).

4.3. Phosphoethanolamine

As said before, P-Et is the precursor of PE, and derives from the phosphorylation of ethanolamine made by ETNK1 or ETNK2 kinases. However, its role is not only limited to the phospholipids biosynthesis.

Phosphoethanolamine is required for the attachment of several proteins to the surface of the plasma membrane through the synthesis of the glycosylphosphatidylinositol (GPI) anchors (Figure 14) (191). In particular, P-Et binds the protein to the glycan core of the anchor.

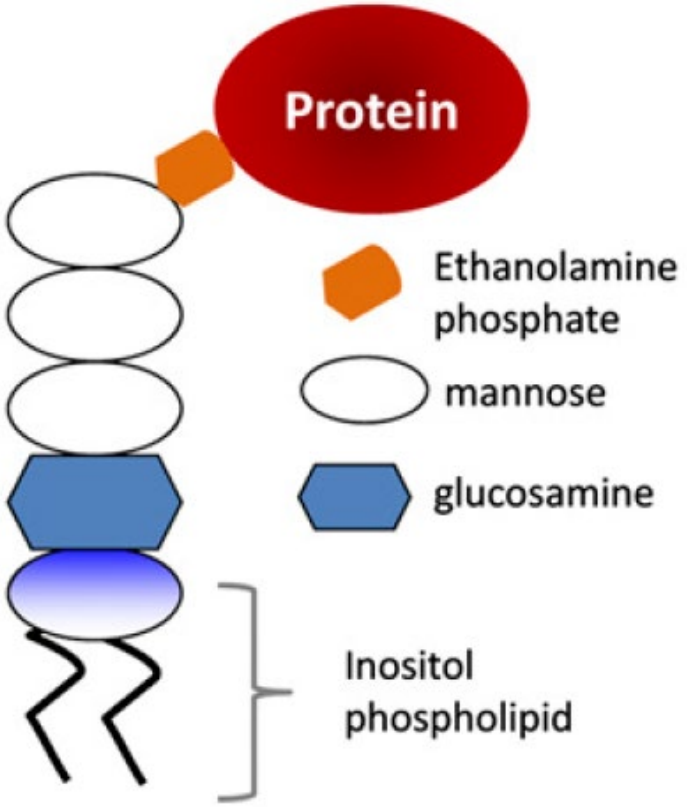

Figure 14. Core structure of the GPI anchor. The inositol-phospholipid is anchored into the lipid bilayer of the plasma membrane. The glycan core consists of a molecule of N-glucosamine, 3 mannose molecules (Man), and a molecule of phosphoethanolamine.

The binding proteins are covalently attached through an amide bond to phosphoethanolamine.
(from Brodsky RA. Paroxysmal nocturnal hemoglobinuria. *Blood*. 2014 Oct 30;**124**(18):2804-11)

4.4. Synthetic phosphoethanolamine as anticancer agent

In the last decade, phosphoethanolamine has been studied as a possible anticancer agent in response to the evidence that it can suppress tumor growth. Several studies of synthetic P-Et, developed in early 1990s by Gilberto Chierice at the University of São Paulo, have been performed (192-198). In 2011, Arruda and colleagues tested the effects of synthetic phosphoethanolamine on macrophage activity in mice bearing solid Ehrlich tumors (192). In this study, the administration of synthetic P-Et resulted in a significant decrease of the macrophage-spreading capacity, and in an increased survival time. Moreover, a smaller amount of hydrogen peroxide (H_2O_2) and nitric oxide (NO) was released by cells collected from treated animals compared to untreated ones, suggesting that H_2O_2 and NO play a role in the modulation of neoplastic growth. These finding corroborated Gordon's results, according to which there is a direct correlation between the presence of P-Et and a decrease in superoxide anion (O_2^-) amount (199).

In addition to the alterations in the cells of the immune response, such as macrophages, the antitumor effects of synthetic P-Et have been reported as well. Synthetic phosphoethanolamine has been tested in various tumor types, in both *in vitro* and *in vivo* models. In particular, the broad antitumor capacity of this compound was evaluated in a variety of tumor cells, such as Ehrlich ascites tumor cells (194), human breast adenocarcinoma MCF-7 cells (194, 196), human SKMEL-28 and MeWo, and murine B16-F10 malignant melanoma cells (193-195), and human mucoepidermoid pulmonary carcinoma H292 cells (194). In *in vitro* assay, it displayed cytotoxic activity against B16-F10 tumor cells, while it preserved healthy cells (193, 195). Moreover, P-Et reduced cell proliferation inducing apoptosis and decreasing the cell cycle progression through both the downregulation of Bax and Bad protein (193), and the activation of caspase-3 and mitochondrial permeability transition-independent apoptosis (195). In mice inoculated with B16-F10 melanoma cells, the treatment with P-Et 7mg/kg and 14mg/kg significantly decreased tumor volume of about 86% compared to control or mice treated with taxol, and reduced the number of metastasis, increasing the survival rate of animals (193). Regarding Ehrlich ascites tumor cells, *in vitro* P-Et exhibited potent cytotoxic activity and caused morphological alterations (194). The treatment induced changes in mitochondrial morphology and transmembrane potential, besides increasing the number of apoptotic cells. Again, P-Et is able to inhibit tumor growth *in vivo* in Ehrlich ascites tumor-bearing mice at 35mg/kg (194). In breast cancer cells, the exposure to synthetic phosphoethanolamine induced cytotoxic effects with an IC_{50} of 20mM, leading to significant

morphological changes in MCF-7 cells. Moreover, the treatment reduced the mitochondrial transmembrane potential, causing changes in mitochondria morphology and their dysfunction. It is also responsible for chromatin condensation and DNA fragmentation, leading to apoptosis via the caspase pathway, and inhibition of the cell cycle (196).

In addition to solid cancers, Ferreira and colleagues evaluated synthetic P-Et effects on leukemic cells that are known to be more sensitive to molecules that impair energy generation by mitochondria compared to their normal counterpart. First, synthetic P-Et exhibited a potent dose-dependent cytotoxic effect against KG-1 (IC_{50}=9mM), K562 (IC_{50}=6mM), and Jurkat (IC_{50}=12mM) cells, decreasing the mitochondrial membrane potential and inducing apoptosis through the mitochondrial-dependent pathway (198). Moreover, in an *in vivo* acute promyelocytic leukemia mouse model, this compound, tested at concentrations of 40mg/kg or 80mg/kg, reduced the percentage of white blood and immature cells in the bone marrow, peripheral blood, spleen, and liver by induction of apoptosis. Moreover, it caused a reduction of $CD117^+$ and $Gr\text{-}1^+$ cells in spleen and liver, a decrease of $CD34^+$ cells in the bone marrow, and an increase of $CD45^+$ cells (198).

Furthermore, it has been demonstrated that synthetic P-Et shows an antiangiogenic activity by inhibition of cell migration and capillaries formation (197), through the reduction in cyclin D1 and VEGFR1 mRNA expression. The same research group also proved the anti-metastatic activity of synthetic P-Et in mice with melanoma (B16-F10) tumors treated with 7mg/kg or 14mg/kg of compound

(197), and in mice injected with murine renal carcinoma cells, treated with 50 or 100mg/kg/day P-Et (193). In both the models, a reduction in metastases was observed compared to untreated mice.

It is of note that in five of these six studies performed by Ferreira and colleagues, the authors did not declare the purity of the test compound (193-197) and in only one study they informed that synthetic P-Et was 99% pure (198). Recently, the same group tested the activity of commercial P-Et on A2058 human melanoma cell line, showing that the compound was able to arrest the cell cycle and to reduce cell mobility, inducing caspase-independent cell death through the impairment of RAS/RAF/MEK/ERK signaling pathway; while in *in vivo* melanoma models P-Et inhibited tumor growth and increased survival rate (200).

On the other hand, besides these eight above-mentioned reports attesting the properties of P-Et as antitumor drug, in literature only a single paper reporting a possible role of P-Et as an inducer of tumor proliferation in the rat mammary carcinoma cell line 64-24 is present (201).

However, the majority of the analyzed papers suggests the possible antitumorigenic potential of synthetic P-Et, although only preclinical studies have been reported. No clinical studies carried on in humans have been published in literature until now (202); therefore, this compound has not received yet the approval for use as an anticancer drug. Even so, some chemists of the Chierice's laboratory at the University of São Paulo, which is not registered for producing medicines, have manufactured the compound for years and distributed free of charge to people with cancer, without any regulatory approval

or clinical oversight. Chierice had been conducting research on synthetic P-Et for over 20 years; he claimed that nearly 40000 individuals have been treated over the years, and a few of those patients have declared remarkable recoveries, perpetuating the compound's reputation as a miracle cure. Moreover, Chierice claimed to have taken part in clinical trials at a reputable cancer center, although the center has denied its involvement. No clinical data on this substance have ever been published. In September 2015, after he retired, the University stopped this unofficial and unsupported distribution of synthetic P-Et, but patients who had been receiving it took the University to court, claming continuous access to the substance. In October 2015, one of the cases reached the Brazilian Supreme Federal Court, who ruled that patients could continue using the substance and that the University should not stop making P-Et, even though the laboratory was not accredited to make compounds for human use, and even before adequate studies were done and evaluated by the Brazilian Health Regulatory Agency (ANVISA). Indeed, the decision not only ignored the opinion of medical specialists who did not believe that synthetic P-Et was active in cancer treatment, but also overlooked the fact that the drug, even if it is not really a 'drug' at all, since it is not approved by Brazil's National Health Surveillance Agency, had only been tested on animals. Despite of all these lacks of experimental and clinical evidences for anticancer efficacy of the P-Et, the Brazilian President Dilma Rousseff signed into law on April 14, 2016 a measure that allows the compound to be produced, prescribed, and dispensed legally as a cancer therapy in Brazil (*Law 13,269/2016*), responding to political pressure and popular demand.

To acquire the pills, consumers must only show medical proof that they have a malignant tumor and sign a consent form. Then, in April 2016, the Science and Technology Ministry created and funded a task force to conduct preclinical studies and clinical trials to evaluate P-Et as cancer treatment. These phase I studies were started in a public hospital sponsored by the São Paulo State Secretary of Health. Notwithstanding the approval, since sponsors did not provide scientifically valid nonclinical and clinical evidence of P-Et potential benefits to cancer patients nor did they present an adequate set of preclinical safety data, the synthetic P-Et trial in cancer patients does not fulfill at least three out of seven key requirements to make a clinical trial ethical. Indeed, as it is known, the authorization to test a new drug in patients without a comprehensive preclinical safety evaluation and in the absence of potential therapeutic usefulness breaks cornerstone rule of human research ethics, the Declaration of Helsinki (203-210). Reports released by the Ministry of Science, Technology and Innovation (MCTI) and issued by the laboratories participating in clinical trials certified that the pills produced by Chierice's group contained only 30% synthetic P-Et. However, it does not appear to be toxic. Studies on toxicity, cytotoxic evaluation, antiproliferative action, genotoxicity and cytotoxic hemolytic potential were made available to the public in order to maintain complete transparency (211). In May 2016, one of the published reports on the effects of synthetic P-Et on Walker's 256 carcinosarcoma described that the drug did not show any antiproliferative action in animals treated with the dose of 1g/kg of body weight per day, for 10

consecutive days. Moreover, a further report on sarcoma 180 cells also showed no inhibitory effects at the same dose and posology (212).

A human trial started on July 25, 2016 and, in phase I, patients with tumors were evaluated. Since no side effects were detected, 200 more people were distributed among ten groups with different type of tumors: head and neck squamous cell carcinoma, non-small cell lung cancer, breast cancer, colorectal adenocarcinoma, cervix cancer, prostate cancer, melanoma, pancreas adenocarcinoma, gastric adenocarcinoma and hepatocellular carcinoma (213). After satisfactory results, other 800 patients would be included in a phase II study (ClinicalTrials.gov Identifier: NCT02950103). However, in April 2017, according to the Director of the Cancer Institute, since the substance had no clinical efficacy in the preliminary study (214), clinical trials were suspended (215).

The lack of more complex studies in humans does not allow a more in-depth and qualitative analysis of the actual toxicological implications of the compound.

It is clear that all the above mentioned use of P-Et did not consider at all the presence of mutated *ETNK1* in the treated cells/animals/patients.

5. Mitochondria

Mitochondria are dynamic organelles present in the cytoplasm of eukaryotic cells but erythrocytes, first observed in the 1840s (216),

even if their name, derived from the Greek words "*mitos*" (*μίτος*) and "*chondros*" (*χονδρίον*), that mean "thread" and "granule" respectively, was coined in 1898 by Carl Benda (217). The first reference to a possible link between mitochondria and respiration, made by Kingsbury (218), is dated back in 1912, and one of the first in-depth descriptions of mitochondria in cells was made by Lewis in 1915 (219), when he observed living and fixed mitochondria, describing mitochondrial movement and dynamics. However, only in the 1990s, thanks to the development of fluorescent probes, fusion and fission of mitochondria were recorded and widely accepted (220), so that nowadays mitochondria are defined as highly dynamic organelles that move throughout the cell whilst constantly fusing and dividing (221).

Mitochondria are thought to have evolved up to two billion years ago from a mutually beneficial relationship between a proteobacteria and a host cell (222). The bacterium was originally endocytosed by the host thereby becoming incorporated into its cytoplasm, conducting cellular respiration in the host cell, which in turn provided the bacteria with a safe environment and more nutrients (223, 224). There may be up to several thousand mitochondria within a single cell depending on the species and the specific energy requirements of the tissue (225).

This organelle is constituted by a double membrane, an outer membrane and an inner one. The outer and the inner membranes re separated by the intermembrane space, while the center of the mitochondrion is known as the matrix. Its diameter is approximately 0.5-1.0μm and its length is about 2-5μm. The structure of a single mitochondrion is shown in Figure 15. The inner mitochondrial

membrane (IMM) is highly folded into cristae to allow for a large surface area, on which many of the mitochondrion's enzymatic reactions occur. In the late 1940s, the mitochondrion was recognized to be a major site of cellular energy production (226), to such an extent that in 1957 Siekevitz named it as "the powerhouse of the cell" (227). Indeed, one of the most important reactions, the oxidative phosphorylation (OXPHOS), occurs on the IMM, since it contains many copies of each of the five electron transport chain (ETC) complexes used to generate ATP, the cellular energy, from adenosine diphosphate (ADP) and phosphate (228). On the other hand, the cristae extend into the central matrix space (229), in which multiple copies of mitochondrial DNA are attached to the inner membrane (228). The intermembrane space is important for mitochondrial respiration as well, since it allows for the generation of a proton (H^+) gradient across the inner membrane that is used in the production of adenosine triphosphate (ATP) (230). In addition to the energy production, mitochondria play other roles, including the generation of reduced electron (e^-) carriers for use in the ETC (231), and the synthesis of metabolic precursors such as amino acids (223), which take place at the citric acid cycle in the mitochondrial matrix. Moreover, mitochondrial are essential for apoptosis, or programmed cell death, which involves the release of cytochrome c from the degraded mitochondrial membrane, to induce the cellular death cascade (232).

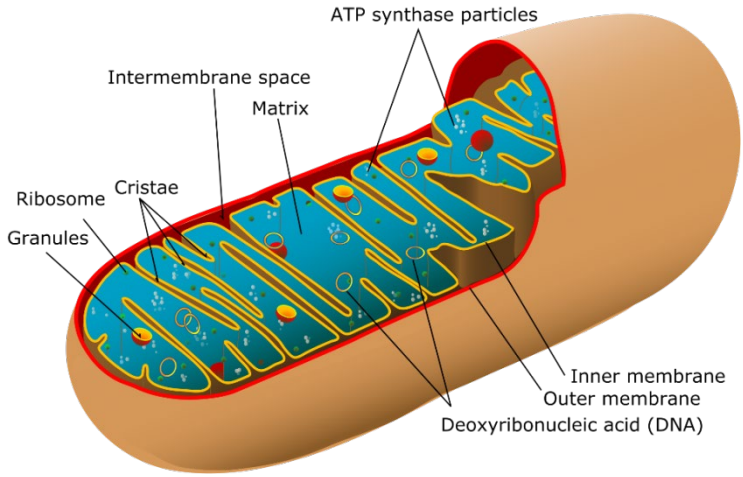

Figure 15. A mitochondrion with its main features.

(from http://teachmephysiology.com/basics/cell-structures/mitochondria /)

5.1. Oxidative phosphorylation and electron transport chain

The ETC is constituted by five multimeric enzyme complexes, termed complex I-V, which are involved in the transport of protons across the mitochondrial inner membrane from the matrix to the intermembrane space, to generate a proton gradient which is then utilized by complex V, the ATP synthase, to generate ATP (Figure 16) (223, 228, 233-235).

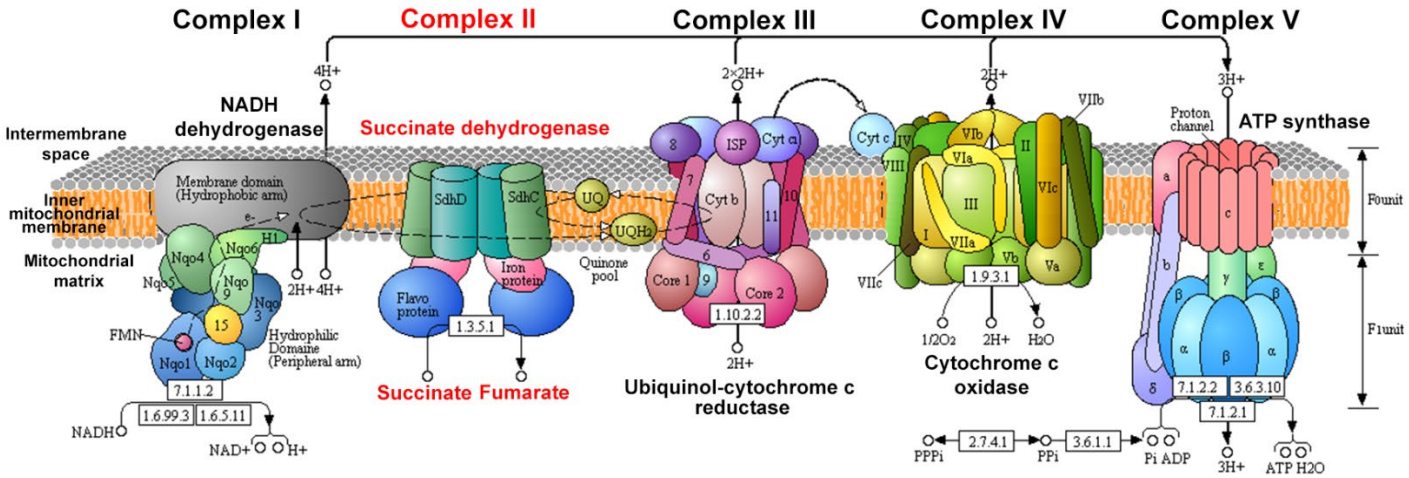
Complex I
Complex II
Complex III
Complex IV
Complex V
4H+
2×2H+
2H+
3H+
NADH dehydrogenase
Succinate dehydrogenase
Intermembrane space
Inner mitochondrial membrane
Mitochondrial matrix
Membrane domain (Hydrophobic arm)
e-
H1
2H+ 4H+
Nqo4
Nqo6
Nqo5
Nqo 9
Nqo 3
15
FMN
Nqo1
Nqo2
Hydrophilic Domaine (Peripheral arm)
7.1.1.2
1.6.99.3
1.6.5.11
NADH
NAD+
H+
SdhD
SdhC
UQ
UQH2
Flavo protein
Iron protein
1.3.5.1
Quinone pool
Succinate Fumarate
8
ISP
Cyt c1
7
Cyt b
10
11
6
Core 1
9
Core 2
1.10.2.2
2H+
Ubiquinol-cytochrome c reductase
Cyt c
IV
VIII
VIIb
VIb
VIa
II
III
VIc
I
VIIa
Vb
Va
VIIc
1.9.3.1
1/2O2
2H+
H2O
Cytochrome c oxidase
Proton channel
ATP synthase
a
c
b
γ
ε
β
α
δ
7.1.2.2
3.6.3.10
7.1.2.1
Founit
F1unit
PPPi
2.7.4.1
PPi
3.6.1.1
Pi ADP
3H+
ATP H2O

Figure 16. Mitochondrial electron transport chain.
(adapted from https://biology.stackexchange.com/questions/42560/how-many-protons-are-pumped-out-per-pair-of-electrons-from-nadh-in-oxidative-pho)

NADH dehydrogenase (complex I) is the first complex in the electron transport chain. It is embedded in the mitochondrial inner membrane, and it is responsible for the oxidation of nicotinamide adenine dinucleotide hydride (NADH) to give NAD^+, transferring two electrons to ubiquinone, which in turn, once reduced to ubiquinol, transfers electrons to complex III. Moreover, complex I pumps protons into the intermembrane space, contributing to the proton gradient used for ATP production (236).

The smallest complex in the electron transport chain is the succinate dehydrogenase (complex II), responsible for the oxidation of succinate to give fumarate. This reaction is coupled with the reduction of flavin adenine dinucleotide (FAD) to $FADH_2$ (237); the electrons are transferred to ubiquinone that, when reduced to ubiquinol, can transfer electrons to complex III. Complex II is located on the matrix side of the inner mitochondrial membrane, and therefore does not contribute directly to the generation of the proton gradient. It consists of four subunits: SDHA, the flavoprotein subunit, which contains FAD bound covalently in the active site; SDHB, the iron-sulfur

protein subunit, which contains a chain of three iron-sulfur clusters; and SDHC and SDHD, the two transmembrane cytochrome b heme subunits, which contain a heme moiety (238).

Ubiquinone-cytochrome c oxidoreductase (complex III) is the third complex and it is responsible for reducing two molecules of cytochrome c, an electron carrier not bound to the membrane (239). The reduction of cytochrome c is coupled to the oxidation of ubiquinol generated by both complexes I and II (240). Moreover, complex III contributes to the proton gradient, pumping hydrogens into the intermembrane space.

Cytochrome c oxidase (complex IV) is the fourth complex and it oxidizes four molecules of cytochrome c reducing one molecule of molecular oxygen to water (241). Again, it contributes to the proton gradient.

The final complex in the oxidative phosphorylation is not involved in electron transfer, but it is responsible for the ATP production, and it is named ATP synthase (complex V). Indeed, the protons stored in the intermembrane space as a reservoir of energy flow back into the matrix through complex V, and the energy derived from the proton motive force drives the ATP synthesis in the mitochondrial matrix from inorganic phosphate and ADP (242).

5.2. Reactive oxygen species

During the process of oxidative phosphorylation, electrons can be leaked from complexes I and III (231, 243-247) during the so-called “electron leak”. These leaked electrons are able to react with

oxygen to generate reactive oxygen species (ROS), a by-product of respiration. As electrons react with oxygen, they initially form superoxide (O_2^-), a radical that contains a single impaired electron, which is responsible of proteins, lipids and nucleic acids oxidation, leading to cell dysfunction due to structural and genetic damage (248-250).

Recently, it has been demonstrated that the complex II activity can produce ROS as well (251-255), at rates similar to those associated to complex I and complex III. In particular, Quinlan and colleagues demonstrated that complex II generates O_2^- or H_2O_2 from site II_F (253), doing so in both the forward reaction from succinate and the reverse reaction from ubiquinol (QH_2).

In physiological circumstances, cells are able to decrease the level of superoxide through the manganese superoxide dismutase (MnSOD) enzyme that converts O_2^- in H_2O_2, that leaves the mitochondria and that is further converted to water by catalase or glutathione peroxidase (223, 234). However, this process could be not completely efficient, and H_2O_2 may undergo the Fenton reaction with iron and copper to generate the hydroxyl radical (OH•) (256-258). Hydroxyl radicals attack DNA rapidly due to their high diffusibility, which results in formation of DNA lesions including oxidized DNA bases, single- and double-strand breaks (259, 260). The oxidative damage occurs when the physiological antioxidative capacity of the cell is no longer able to contrast the ROS generation (261).

5.3. Mitochondrial ROS and cancer

Several studies have demonstrated a possible correlation between increasing ROS level and cancer (262-265). Indeed, mitochondrial ROS production and its subsequent accumulation favor the interaction between these molecules and DNA components, causing single- and/or double-strand breaks resulting in base modifications and genomic instability, respectively, which in turn can activate potentially oncogenic signaling pathway, or cause alterations in gene expression, promoting carcinogenesis (266). For example, mitochondrial-generated ROS are known to trigger the formation of adducts such as 8-oxo-deoxyguanosine (8-oxo-dG), which if not repaired can induce DNA strand breaks and DNA base transversions (267).

5.4. Mitochondria and cancer

In the 1920s, Otto Warburg first reported the metabolic distinction between normal and tumor cells (268), named as “the Warburg effect”. According to this process, in the presence of sufficient oxygen, the malignant cells prefer to produce ATP via glycolysis instead of OXPHOS (269). However, some tumor cells exhibit high rates of OXPHOS (270-272), and that implies that tumors do not consistently inhibit mitochondrial bioenergetics as suggested by Warburg. Indeed, it was observed that stromal fibroblasts that are associated with breast cancer epithelial cells are glycolytic, and it was

proved that the H_2O_2 secreted by the adjacent cancer cells (273) induces the fibroblasts conversion from oxidative to glycolytic metabolism. In this scenario, the stroma synthetizes energy, which in turn is taken by tumor cells for their tricarboxylic acid (TCA) cycle activity, and consequently for oxidative phosphorylation. This intercellular cooperation has been designated as “stromal-epithelial metabolic coupling” or “reverse Warburg effect” (274). Since extensive studies have demonstrated that tumor cells, such as breast cancer and leukemia cells, are more dependent on mitochondria compared to their normal counterparts to meet energy demands for growth and survival (275-278), targeting the mitochondria in cancer cells may reveal a novel strategy for cancer treatment. Therefore, considerable efforts were made on the development of molecules able to target mitochondria. For example, the induction of mitochondrial ROS production may lead to cancer cell death by using a strategy of chemo- or radio-sensitization (279, 280). Some of these agents are nowadays in clinical practice, for example metformin, which is widely used for the treatment of diabetes. Since metformin reduces citric acid cycle activity in isolated mitochondria and inhibits OXPHOS (281), could be repurposed for cancer treatment. Moreover, in the last years, the antibiotic tigecycline is becoming a promising drug for cancer treatment (282).

5.5. Tigecycline

Tigecycline (Tigacil®;Pfizer) (Figure 17) is a new antimicrobial agent for intravenous infusion, belonging to the

glycylcycline class. From a structural and functional point of view, it is similar to tetracycline (283). The chemical name of tigecycline is (4*S*,4a*S*,5a*R*,12a*S*)-9-[2-(*tert*-butylamino)acetamido]-4,7-bis(dimethylamino)-1,4,4a,5,5a,6,11,12a-octahydro-3,10,12,12a-tetrahydroxy-1,11-dioxo-2-naphthacenecarboxamide. The empiric formula is $C_{29}H_{39}N_5O_8$ and the molecular weight is 585.65g/mol.

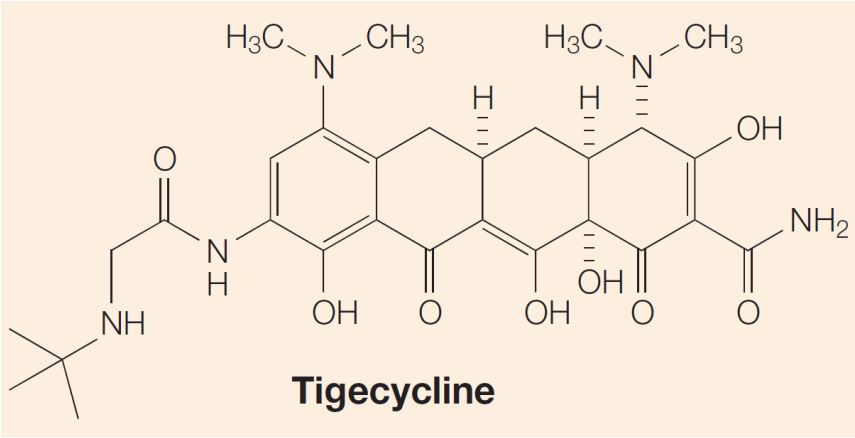

Figure 17. Structure of tigecycline is reported.
(from Wenzel R *et al.* Tigecycline. *Nat Rev Drug Discov*. 2005 Oct;**4**(10):809-10)

Tigecycline received the US FDA approval for clinical antibacterial treatment on June 15, 2005, and, currently, it is the only one FDA-approved glycylcycline. Tigecycline is active against a broad range of Gram-positive and Gram-negative bacteria, particularly drug-resistant pathogens (284, 285), such as *Staphylococcus aureus* (286), *Acinetobacter baumannii* (287), and Enterobacteriaceae (288). Now, it is widely used for complicated skin or intraperitoneal

infection, in particular for complicated intra-abdominal infections (cIAIs), complicated skin-structure infections (cSSIs) (289), and community-acquired bacterial pneumonia (CAP) (290); while it is not indicated for the treatment of diabetic foot infection or hospital-acquired pneumonia, including ventilator-associated pneumonia (290). However, tigecycline is clinically available, with a good safety and tolerable profile, for antibiotic therapies in cancer patients with a pathogen infection (291, 292). The recommended dosage regimen for tigecycline is an initial intravenous infusion of 100mg, followed by doses of 50mg every 12 hours. The duration of treatment for cSSIs or cIAIs is 5 to 14 days, while for CAP is 7 to 14 days, depending upon the severity and the site of the infection. The predominant adverse events reported with tigecycline use have been gastrointestinal ones, such as nausea, vomiting, and diarrhea (290), but they appear to be manageable with the use of standard antiemetic therapies (293). To date, the development of resistance to tigecycline by organisms normally sensitive to the drug has not been noted yet, either in nature or in laboratory (294, 295).

Tigecycline mechanism of action is similar to tetracycline one. It exerts its bacteriostatic activity due to a reversibly binding to the 30S bacterial ribosomal subunit of pathogens, that prevents the docking of the transfer RNA with its codon into the A site of the ribosome complex, leading to inhibition of protein synthesis through the blocking of the peptide chain elongation (295-297).

As said before in paragraph 5, since mitochondria evolved from engulfed bacteria (298, 299), many antibiotics actually target mitochondria, as a mild side-effect, which is well tolerated in most

patients. In particular, tigecycline binds with high affinity the 28S mitochondrial ribosomal subunit (Figure 18). Regarding the role of tigecycline in eukaryotes, and especially in cancer cells, it has been shown that tigecycline blocks only the mitochondrial protein synthesis through binding to its ribosomal subunit, but not to cytoplasmic ribosome subunit (276).

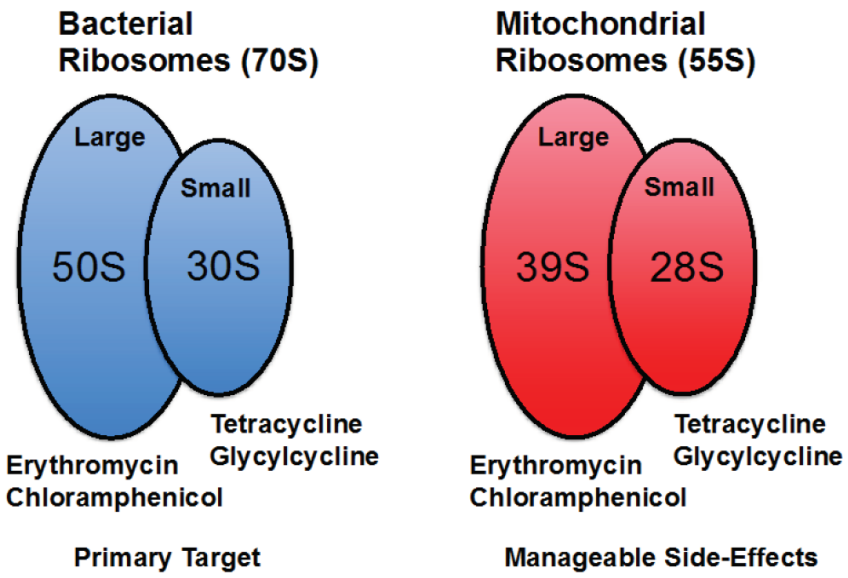

Figure 18. Bacterial and mitochondrial ribosomes are closely related. Erythromycins and chloramphenicol target the large mitochondrial ribosome, while tetracyclines and glycylcyclines target the small mitochondrial ribosomes, because of conserved similarities with bacterial ribosomes.

(from Lamb R *et al*. Antibiotics that target mitochondria effectively eradicate cancer stem cells, across multiple tumor types: Treating cancer like an infectious disease. *Oncotarget* 2015 Mar 10; **6**(7): 4569-4584)

As all electron transport chain complexes but complex II are encoded by mitochondrial DNA and translated by mitochondrial ribosomes, a suppression of mitochondrial respiration occurs because of the inhibition of protein synthesis by tigecycline (300, 301), inhibiting mitochondrial biogenesis, as well (297). For these reasons, tigecycline could be repurposed for the treatment of cancer, even if the mechanism of action of tigecycline appears to vary in different tumor types.

Recently, several studies have shown tigecycline properties against solid cancers. In particular, tigecycline inhibits tumor-sphere formation in a panel of 12 tumor cell lines, across 8 different tumor types, including MCF7, T47D and MDA-MB-231 breast cancer cells, DCIS.com ductal carcinoma in situ cell line, SKOV3, ES2 and Tov21G ovarian cancer cells, A549 lung cancer cells, A375 melanoma cancer cells, PC3 prostate cancer cells, MIA PaCa2 pancreatic cancer cells, and U-87 MG glioblastoma cell line (297). Notably, tigecycline is known to cross the blood-brain barrier, making the treatment of brain cancer feasible. Recently *in vitro* studies have showed that tigecycline is able to inhibit cell proliferation by inducing cell cycle arrest via the AKT pathway in glioma cells (302). Furthermore, Zhong observed the same activity in neuroblastoma cells (303), establishing the effectiveness of tigecycline as a therapeutic agent for glioblastoma. Moreover, tigecycline has been shown to inhibit cell proliferation and induce autophagy in gastric cancer cells through the suppression of mTOR and p70S6K (304); while tigecycline inhibits proliferation and induces apoptosis in NSCLC cell

lines both *in vitro* and *in vivo*, through its ability to disrupt mitochondrial functions (305). Hu and colleagues demonstrated the activity of tigecycline in the inhibition of the cell growth and proliferation in human melanoma cells, and in suppressing tumor growth in a xenograft model of human melanoma, as well (306). Besides, it is a very potent inhibitor of human oral squamous cell carcinoma (OSCC) cell growth, both *in vitro* and *in vivo*, where it inhibits tumorigenesis in a xenograft model when administered intraperitoneally (307). Tigecycline is a potential candidate for the human hepatocellular carcinoma (HCC) treatment, via inhibiting mitochondrial translation and inducing oxidative stress and damage (308). Again, tigecycline inhibits mitochondrial translation in renal cell carcinoma (RCC) cells, and sensitize RCC cells to chemotherapy in both *in vitro* and *in vivo* xenograft mouse model (309). Regarding the cervical squamous cell carcinoma, Li and colleagues reported that tigecycline targets cervical squamous cancer cells in both *in vitro* and *in vivo*, suppressing the Wnt-β-catenin signaling (310). Moreover, it has been demonstrated that tigecycline is able to inhibit the mitochondrial protein translation in triple-negative breast cancer cells (311).

Besides solid tumors, the anti-cancer activities of tigecycline have been shown in hematological malignancies, as well. Škrtić and colleagues firstly demonstrated the role of tigecycline in inducing cell death on a broader spectrum of human and murine AML cell lines (276). Moreover, tigecycline induces selectively death of primary AML cells and progenitor stem cells without affecting the normal hematopoietic counterparts, by the direct inhibition of the

mitochondrial translation. The same activity was also shown in xenograft model of human leukemia (276). Besides AML, tigecycline effects were tested also in other hematological disease. In both diffuse large B-cell lymphoma (DLBCL) cell lines and primary tumors tigecycline showed an antiproliferative effect on cell lines starting from 2.5μM due to the perturbation of the mitochondrial translation pathway, that is responsible for complexes I, III and IV formation. A recent study by Kuntz and coworkers proposes the use of tigecycline together with imatinib to treat patient affected by CML with minimal residual disease (312). First of all they demonstrated that primitive $CD34^+$ CML cells present an increase in oxidative metabolism compared to both differentiated $CD34^-$ CML cells and undifferentiated $CD34^+$ hematopoietic cells from healthy donors. Consequently, the inhibition of aberrant oxidative metabolism can target only CML progenitors and leukemic stem cells (LSCs), preserving the normal counterpart. Basing on these findings, they treated both primary CML cells and murine xenotransplant model of human CML with tigecycline alone or in combination with imatinib, showing that the combined treatment strongly impaired the proliferation of $CD34^+$ CML cells (312). In September 2016, an *in vitro* study for the evaluation of tigecycline for the treatment of CML was approved (ClinicalTrials.gov Identifier: NCT02883036). In this study, investigators should have collected bone marrow and/or peripheral blood mononuclear cells from 100 untreated CML patients, as well as healthy donor, in order to analyze the mitochondrial biogenesis and the basal metabolic characteristic of mononuclear cells, to test the cell viability and apoptosis after tigecycline administration, and to detect

changes of cell mitochondrial biogenesis after the treatment. However, up to date, patients recruitment has not begun yet.

Recently, based on the above-mentioned pre-clinical data from Škrtić, tigecycline has completed a Phase I clinical trial (ClinicalTrials.gov Identifier: NCT01332786) for the treatment of relapsed and refractory AML patients (313). It was an open-label, multicentric, dose-escalation study. The maximal evaluated dose was 350mg/day and the maximal tolerated dose was 300mg/day. The most frequent adverse events reported were nausea and vomiting. However, no clinical responses were seen, and the study was stopped after administration of tigecycline to 27 patients for 42 cycles over seven doses (313).

Scope of this thesis

The work performed in this three-year PhD project has been focused on the characterization of the role of mutated *ETNK1* in the onset of atypical Chronic Myeloid Leukemia.

The project has been developed as follow:

- First, I created a new isogenic CRISPR/Cas9 cellular model in which *ETNK1* mutation was present as heterozygous variant.
- Second, I provided evidences regarding the molecular mechanism by which phosphoethanolamine acts on mitochondria.
- Then, I investigated the functional effect of phosphoethanolamine modulation, with particular attention toward the impaired mitochondrial activity.
- Finally I discovered the role of *ETNK1* in the onset of the disease, and I proposed two possible therapeutic strategies.

References

1. Thomas X. First contributors in the history of leukemia. *World J Hematol* 2013 Aug 6; **2**(3)**:** 62-70.

2. Kampen KR. The discovery and early understanding of leukemia. *Leukemia Res* 2012 Jan; **36**(1)**:** 6-13.

3. Degos L. John Hughes Bennett, Rudolph Virchow... and Alfred Donne: the first description of leukemia. *The hematology journal : the official journal of the European Haematology Association* 2001; **2**(1)**:** 1.

4. Lichtman MA. Battling the hematological malignancies: the 200 years' war. *The oncologist* 2008 Feb; **13**(2)**:** 126-138.

5. Beutler E. The treatment of acute leukemia: past, present, and future. *Leukemia* 2001 Apr; **15**(4)**:** 658-661.

6. Geary CG. The story of chronic myeloid leukaemia. *Brit J Haematol* 2000 Jul; **110**(1)**:** 2-11.

7. Seufert W, Seufert WD. The Recognition of Leukemia as a Systemic-Disease. *J Hist Med All Sci* 1982 Jan; **37**(1)**:** 34-50.

8. Kiple KF. The Cambridge world history of human disease. *Cambridge University Press* 1993 Jan 29; **vol. VIII:** 82-848.

9. Goldman JM. Chronic Myeloid Leukemia: A Historical Perspective. *Semin Hematol* 2010 Oct; **47**(4)**:** 302-311.

10. Cullen P. Case of splenitis acutus in which the serum of the blood draw from the arm had the appearance of milk. *Edinburgh Med J* 1811; **7:** 169-171.

11. Velpeau A. Sur la résorption du pus et sur l'altération du sang dans les maladies. *Revue Médicale Française et étrangère* 1827; **2:** 216-240.

12. Velpeau A. Altération du sang. *Archives Générales de Medecine; Journal publié par une société de médecins, Paris* 1825**:** 462-463.

13. Vidal E. De la leucocythémie splénique ou de l'hypertrophie de la rate avec altération du sang consistant dans une augmentation considérable du nombre des globules blancs. *Gazette hebdomadaire de médecine et de chirurgie* 1856**:** 201-202.

14. Donné A. Globules purulent: Du pus dans le sang, Cours de Microscopie complémentaire des études médicales: anatomie microscopique et physiologie de fluides de l'économie. Paris. *Chez J & Bailliere B* 1844**:** 195-201.

15. Donné A, Foucault L. Cours de microscopie complémentaire des études médicales: anatomie microscopique et physiologie des fluides de l'économie. Atlas au Microscope-Daggueréotype. Paris. *Chez J & Baillière B* 1845**:** 24-41.

16. Donné A. Bulletins et mémoires de la Société Médicale des Hôpitaux de Paris. *Paris: Ballière* 1855**:** 39.

17. Bennett JH. Case 2, case of hypertrophy of the spleen and liver, in which death took place from suppuration of the blood. *The Edinburgh Medical and Surgical Journal* 1845; **64:** 413-423.

18. Bennett JH. Leucocythaemia or white cell blood. *Edinb Med Surg J* 1852; **72:** 7-82.

19. Bennett JH. Leucocythemia (1845), clinical lectures on the principles and practice of medicine. *Last Edinburgh edition New York: Samuel S & Wood W* 1860**:** 814-844.

20. Bennett JH. Professors Kölliker and Bennett on the discovery of leucocythaemia. *Monthly J Med Sci* 1854; **19:** 377-381.

21. Virchow R. Weisses blut. *Froriep's Notizen* 1845; **36:** 151-156.

22. Virchow R. Zur pathologischen physiologie des blutes. II. Weisses blut. *Arch Pathol Anat Phys* 1847; **1:** 563-572.

23. Virchow R. Leukamie, Gesammelte Abhandlungen zur wissenschaftlichen medicin. *Frankfurt: Meidinger Sohn & comp* 1856**:** 149-154.

24. Virchow R. Zur pathologischen physiologie des blutes. IV. Farblose, pigmentierte und geschwantze nicht spezifische zellen im blut. *Arch Pathol Anat Phys* 1849; **2:** 587-598.

25. Saadatpour A, Guo GJ, Orkin SH, Yuan GC. Characterizing heterogeneity in leukemic cells using single-cell gene expression analysis. *Genome Biol* 2014 Dec 3; **15**(12)**:** 525.

26. Andral G. Pathological Haematology. An essay on the blood in disease. *Philadelphia: Lea and Blanchard* 1844.

27. Friedreich N. Ein neuer fall von Leukamie. *Virchows Arch Pathol Anat* 1857; **12:** 37-58.

28. Neumann E. Uber myelogene Leukamie. *Berlin Klin Wochenschr* 1878; **15:** 69.

29. Ehrlich P. Methodologische beiträge zur physiologie und pathologie der verschisdenen formen der leukocyten. *Zeitschrift Klin Medizin* 1879; **1:** 553-560.

30. Neumann E. Ueber die bedeutung des knochenmarkes für die blutbildung. *Archiv der Heilkunde Leipzig* 1869**:** 68-102.

31. Neumann E. Ein fall von Leukamie mit erkrankung des knochenmarks. *Arch Heilkunde* 1870; **11:** 1.

32. Bizzozero G. Sulla funzione ematopoietica del midollo delle ossa. *Centralblatt Medizin Wissenschaft* 1868; **6:** 885.

33. Bizzozero G. Sulla funzione ematopoietica del midollo delle ossa, seconda communicazione preventia. *Centralblatt Medizin Wissenschaft* 1869; **10:** 149-150.

34. Neumann E. Ein neuer fall von Leukamie mit erkrankung des knochenmarks. *Arch Heilkunde* 1872; **13:** 502-508.

35. Mosler F. Klinische symptome und therapie des medullaren Leukämia. *Berlin Klin Wochenschr* 1876; **13:** 702.

36. Piller GJ. Leukaemia - a brief historical review from ancient times to 1950. *Brit J Haematol* 2001 Feb; **112**(2)**:** 282-292.

37. Cutler EG, Bradford EH. Action of iron, cod liver oil and arsenic on the globular richness of the blood. *American Journal of Medical Science* 1878; **75:** 74-84.

38. Röntgen WC. On a new kind of rays. *Science* 1896; **3**(59)**:** 227-231.

39. Osler W. The Principles and Practice of Medicine: Designed for the use of practitioners and students of medicine. 8th edn. *New York, London: D Appleton and Company* 1916**:** 746.

40. Forkner CE. Leukemia and allied disorders. A monograph. *New York: Macmillan Co* 1938.

41. Wintrobe MM. Clinical Haematology. 2nd edn. *London: Henry Kimpton* 1946**:** 712.

42. Bessis M, Bernard J. Remarquables résultats du traitement par l'exsanguino-transfusion d'un cas de leucémie aiguë. *Bull Mem Soc Med Hop Paris* 1947 Oct; **63**(28-29)**:** 871-877.

43. Gilman A, Philips FS. The biological actions and therapeutic applications of the B-chloroethyl amines and sulfides. *Science* 1946 Apr 5; **103**(2675)**:** 409-415.

44. Foye LV, Chapman CG, Willett FM, Adams WS. Cyclophosphamide. A preliminary study of a new alkylating agent. *Cancer Chemother Rep* 1960 Feb; **6:** 39-40.

45. Farber S, Schwachman H, Toch R. The Effect of ACTH in Acute Leukemia in Childhood. *In Proceedings of the First*

Clinical ACTH Conference (ed by Mote JR), New York: Blakiston, Co 1950**:** 328-330.

46. Pearson OH, Eliel LP, Rawson RW, Dobriner K, Rhoads CP. ACTH and cortisone induced regression of lymphoid tumors in man. *Cancer* 1949 Nov; **2:** 943-945.

47. Elion GB, Hitchings GH, van der Werff H. Antagonists of nucleic acid derivatives. VI. Purines. *Journal of Biological Chemistry* 1951 Oct; **192:** 505.

48. Elion GB, Burgi E, Hitchings GH. Studies on condensed pyrimidine systems. IX. The synthesis of some 6-substituted purines. *Journal of the American Chemistry Society* 1952 Jan; **74:** 411-414.

49. Boveri R. Zur frage der entstehung maligner tumoren. *Jena: Fischer* 1914.

50. Nowell PC, Hungerford DA. A minute chromosome in human chronic granulocytic leukemia. Abstract. *Science* 1960; **132:** 1497.

51. Druker BJ, Tamura S, Buchdunger E, Ohno S, Segal GM, Fanning S*, et al.* Effects of a selective inhibitor of the Abl tyrosine kinase on the growth of Bcr-Abl positive cells. *Nat Med* 1996 May; **2**(5)**:** 561-566.

52. Druker BJ, Talpaz M, Resta DJ, Peng B, Buchdunger E, Ford JM*, et al.* Efficacy and safety of a specific inhibitor of the BCR-ABL tyrosine kinase in chronic myeloid leukemia. *N Engl J Med* 2001 Apr 5; **344**(14)**:** 1031-1037.

53. Kantarjian H, Sawyers C, Hochhaus A, Guilhot F, Schiffer C, Gambacorti-Passerini C*, et al.* Hematologic and cytogenetic responses to imatinib mesylate in chronic myelogenous leukemia. *New Engl J Med* 2002 Feb 28; **346**(9)**:** 645-652.

54. Sawyers CL, Hochhaus A, Feldman E, Goldman JM, Miller CB, Ottmann OG*, et al.* Imatinib induces hematologic and cytogenetic responses in patients with chronic myelogenous

leukemia in myeloid blast crisis: results of a phase II study. *Blood* 2002 May 15; **99**(10)**:** 3530-3539.

55. Hochhaus A, Druker B, Sawyers C, Guilhot F, Schiffer CA, Cortes J*, et al.* Favorable long-term follow-up results over 6 years for response, survival, and safety with imatinib mesylate therapy in chronic-phase chronic myeloid leukemia after failure of interferon-alpha treatment. *Blood* 2008 Feb 1; **111**(3)**:** 1039-1043.

56. Gambacorti-Passerini C. Part I: Milestones in personalised medicine - imatinib. *Lancet Oncol* 2008 Jun; **9**(6)**:** 600-600.

57. Arber DA, Orazi A, Hasserjian R, Thiele J, Borowitz MJ, Le Beau MM*, et al.* The 2016 revision to the World Health Organization classification of myeloid neoplasms and acute leukemia. *Blood* 2016 May 19; **127**(20)**:** 2391-2405.

58. Vardiman JW, Harris NL, Brunning RD. The World Health Organization (WHO) classification of the myeloid neoplasms. *Blood* 2002 Oct 1; **100**(7)**:** 2292-2302.

59. Kurzrock R, Bueso-Ramos CE, Kantarjian H, Freireich E, Tucker SL, Siciliano M*, et al.* BCR rearrangement-negative chronic myelogenous leukemia revisited. *Journal of clinical oncology : official journal of the American Society of Clinical Oncology* 2001 Jun 1; **19**(11)**:** 2915-2926.

60. Pugh WC, Pearson M, Vardiman JW, Rowley JD. Philadelphia Chromosome-Negative Chronic Myelogenous Leukemia - a Morphological Reassessment. *Brit J Haematol* 1985 Jul; **60**(3)**:** 457-467.

61. Travis LB, Pierre RV, DeWald GW. Ph1-negative chronic granulocytic leukemia: a nonentity. *Am J Clin Pathol* 1986 Feb; **85**(2)**:** 186-193.

62. Fend F, Horn T, Koch I, Vela T, Orazi A. Atypical chronic myeloid leukemia as defined in the WHO classification is a JAK2 V617F negative neoplasm. *Leukemia Res* 2008 Dec; **32**(12)**:** 1931-1935.

63. Shepherd PC, Ganesan TS, Galton DA. Haematological classification of the chronic myeloid leukaemias. *Bailliere's clinical haematology* 1987 Dec; **1**(4)**:** 887-906.

64. Kantarjian HM, Shtalrid M, Kurzrock R, Blick M, Dalton WT, LeMaistre A*, et al.* Significance and correlations of molecular analysis results in patients with Philadelphia chromosome-negative chronic myelogenous leukemia and chronic myelomonocytic leukemia. *The American Journal of Medicine* 1988 Nov; **85**(5)**:** 639-644.

65. Wiedemann LM, Karhi KK, Shivji MKK, Rayter SI, Pegram SM, Dowden G*, et al.* The Correlation of Breakpoint Cluster Region Rearrangement and P210 Phl/Abl Expression with Morphological Analysis of Ph-Negative Chronic Myeloid-Leukemia and Other Myeloproliferative Diseases. *Blood* 1988 Feb; **71**(2)**:** 349-355.

66. Galton DA. Haematological differences between chronic granulocytic leukaemia, atypical chronic myeloid leukaemia, and chronic myelomonocytic leukaemia. *Leukemia & lymphoma* 1992 Aug; **7**(5-6)**:** 343-350.

67. Martiat P, Michaux JL, Rodhain J. Philadelphia-negative (Ph-) chronic myeloid leukemia (CML): comparison with Ph+ CML and chronic myelomonocytic leukemia. The Groupe Francais de Cytogenetique Hematologique. *Blood* 1991 Jul 1; **78**(1)**:** 205-211.

68. Cogswell PC, Morgan R, Dunn M, Neubauer A, Nelson P, Poland-Johnston NK*, et al.* Mutations of the ras protooncogenes in chronic myelogenous leukemia: a high frequency of ras mutations in bcr/abl rearrangement-negative chronic myelogenous leukemia. *Blood* 1989 Dec; **74**(8)**:** 2629-2633.

69. Kurzrock R, Kantarjian HM, Shtalrid M, Gutterman JU, Talpaz M. Philadelphia chromosome-negative chronic myelogenous leukemia without breakpoint cluster region

rearrangement: a chronic myeloid leukemia with a distinct clinical course. *Blood* 1990 Jan 15; **75**(2)**:** 445-452.

70. Bennett JM, Catovsky D, Daniel MT, Flandrin G, Galton DA, Gralnick H*, et al.* The chronic myeloid leukaemias: guidelines for distinguishing chronic granulocytic, atypical chronic myeloid, and chronic myelomonocytic leukaemia. Proposals by the French-American-British Cooperative Leukaemia Group. *Br J Haematol* 1994 Aug; **87**(4)**:** 746-754.

71. Oscier DG. Atypical chronic myeloid leukaemia, a distinct clinical entity related to the myelodysplastic syndrome? *Br J Haematol* 1996 Mar; **92**(3)**:** 582-586.

72. Hernandez JM, del Canizo MC, Cuneo A, Garcia JL, Gutierrez NC, Gonzalez M*, et al.* Clinical, hematological and cytogenetic characteristics of atypical chronic myeloid leukemia. *Annals of oncology : official journal of the European Society for Medical Oncology* 2000 Apr; **11**(4)**:** 441-444.

73. Jaffe ES, Harris NL, Stein H, Vardiman JW. Pathology and Genetics of Tumours of Haematopoietic and Lymphoid Tissues WHO Classification of Tumours, 3rd Edition, Volume 3. *Lyon: IARC Press* 2001.

74. Harris NL, Jaffe ES, Diebold J, Flandrin G, Muller-Hermelink HK, Vardiman J*, et al.* World Health Organization classification of neoplastic diseases of the hematopoietic and lymphoid tissues: report of the Clinical Advisory Committee meeting-Airlie House, Virginia, November 1997. *Journal of clinical oncology : official journal of the American Society of Clinical Oncology* 1999 Dec; **17**(12)**:** 3835-3849.

75. Vardiman JW, Bain B, Inbert M, Brunning RD, Pierre RV, Flandrin G. Atypical chronic myeloid leukemia. In Jaffe E, Harris NL, Stein H, Vardiman J, editors. WHO classification of tumours: pathology and genetics of tumours of haematopoietic and lymphoid tissues. Lyon: IARC Press. *Lyon: IARC Press* 2001**:** 53-57.

76. Onida F, Ball G, Kantarjian HM, Smith TL, Glassman A, Albitar M*, et al.* Characteristics and outcome of patients with Philadelphia chromosome negative, bcr/abl negative chronic myelogenous leukemia. *Cancer* 2002 Oct 15; **95**(8)**:** 1673-1684.

77. Sabattini E, Bacci F, Sagramoso C, Pileri SA. WHO classification of tumours of haematopoietic and lymphoid tissues in 2008: an overview. *Pathologica* 2010 Jun; **102**(3)**:** 83-87.

78. Swerdlow SH, Campo E, Harris NL, Jaffe ES, Pileri SA, Stein H*, et al.* WHO Classification of Tumours of Haematopoietic and Lymphoid Tissues. WHO Classification of Tumours, Revised 4th Edition, Volume 2. *Lyon: IARC Press* 2008.

79. Vardiman JW, Thiele J, Arber DA, Brunning RD, Borowitz MJ, Porwit A*, et al.* The 2008 revision of the World Health Organization (WHO) classification of myeloid neoplasms and acute leukemia: rationale and important changes. *Blood* 2009 Jul 30; **114**(5)**:** 937-951.

80. Oscier D. Atypical chronic myeloid leukemias. *Pathologie-biologie* 1997 Sep; **45**(7)**:** 587-593.

81. Breccia M, Biondo F, Latagliata R, Carmosino I, Mandelli F, Alimena G. Identification of risk factors in atypical chronic myeloid leukemia. *Haematologica* 2006 Nov; **91**(11)**:** 1566-1568.

82. Cazzola M, Malcovati L, Invernizzi R. Myelodysplastic/myeloproliferative neoplasms. *Hematology Am Soc Hematol Educ Program* 2011; **1:** 264-272.

83. Orazi A, Germing U. The myelodysplastic/myeloproliferative neoplasms: myeloproliferative diseases with dysplastic features. *Leukemia* 2008 Jul; **22**(7)**:** 1308-1319.

84. Tiu RV, Sekeres MA. Making sense of the myelodysplastic/myeloproliferative neoplasms overlap

syndromes. *Current opinion in hematology* 2014 Mar; **21**(2)**:** 131-140.

85. Orazi A, O'Malley DP, Arber DA. Illustrated Pathology of the Bone Marrow. *Cambridge University Press: Cambridge, UK* 2006**:** 88-92.

86. Tefferi A, Elliot MA, Pardanani A. Atypical myeloproliferative disorders: Diagnosis and management. *Mayo Clin Proc* 2006 Apr; **81**(4)**:** 553-563.

87. Jones AV, Kreil S, Zoi K, Waghorn K, Curtis C, Zhang LY*, et al.* Widespread occurrence of the JAK2 V617F mutation in chronic myeloproliferative disorders. *Blood* 2005 Sep 15; **106**(6)**:** 2162-2168.

88. Carulli G, Fabiani O, Azzara A. The syndrome of abnormal chromatin clumping in leukocytes. *Haematologica* 1997 Sep-Oct; **82**(5)**:** 635-636.

89. Piazza R, Valletta S, Winkelmann N, Redaelli S, Spinelli R, Pirola A*, et al.* Recurrent SETBP1 mutations in atypical chronic myeloid leukemia. *Nat Genet* 2013 Jan; **45**(1)**:** 18-24.

90. Gambacorti-Passerini CB, Donadoni C, Parmiani A, Pirola A, Redaelli S, Signore G*, et al.* Recurrent ETNK1 mutations in atypical chronic myeloid leukemia. *Blood* 2015 Jan 15; **125**(3)**:** 499-503.

91. Meggendorfer M, Bacher U, Alpermann T, Haferlach C, Kern W, Gambacorti-Passerini C*, et al.* SETBP1 mutations occur in 9% of MDS/MPN and in 4% of MPN cases and are strongly associated with atypical CML, monosomy 7, isochromosome i(17)(q10), ASXL1 and CBL mutations. *Leukemia* 2013 Sep; **27**(9)**:** 1852-1860.

92. Zoi K, Cross NC. Molecular pathogenesis of atypical CML, CMML and MDS/MPN-unclassifiable. *International journal of hematology* 2015 Mar; **101**(3)**:** 229-242.

93. Gotlib J, Maxson JE, George TI, Tyner JW. The new genetics of chronic neutrophilic leukemia and atypical CML: implications for diagnosis and treatment. *Blood* 2013 Sep 5; **122**(10)**:** 1707-1711.

94. Reiter A, Invernizzi R, Cross NCP, Cazzola M. Molecular basis of myelodysplastic/myeloproliferative neoplasms. *Haematol-Hematol J* 2009 Dec; **94**(12)**:** 1634-1638.

95. Sakaguchi H, Okuno Y, Muramatsu H, Yoshida K, Shiraishi Y, Takahashi M*, et al.* Exome sequencing identifies secondary mutations of SETBP1 and JAK3 in juvenile myelomonocytic leukemia. *Nat Genet* 2013 Aug; **45**(8)**:** 937-941.

96. Makishima H, Yoshida K, Nguyen N, Przychodzen B, Sanada M, Okuno Y*, et al.* Somatic SETBP1 mutations in myeloid malignancies. *Nat Genet* 2013 Aug; **45**(8)**:** 942-946.

97. Inoue D, Kitaura J, Matsui H, Hou HA, Chou WC, Nagamachi A*, et al.* SETBP1 mutations drive leukemic transformation in ASXL1-mutated MDS. *Leukemia* 2015 Apr; **29**(4)**:** 847-857.

98. Fabiani E, Falconi G, Fianchi L, Criscuolo M, Leone G, Voso MT. SETBP1 mutations in 106 patients with therapy-related myeloid neoplasms. *Haematologica* 2014 Sep; **99**(9)**:** e152-153.

99. Patnaik MM, Itzykson R, Lasho T, Kosmider O, Finke C, Hanson C*, et al.* ASXL1 and SETBP1 mutations and their prognostic contribution in chronic myelomonocytic leukemia: a two-center study of 466 patients. *Leukemia* 2014 Nov; **28**(11)**:** 2206-2212.

100. Thol F, Suchanek KJ, Koenecke C, Stadler M, Platzbecker U, Thiede C*, et al.* SETBP1 mutation analysis in 944 patients with MDS and AML. *Leukemia* 2013 Oct; **27**(10)**:** 2072-2075.

101. Wang XA, Muramatsu H, Okuno Y, Sakaguchi H, Yoshida K, Kawashima N*, et al.* GATA2 and secondary mutations in familial myelodysplastic syndromes and pediatric myeloid malignancies. *Haematologica* 2015 Oct; **100**(10)**:** E398-E401.

102. Lasho TL, Finke CM, Zblewski D, Patnaik M, Ketterling RP, Chen D*, et al.* Novel recurrent mutations in ethanolamine kinase 1 (ETNK1) gene in systemic mastocytosis with eosinophilia and chronic myelomonocytic leukemia. *Blood Cancer J* 2015 Jan 23; **5:** e275.

103. Koopmans SM, van Marion AMW, Schouten HC. Myeloproliferative neoplasia: a review of clinical criteria and treatment. *Neth J Med* 2012 May; **70**(4)**:** 159-167.

104. Dameshek W. Some speculations on the myeloproliferative syndromes. *Blood* 1951 Apr; **6**(4)**:** 372-375.

105. Kurzrock R. Myelodysplastic syndrome overview. *Semin Hematol* 2002 Jul; **39**(3)**:** 18-25.

106. Leube W. A macrocytic anemia progressing to acute leukemia. *Berl Klin Wochenschr* 1900; **37:** 851.

107. Maxson JE, Tyner JW. Genomics of chronic neutrophilic leukemia. *Blood* 2017 Feb 9; **129**(6)**:** 715-722.

108. Wang SA, Hasserjian RP, Fox PS, Rogers HJ, Geyer JT, Chabot-Richards D*, et al.* Atypical chronic myeloid leukemia is clinically distinct from unclassifiable myelodysplastic/myeloproliferative neoplasms. *Blood* 2014 Apr 24; **123**(17)**:** 2645-2651.

109. Gotlib J. How I treat atypical chronic myeloid leukemia. *Blood* 2017 Feb 16; **129**(7)**:** 838-845.

110. Dhakal P, Gundabolu K, Amador C, Rayamajhi S, Bhatt VR. Atypical chronic myeloid leukemia: a rare entity with management challenges. *Future Oncol* 2018 Jan; **14**(2)**:** 177-185.

111. Mittal P, Saliba RM, Giralt SA, Shahjahan M, Cohen AI, Karandish S*, et al.* Allogeneic transplantation: a therapeutic option for myelofibrosis, chronic myelomonocytic leukemia and Philadelphia-negative/BCR-ABL-negative chronic

myelogenous leukemia. *Bone marrow transplantation* 2004 May; **33**(10)**:** 1005-1009.

112. Koldehoff M, Beelen DW, Trenschel R, Steckel NK, Peceny R, Ditschkowski M*, et al.* Outcome of hematopoietic stem cell transplantation in patients with atypical chronic myeloid leukemia. *Bone marrow transplantation* 2004 Dec; **34**(12)**:** 1047-1050.

113. Koldehoff M, Steckel NK, Hegerfeldt Y, Ditschkowski M, Beelen DW, Elmaagacli AH. Clinical course and molecular features in 21 patients with atypical chronic myeloid leukemia. *Int J Lab Hematol* 2012 Feb; **34**(1)**:** e3-e5.

114. Onida F, de Wreede LC, van Biezen A, Eikema DJ, Byrne JL, Iori AP*, et al.* Allogeneic stem cell transplantation in patients with atypical chronic myeloid leukaemia: a retrospective study from the Chronic Malignancies Working Party of the European Society for Blood and Marrow Transplantation. *Brit J Haematol* 2017 Jun; **177**(5)**:** 759-765.

115. Lim SN, Lee JH, Kim DY, Kim SD, Kang YA, Lee YS*, et al.* Allogeneic hematopoietic cell transplantation in adult patients with myelodysplastic/myeloproliferative neoplasms. *Blood research* 2013 Sep; **48**(3)**:** 178-184.

116. Patnaik MM, Barraco D, Lasho TL, Finke CM, Reichard K, Hoversten KP*, et al.* Targeted next generation sequencing and identification of risk factors in World Health Organization defined atypical chronic myeloid leukemia. *Am J Hematol* 2017 Jun; **92**(6)**:** 542-548.

117. Montefusco E, Alimena G, Lo Coco F, De Cuia MR, Wang YZ, Aloe Spiriti MA*, et al.* Ph-negative and bcr-negative atypical chronic myelogenous leukemia: biological features and clinical outcome. *Annals of hematology* 1992 Jul; **65**(1)**:** 17-21.

118. Costello R, Lafage M, Toiron Y, Brunel V, Sainty D, Arnoulet C*, et al.* Philadelphia chromosome-negative chronic myeloid

leukaemia: a report of 14 new cases. *Br J Haematol* 1995 Jun; **90**(2)**:** 346-352.

119. Costello R, Sainty D, LafagePochitaloff M, Gabert J. Clinical and biological aspects of Philadelphia-negative/BCR-negative chronic myeloid leukemia. *Leukemia & lymphoma* 1997 Apr; **25**(3-4)**:** 225-232.

120. Jabbour E, Kantarjian H, Cortes J, Thomas D, Garcia-Manero G, Ferrajoli A*, et al.* PEG-IFN-alpha-2b therapy in BCR-ABL-negative myeloproliferative disorders - Final result of a phase 2 study. *Cancer* 2007 Nov 1; **110**(9)**:** 2012-2018.

121. Gerds AT. I Walk the Other Line: Myelodysplastic/Myeloproliferative Neoplasm Overlap Syndromes. *Curr Hematol Malig R* 2014 Dec; **9**(4)**:** 400-406.

122. Hausmann H, Bhatt VR, Yuan J, Maness LJ, Ganti AK. Activity of single-agent decitabine in atypical chronic myeloid leukemia. *Journal of oncology pharmacy practice : official publication of the International Society of Oncology Pharmacy Practitioners* 2016 Dec; **22**(6)**:** 790-794.

123. Ades L, Sekeres MA, Wolfromm A, Teichman ML, Tiu RV, Itzykson R*, et al.* Predictive factors of response and survival among chronic myelomonocytic leukemia patients treated with azacitidine. *Leuk Res* 2013 Jun; **37**(6)**:** 609-613.

124. Kantarjian HM, O'Brien S, Cortes J, Giles FJ, Faderl S, Issa JP*, et al.* Results of decitabine (5-Aza-2 ' deoxycytidine) therapy in 130 patients with chronic myelogenous leukemia. *Cancer* 2003 Aug 1; **98**(3)**:** 522-528.

125. Tong XZ, Li J, Zhou ZH, Zheng D, Liu JR, Su C. Efficacy and side-effects of decitabine in treatment of atypical chronic myeloid leukemia. *Leukemia & lymphoma* 2015 Jun; **56**(6)**:** 1911-1913.

126. Mao L, You L, Yang M, Li Y, Ye X, Tong H. The First Case of Decitabine Successfully in Treatment of Atypical Chronic

Myeloid Leukemia with CEBPA Double Mutation. *Chemotherapy* 2013 Jul 11; **2:** 114.

127. Jiang HF, Wu ZL, Ren L, Tao DH, Tong HY. Decitabine for the treatment of atypical chronic myeloid leukemia: A report of two cases. *Oncol Lett* 2016 Jan; **11**(1)**:** 689-692.

128. Patnaik MM, Tefferi A. Chronic myelomonocytic leukemia: 2016 update on diagnosis, risk stratification, and management. *American Journal of Hematology* 2016 Jun; **91**(6)**:** 632-642.

129. Lierman E, Selleslag D, Smits S, Billiet J, Vandenberghe P. Ruxolitinib inhibits transforming JAK2 fusion proteins in vitro and induces complete cytogenetic remission in t(8;9)(p22;p24)/PCM1-JAK2-positive chronic eosinophilic leukemia. *Blood* 2012 Aug 16; **120**(7)**:** 1529-1531.

130. Schwaab J, Knut M, Haferlach C, Metzgeroth G, Horny HP, Chase A*, et al.* Limited duration of complete remission on ruxolitinib in myeloid neoplasms with PCM1-JAK2 and BCR-JAK2 fusion genes. *Annals of hematology* 2015 Feb; **94**(2)**:** 233-238.

131. Rumi E, Milosevic JD, Selleslag D, Casetti I, Lierman E, Pietra D*, et al.* Efficacy of ruxolitinib in myeloid neoplasms with PCM1-JAK2 fusion gene. *Annals of hematology* 2015 Nov; **94**(11)**:** 1927-1928.

132. Maxson JE, Gotlib J, Pollyea DA, Fleischman AG, Agarwal A, Eide CA*, et al.* Oncogenic CSF3R Mutations in Chronic Neutrophilic Leukemia and Atypical CML. *New Engl J Med* 2013 May 9; **368**(19)**:** 1781-1790.

133. Ammatuna E, Eefting M, van Lom K, Kavelaars FG, Valk PJM, Touw IP. Atypical chronic myeloid leukemia with concomitant CSF3R T618I and SETBP1 mutations unresponsive to the JAK inhibitor ruxolitinib. *Annals of hematology* 2015 May; **94**(5)**:** 879-880.

134. Khanna V, Pierce ST, Dao KH, Tognon CE, Hunt DE, Junio B*, et al.* Durable Disease Control with MEK Inhibition in a

Patient with NRAS-mutated Atypical Chronic Myeloid Leukemia. *Cureus* 2015 Dec 17; **7**(12)**:** e414.

135. Hoischen A, van Bon BW, Gilissen C, Arts P, van Lier B, Steehouwer M*, et al.* De novo mutations of SETBP1 cause Schinzel-Giedion syndrome. *Nat Genet* 2010 Jun; **42**(6)**:** 483-485.

136. Ko JM, Lim BC, Kim KJ, Hwang YS, Ryu HW, Lee JH*, et al.* Distinct neurological features in a patient with Schinzel-Giedion syndrome caused by a recurrent SETBP1 mutation. *Child's nervous system : ChNS : official journal of the International Society for Pediatric Neurosurgery* 2013 Apr; **29**(4)**:** 525-529.

137. Chen M, Yao H, Chen S, Wang Q, Wen L, Xie J*, et al.* Rare occurrence of SET binding protein 1 mutation in patients with acute lymphoblastic leukemia, mixed phenotype acute leukemia and chronic myeloid leukemia in blast crisis. *Leukemia & lymphoma* 2014 Sep; **55**(9)**:** 2209-2210.

138. Minakuchi M, Kakazu N, Gorrin-Rivas MJ, Abe T, Copeland TD, Ueda K*, et al.* Identification and characterization of SEB, a novel protein that binds to the acute undifferentiated leukemia-associated protein SET. *Eur J Biochem* 2001 Mar; **268**(5)**:** 1340-1351.

139. Janssens V, Goris J. Protein phosphatase 2A: a highly regulated family of serine/threonine phosphatases implicated in cell growth and signalling. *Biochemical Journal* 2001 Feb 1; **353:** 417-439.

140. Wang GL, Iakova P, Wilde M, Awad S, Timchenko NA. Liver tumors escape negative control of proliferation via PI3K/Akt-mediated block of C/EBP alpha growth inhibitory activity. *Gene Dev* 2004 Apr 15; **18**(8)**:** 912-925.

141. Kawabe T, Muslin AJ, Korsmeyer SJ. HOX11 interacts with protein phosphatases PP2A and PP1 and disrupts a G2/M cell-cycle checkpoint. *Nature* 1997 Jan 30; **385**(6615)**:** 454-458.

142. Mumby M. PP2A: Unveiling a reluctant tumor suppressor. *Cell* 2007 Jul 13; **130**(1)**:** 21-24.

143. Westermarck J, Hahn WC. Multiple pathways regulated by the tumor suppressor PP2A in transformation. *Trends Mol Med* 2008 Apr; **14**(4)**:** 152-160.

144. Janssens V, Goris J, Van Hoof C. PP2A: the expected tumor suppressor. *Curr Opin Genet Dev* 2005 Feb; **15**(1)**:** 34-41.

145. Schönthal AH. Role of serine/threonine protein phosphatase 2A in cancer. *Cancer Lett* 2001 Sep 10; **170**(1)**:** 1-13.

146. Cristobal I, Garcia-Orti L, Cirauqui C, Alonso MM, Calasanz MJ, Odero MD. PP2A impaired activity is a common event in acute myeloid leukemia and its activation by forskolin has a potent anti-leukemic effect. *Leukemia* 2011 Apr; **25**(4)**:** 606-614.

147. Arnold HK, Sears RC. A tumor suppressor role for PP2A-B56 alpha through negative regulation of c-Myc and other key oncoproteins. *Cancer Metast Rev* 2008 Jun; **27**(2)**:** 147-158.

148. Sablina AA, Hahn WC. The Role of PP2A A Subunits in Tumor Suppression. *Cell Adhes Migr* 2007 Jul-Sep; **1**(3)**:** 140-141.

149. Cristobal I, Blanco FJ, Garcia-Orti L, Marcotegui N, Vicente C, Rifon J*, et al.* SETBP1 overexpression is a novel leukemogenic mechanism that predicts adverse outcome in elderly patients with acute myeloid leukemia. *Blood* 2010 Jan 21; **115**(3)**:** 615-625.

150. Piazza R, Magistroni V, Redaelli S, Mauri M, Massimino L, Sessa A*, et al.* SETBP1 induces transcription of a network of development genes by acting as an epigenetic hub. *Nature Communications* 2018 Jun 6; **9**(1)**:** 2192.

151. Kataoka K, Kurokawa M. Ecotropic viral integration site 1, stem cell self-renewal and leukemogenesis. *Cancer Sci* 2012 Aug; **103**(8)**:** 1371-1377.

152. Oakley K, Han YF, Vishwakarma BA, Chu S, Bhatia R, Gudmundsson KO*, et al.* Setbp1 promotes the self-renewal of murine myeloid progenitors via activation of Hoxa9 and Hoxa10. *Blood* 2012 Jun 21; **119**(25)**:** 6099-6108.

153. Vishwakarma BA, Nguyen N, Makishima H, Hosono N, Gudmundsson KO, Negi V*, et al.* Runx1 repression by histone deacetylation is critical for Setbp1-induced mouse myeloid leukemia development. *Leukemia* 2016 Jan; **30**(1)**:** 200-208.

154. Ichikawa M, Asai T, Saito T, Seo S, Yamazaki I, Yamagata T*, et al.* AML-1 is required for megakaryocytic maturation and lymphocytic differentiation, but not for maintenance of hematopoietic stem cells in adult hematopoiesis. *Nat Med* 2004 Mar; **10**(3)**:** 299-304.

155. Growney JD, Shigematsu H, Li Z, Lee BH, Adeisperger J, Rowan R*, et al.* Loss of Runx1 perturbs adult hematopoiesis and is associated with a myeloproliferative phenotype. *Blood* 2005 Jul 15; **106**(2)**:** 494-504.

156. Lykidis A, Wang J, Karim MA, Jackowski S. Overexpression of a mammalian ethanolamine-specific kinase accelerates the CDP-ethanolamine pathway. *The Journal of biological chemistry* 2001 Jan 19; **276**(3)**:** 2174-2179.

157. Kennedy EP, Weiss SB. The function of cytidine coenzymes in the biosynthesis of phospholipides. *The Journal of biological chemistry* 1956 Sep; **222**(1)**:** 193-214.

158. Simossis VA, Kleinjung J, Heringa J. Homology-extended sequence alignment. *Nucleic acids research* 2005 Feb 7; **33**(3)**:** 816-824.

159. Behjati S, Tarpey PS, Sheldon H, Martincorena I, Van Loo P, Gundem G*, et al.* Recurrent PTPRB and PLCG1 mutations in angiosarcoma. *Nat Genet* 2014 Apr; **46**(4)**:** 376-379.

160. Behjati S, Tarpey PS, Presneau N, Scheipl S, Pillay N, Van Loo P*, et al.* Distinct H3F3A and H3F3B driver mutations

define chondroblastoma and giant cell tumor of bone. *Nat Genet* 2013 Dec; **45**(12)**:** 1479-1482.

161. Tarpey PS, Behjati S, Cooke SL, Van Loo P, Wedge DC, Pillay N*, et al.* Frequent mutation of the major cartilage collagen gene COL2A1 in chondrosarcoma. *Nat Genet* 2013 Aug; **45**(8)**:** 923-926.

162. Bolli N, Avet-Loiseau H, Wedge DC, Van Loo P, Alexandrov LB, Martincorena I*, et al.* Heterogeneity of genomic evolution and mutational profiles in multiple myeloma. *Nat Commun* 2014; **5**(2997).

163. Papaemmanuil E, Rapado I, Li Y, Potter NE, Wedge DC, Tubio J*, et al.* RAG-mediated recombination is the predominant driver of oncogenic rearrangement in ETV6-RUNX1 acute lymphoblastic leukemia. *Nat Genet* 2014 Feb; **46**(2)**:** 116-125.

164. Stephens PJ, Tarpey PS, Davies H, Van Loo P, Greenman C, Wedge DC*, et al.* The landscape of cancer genes and mutational processes in breast cancer. *Nature* 2012 May 16; **486**(7403)**:** 400-404.

165. Varela I, Tarpey P, Raine K, Huang D, Ong CK, Stephens P*, et al.* Exome sequencing identifies frequent mutation of the SWI/SNF complex gene PBRM1 in renal carcinoma. *Nature* 2011 Jan 27; **469**(7331)**:** 539-542.

166. Tian Y, Jackson P, Gunter C, Wang J, Rock CO, Jackowski S. Placental thrombosis and spontaneous fetal death in mice deficient in ethanolamine kinase 2. *The Journal of biological chemistry* 2006 Sep 22; **281**(38)**:** 28438-28449.

167. Vance JE. Phospholipid synthesis and transport in mammalian cells. *Traffic* 2015 Jan; **16**(1)**:** 1-18.

168. Borkenhagen LF, Kennedy EP, Fielding L. Enzymatic formation and decarboxylation of phosphatidylserine. *J Biol Chem* 1961 Jun 1; **236** 28–32.

169. Podo F. Tumour phospholipid metabolism. *NMR in biomedicine* 1999 Nov; **12**(7)**:** 413-439.

170. Vance JE. Historical perspective: phosphatidylserine and phosphatidylethanolamine from the 1800s to the present. *Journal of lipid research* 2018 Jun; **59**(6)**:** 923-944.

171. Dawaliby R, Trubbia C, Delporte C, Noyon C, Ruysschaert JM, Van Antwerpen P*, et al.* Phosphatidylethanolamine Is a Key Regulator of Membrane Fluidity in Eukaryotic Cells. *Journal of Biological Chemistry* 2016 Feb 12; **291**(7)**:** 3658-3667.

172. Birner R, Burgermeister M, Schneiter R, Daum G. Roles of phosphatidylethanolamine and of its several biosynthetic pathways in Saccharomyces cerevisiae. *Mol Biol Cell* 2001 Apr; **12**(4)**:** 997-1007.

173. Mileykovskaya E, Dowhan W. Role of membrane lipids in bacterial division-site selection. *Curr Opin Microbiol* 2005 Apr; **8**(2)**:** 135-142.

174. Dill KA, Stigter D. Lateral interactions among phosphatidylcholine and phosphatidylethanolamine head groups in phospholipid monolayers and bilayers. *Biochemistry* 1988 May 3; **27**(9)**:** 3446-3453.

175. van den Brink-van der Laan E, Killian JA, de Kruijff B. Nonbilayer lipids affect peripheral and integral membrane proteins via changes in the lateral pressure profile. *Biochimica et biophysica acta* 2004 Nov 3; **1666**(1-2)**:** 275-288.

176. Siegel DP, Epand RM. The mechanism of lamellar-to-inverted hexagonal phase transitions in phosphatidylethanolamine: implications for membrane fusion mechanisms. *Biophysical journal* 1997 Dec; **73**(6)**:** 3089-3111.

177. Storey MK, Clay KL, Kutateladze T, Murphy RC, Overduin M, Voelker DR. Phosphatidylethanolamine has an essential role in Saccharomyces cerevisiae that is independent of its

ability to form hexagonal phase structures. *The Journal of biological chemistry* 2001 Dec 21; **276**(51)**:** 48539-48548.

178. Epand RM. Lipid polymorphism and protein-lipid interactions. *Biochimica et biophysica acta* 1998 Nov 10; **1376**(3)**:** 353-368.

179. Cullis PR, De Kruijff B. Polymorphic phase behaviour of lipid mixtures as detected by 31P NMR. Evidence that cholesterol may destabilize bilayer structure in membrane systems containing phosphatidylethanolamine. *Biochimica et biophysica acta* 1978 Feb 21; **507**(2)**:** 207-218.

180. Martens S, McMahon HT. Mechanisms of membrane fusion: disparate players and common principles. *Nature reviews Molecular cell biology* 2008 Jul; **9**(7)**:** 543-556.

181. Emoto K, Kobayashi T, Yamaji A, Aizawa H, Yahara I, Inoue K*, et al.* Redistribution of phosphatidylethanolamine at the cleavage furrow of dividing cells during cytokinesis. *Proc Natl Acad Sci U S A* 1996 Nov 12; **93**(23)**:** 12867-12872.

182. Emoto K, Umeda M. An essential role for a membrane lipid in cytokinesis. Regulation of contractile ring disassembly by redistribution of phosphatidylethanolamine. *J Cell Biol* 2000 Jun 12; **149**(6)**:** 1215-1224.

183. Signorell A, Gluenz E, Rettig J, Schneider A, Shaw MK, Gull K*, et al.* Perturbation of phosphatidylethanolamine synthesis affects mitochondrial morphology and cell-cycle progression in procyclic-form Trypanosoma brucei. *Molecular microbiology* 2009 May; **72**(4)**:** 1068-1079.

184. Pécheur EI, Martin I, Maier O, Bakowsky U, Ruysschaert JM, Hoekstra D. Phospholipid species act as modulators in p97/p47-mediated fusion of Golgi membranes. *Biochemistry* 2002 Aug 6; **41**(31)**:** 9813-9823.

185. Horvath SE, Bottinger L, Vogtle FN, Wiedemann N, Meisinger C, Becker T*, et al.* Processing and topology of the yeast mitochondrial phosphatidylserine decarboxylase 1. *The*

Journal of biological chemistry 2012 Oct 26; **287**(44)**:** 36744-36755.

186. Böttinger L, Horvath SE, Kleinschroth T, Hunte C, Daum G, Pfanner N*, et al.* Phosphatidylethanolamine and cardiolipin differentially affect the stability of mitochondrial respiratory chain supercomplexes. *J Mol Biol* 2012 Nov 9; **423**(5)**:** 677-686.

187. Parsons DF, Williams GR, Chance B. Characteristics of isolated and purified preparations of the outer and inner membranes of mitochondria. *Annals of the New York Academy of Sciences* 1966 Jul 14; **137**(2)**:** 643-666.

188. Frey TG, Mannella CA. The internal structure of mitochondria. *Trends in biochemical sciences* 2000 Jul; **25**(7)**:** 319-324.

189. Tasseva G, Bai HD, Davidescu M, Haromy A, Michelakis E, Vance JE. Phosphatidylethanolamine deficiency in Mammalian mitochondria impairs oxidative phosphorylation and alters mitochondrial morphology. *The Journal of biological chemistry* 2013 Feb 8; **288**(6)**:** 4158-4173.

190. Steenbergen R, Nanowski TS, Beigneux A, Kulinski A, Young SG, Vance JE. Disruption of the phosphatidylserine decarboxylase gene in mice causes embryonic lethality and mitochondrial defects. *The Journal of biological chemistry* 2005 Dec 2; **280**(48)**:** 40032-40040.

191. Paulick MG, Bertozzi CR. The glycosylphosphatidylinositol anchor: a complex membrane-anchoring structure for proteins. *Biochemistry* 2008 Jul 8; **47**(27)**:** 6991-7000.

192. Arruda MSPd, Correa MA, Venturini J, Félix MC, Rosis AMBD, Galhiane MS*, et al.* The effect of phosphoethanolamine intake on mortality and macrophage activity in mice with solid ehrlich tumors. *Brazilian Archives of Biology and Technology* 2011; **54:** 1203-1210.

193. Ferreira AK, Meneguelo R, Neto SC, Chierice GO, Maria DA. Synthetic Phosphoethanolamine Induces Apoptosis Through Caspase-3 Pathway by Decreasing Expression of Bax/Bad Protein and Changes Cell Cycle in Melanoma. *J Cancer Sci Ther* 2011; **3:** 053-059.

194. Ferreira AK, Meneguelo R, Pereira A, Filho OMR, Chierice GO, Maria DA. Anticancer Effects of Synthetic Phosphoethanolamine on Ehrlich Ascites Tumor: An Experimental Study. *Anticancer Res* 2012 Jan; **32**(1)**:** 95-104.

195. Ferreira AK, Meneguelo R, Marques FLN, Radin A, Filho OMR, Neto SC*, et al.* Synthetic phosphoethanolamine a precursor of membrane phospholipids reduce tumor growth in mice bearing melanoma B16-F10 and in vitro induce apoptosis and arrest in G2/M phase. *Biomed Pharmacother* 2012 Oct; **66**(7)**:** 541-548.

196. Ferreira AK, Meneguelo R, Pereira A, Filho OMR, Chierice GO, Maria DA. Synthetic phosphoethanolamine induces cell cycle arrest and apoptosis in human breast cancer MCF-7 cells through the mitochondrial pathway. *Biomed Pharmacother* 2013 Jul; **67**(6)**:** 481-487.

197. Ferreira AK, Freitas VM, Levy D, Ruiz JLM, Bydlowski SP, Rici REG*, et al.* Anti-Angiogenic and Anti-Metastatic Activity of Synthetic Phosphoethanolamine. *Plos One* 2013 Mar 14; **8**(3).

198. Ferreira AK, Santana-Lemos BAA, Rego EM, Filho OMR, Chierice GO, Maria DA. Synthetic phosphoethanolamine has in vitro and in vivo anti-leukemia effects. *Brit J Cancer* 2013 Nov 26; **109**(11)**:** 2819-2828.

199. Gordon LI, Weiss D, Prachand S, Weitzman SA. Scavenging of superoxide anion by phosphorylethanolamine: studies in human neutrophils and in a cell free system. *Free radical research communications* 1991; **15**(1)**:** 65-71.

200. Mambelli LI, Teixeira SF, Jorge SD, Kawamura B, Meneguelo R, Barbuto JAM*, et al.* Phosphoethanolamine induces caspase-

independent cell death by reducing the expression of C-RAF and inhibits tumor growth in human melanoma model. *Biomed Pharmacother* 2018 Jul; **103:** 18-28.

201. Kano-Sueoka T, Cohen DM, Yamaizumi Z, Nishimura S, Mori M, Fujiki H. Phosphoethanolamine as a growth factor of a mammary carcinoma cell line of rat. *Proceedings of the National Academy of Sciences of the United States of America* 1979 Nov; **76**(11)**:** 5741-5744.

202. Anastacio LD, Delmaschio CR, Oliveira DA, Chequer FMD. Synthetic phosphoethanolamine: the state of the art of scientific production. *Braz J Pharm Sci* 2017; **53**(4).

203. Paumgartten FJR. Ethical issues on the "synthetic" phosphoethanolamine clinical trial. *Rev Assoc Med Bras* 2017 May; **63**(5)**:** 388-392.

204. Oliveira Caetano NA, Cavajes Moreira T, Ugrinovich LA, do Carmo TA, Ucelli Simioni P. Synthetic phosphoethanolamine as an inhibitor of tumor progression. *A pesquisa com a fosfoetanolamina sintética como inibidor da progressão de tumores* 2017; **19**(3)**:** 111-116.

205. Paumgartten FJR. Phosphoethanolamine: anticancer pill bandwagon effect. *Cadernos de Saúde Pública* 2016; **32**.

206. Ponde N, de Azambuja E, Ades F. Phosphoethanolamine and the danger of unproven drugs. *Ecancermedicalscience* 2016; **10:** 681.

207. Rego JF, Lopes G, Riechelmann RP, Sternberg C, Ferrari C, Fernandes G. A "miracle" cancer drug in the era of social media: A survey of Brazilian oncologists' opinions and experience with phosphoethanolamine. *Rev Assoc Med Bras (1992)* 2017 Jan 1; **63**(1)**:** 70-77.

208. Fernandes GdS, Jr GdLL. More Convoluted Than a Brazilian Soap Opera: How an Eager Chemistry Professor and a Well-Intended but Misguided Federal Judge Ignited an Industry of False Hopes. *Journal of Global Oncology* 2016; **2**(4)**:** 167-168.

209. Ledford H. Brazilian courts tussle over unproven cancer treatment. *Nature* 2015 Nov **527:** 420-421.

210. Escobar H. Brazil president signs law legalizing renegade cancer pill. *Science* 2016 Apr.

211. Centro de Inovação e Ensaios Pré-Clínicos. Avaliação da possível atividade antitumoral da fosfoetanolamina (UNICAMP) em modelo de tumor xenográfico de melanoma humano em camundongos. *Florianópolis: CIEnP* 2016.

212. Moraes Filho MO. Avaliação da possível atividade anticâncer da fosfoetanolamina sintética (FS) nosarcoma 18: laudo técnico do estudo da fosfaetanolamina sintética. *Fortaleza: Universidade Federal do Ceará/Faculdade de Medicina/Núcleo de Pesquisa e Desenvolvimento de Medicamentos/Laboratório de Oncologia Experimental* 2016.

213. São Paulo. Secretaria de Estado da Saúde. Avaliação da eficácia da fosfoetanolamina sintética em pacientes com tumores sólidos avançados. 2016.

214. Núcleo de Divulgação Científica da USP. Estudo no Icesp sugere que fosfoetanolamina não é eficiente contra o câncer. *J USP* 2017.

215. Sociedade Brasileira de Oncologia Clínica. Estudo sobre fosfoetanolamina é suspenso por não constatar benefício. 2017.

216. Henle J. Allgemeine Anatomie: Lehre von den Mischungs- und Formbestandtheilen des menschlichen Körpers. *Sömmering, Samuel Thomas von Vom Baue des menschlichen Körpers* 1841; **6**.

217. Benda C. Ueber die Spermatogenese der Vertebraten und höherer Evertebraten, II Theil: die Histiogenese der Spermien. *Arch Anal Physiol* 1898; **73:** 393-398.

218. Kingsbury BF. Cytoplasmic fixation. *Anat Rec* 1912; **6:** 39-52.

219. Lewis MR, Lewis WH. Mitochondria (and other cytoplasmic structures) in tissue cultures. *Am J Anat* 1915; **17:** 339-401.

220. Bereiter-Hahn J, Voth M. Dynamics of mitochondria in living cells: shape changes, dislocations, fusion, and fission of mitochondria. *Microscopy research and technique* 1994 Feb 15; **27**(3)**:** 198-219.

221. Bereiter-Hahn J, Jendrach M. Mitochondrial dynamics. *International review of cell and molecular biology* 2010; **284:** 1-65.

222. Grivell LA. Mitochondrial DNA. *Scientific American* 1983 Mar; **248**(3)**:** 78-89.

223. Berg OG, Kurland CG. Why mitochondrial genes are most often found in nuclei. *Molecular biology and evolution* 2000 Jun; **17**(6)**:** 951-961.

224. Searcy DG. Metabolic integration during the evolutionary origin of mitochondria. *Cell research* 2003 Aug; **13**(4)**:** 229-238.

225. Youle RJ, van der Bliek AM. Mitochondrial fission, fusion, and stress. *Science* 2012 Aug 31; **337**(6098)**:** 1062-1065.

226. Kennedy EP, Lehninger AL. Oxidation of fatty acids and tricarboxylic acid cycle intermediates by isolated rat liver mitochondria. *The Journal of biological chemistry* 1949 Jun; **179**(2)**:** 957-972.

227. Siekevitz P. Powerhouse of the Cell. *Scientific American* 1957; **197**(1)**:** 131-144.

228. Scheffler IE. Mitochondria, Second Edition. *Wiley-Liss A John Wiley & Sons, Inc, Publication* 2007.

229. Palade GE. An electron microscope study of the mitochondrial structure. *The journal of histochemistry and cytochemistry :*

official journal of the Histochemistry Society 1953 Jul; **1**(4)**:** 188-211.

230. Wallace DC. Mitochondrial genetics: a paradigm for aging and degenerative diseases? *Science* 1992 May 1; **256**(5057)**:** 628-632.

231. Wojtovich AP, Smith CO, Haynes CM, Nehrke KW, Brookes PS. Physiological consequences of complex II inhibition for aging, disease, and the mKATP channel. *Biochimica et biophysica acta* 2013 May; **1827**(5)**:** 598-611.

232. Paz ML, Gonzalez Maglio DH, Weill FS, Bustamante J, Leoni J. Mitochondrial dysfunction and cellular stress progression after ultraviolet B irradiation in human keratinocytes. *Photodermatology, photoimmunology & photomedicine* 2008 Jun; **24**(3)**:** 115-122.

233. Elston T, Wang H, Oster G. Energy transduction in ATP synthase. *Nature* 1998 Jan 29; **391**(6666)**:** 510-513.

234. Birch-Machin MA. The role of mitochondria in ageing and carcinogenesis. *Clinical and experimental dermatology* 2006 Jul; **31**(4)**:** 548-552.

235. Tulah AS, Birch-Machin MA. Stressed out mitochondria: the role of mitochondria in ageing and cancer focussing on strategies and opportunities in human skin. *Mitochondrion* 2013 Sep; **13**(5)**:** 444-453.

236. Lenaz G, Fato R, Genova ML, Bergamini C, Bianchi C, Biondi A. Mitochondrial Complex I: structural and functional aspects. *Biochimica et biophysica acta* 2006 Sep-Oct; **1757**(9-10)**:** 1406-1420.

237. Rutter J, Winge DR, Schiffman JD. Succinate dehydrogenase - Assembly, regulation and role in human disease. *Mitochondrion* 2010 Jun; **10**(4)**:** 393-401.

238. Sun F, Huo X, Zhai Y, Wang A, Xu J, Su D*, et al.* Crystal structure of mitochondrial respiratory membrane protein complex II. *Cell* 2005 Jul 1; **121**(7)**:** 1043-1057.

239. Spaar A, Flock D, Helms V. Association of cytochrome c with membrane-bound cytochrome c oxidase proceeds parallel to the membrane rather than in bulk solution. *Biophysical journal* 2009 Mar 4; **96**(5)**:** 1721-1732.

240. Matsuno-Yagi A, Hatefi Y. Ubiquinol:cytochrome c oxidoreductase (complex III). Effect of inhibitors on cytochrome b reduction in submitochondrial particles and the role of ubiquinone in complex III. *The Journal of biological chemistry* 2001 Jun 1; **276**(22)**:** 19006-19011.

241. Li Y, Park JS, Deng JH, Bai Y. Cytochrome c oxidase subunit IV is essential for assembly and respiratory function of the enzyme complex. *J Bioenerg Biomembr* 2006 Dec; **38**(5-6)**:** 283-291.

242. Dimroth P, Kaim G, Matthey U. Crucial role of the membrane potential for ATP synthesis by F1Fo ATP synthases. *J Exp Biol* 2000 Jan; **203**(1)**:** 51-59.

243. Cadenas E, Boveris A, Ragan CI, Stoppani AO. Production of superoxide radicals and hydrogen peroxide by NADH-ubiquinone reductase and ubiquinol-cytochrome c reductase from beef-heart mitochondria. *Arch Biochem Biophys* 1977 Apr 30; **180**(2)**:** 248-257.

244. Turrens JF, Alexandre A, Lehninger AL. Ubisemiquinone is the electron donor for superoxide formation by complex III of heart mitochondria. *Arch Biochem Biophys* 1985 Mar; **237**(2)**:** 408-414.

245. Hirst J, King MS, Pryde KR. The production of reactive oxygen species by complex I. *Biochemical Society transactions* 2008 Oct; **36**(Pt 5)**:** 976-980.

246. Murphy MP. How mitochondria produce reactive oxygen species. *Biochem J* 2009 Jan 1; **417**(1)**:** 1-13.

247. Bleier L, Drose S. Superoxide generation by complex III: from mechanistic rationales to functional consequences. *Biochimica et biophysica acta* 2013 Nov-Dec; **1827**(11-12)**:** 1320-1331.

248. Brand MD, Buckingham JA, Esteves TC, Green K, Lambert AJ, Miwa S*, et al.* Mitochondrial superoxide and aging: uncoupling-protein activity and superoxide production. *Biochemical Society symposium* 2004; (71)**:** 203-213.

249. Cecarini V, Gee J, Fioretti E, Amici M, Angeletti M, Eleuteri AM*, et al.* Protein oxidation and cellular homeostasis: Emphasis on metabolism. *Biochimica et biophysica acta* 2007 Feb; **1773**(2)**:** 93-104.

250. Krishnan KJ, Greaves LC, Reeve AK, Turnbull D. The ageing mitochondrial genome. *Nucleic acids research* 2007 Oct; **35**(22)**:** 7399-7405.

251. Guo J, Lemire BD. The ubiquinone-binding site of the Saccharomyces cerevisiae succinate-ubiquinone oxidoreductase is a source of superoxide. *The Journal of biological chemistry* 2003 Nov 28; **278**(48)**:** 47629-47635.

252. Lemarie A, Huc L, Pazarentzos E, Mahul-Mellier AL, Grimm S. Specific disintegration of complex II succinate:ubiquinone oxidoreductase links pH changes to oxidative stress for apoptosis induction. *Cell death and differentiation* 2011 Feb; **18**(2)**:** 338-349.

253. Quinlan CL, Orr AL, Perevoshchikova IV, Treberg JR, Ackrell BA, Brand MD. Mitochondrial complex II can generate reactive oxygen species at high rates in both the forward and reverse reactions. *The Journal of biological chemistry* 2012 Aug; **287**(32)**:** 27255-27264.

254. Ralph SJ, Moreno-Sánchez R, Neuzil J, Rodríguez-Enríquez S. Inhibitors of succinate: quinone reductase/Complex II regulate production of mitochondrial reactive oxygen species and protect normal cells from ischemic damage but induce specific cancer cell death. *Pharm Res* 2011 Nov; **28**(11)**:** 2695-2730.

255. Moreno-Sánchez R, Hernández-Esquivel L, Rivero-Segura NA, Marín-Hernández A, Neuzil J, Ralph SJ*, et al.* Reactive oxygen species are generated by the respiratory complex II--evidence for lack of contribution of the reverse electron flow in complex I. *FEBS J* 2013 Feb; **280**(3)**:** 927-938.

256. Hogg N, Darley-Usmar VM, Wilson MT, Moncada S. Production of hydroxyl radicals from the simultaneous generation of superoxide and nitric oxide. *Biochem J* 1992 Jan 15; **281** (Pt 2)**:** 419-424.

257. Turrens JF. Mitochondrial formation of reactive oxygen species. *J Physiol* 2003 Oct 15; **552**(Pt 2)**:** 335-344.

258. Imlay JA, Chin SM, Linn S. Toxic DNA damage by hydrogen peroxide through the Fenton reaction in vivo and in vitro. *Science* 1988 Apr 29; **240**(4852)**:** 640-642.

259. Maynard S, Schurman SH, Harboe C, de Souza-Pinto NC, Bohr VA. Base excision repair of oxidative DNA damage and association with cancer and aging. *Carcinogenesis* 2009 Jan; **30**(1)**:** 2-10.

260. Wiseman H, Halliwell B. Damage to DNA by reactive oxygen and nitrogen species: Role in inflammatory disease and progression to cancer. *Biochemical Journal* 1996 Jan 1; **313:** 17-29.

261. Ray PD, Huang BW, Tsuji Y. Reactive oxygen species (ROS) homeostasis and redox regulation in cellular signaling. *Cell Signal* 2012 May; **24**(5)**:** 981-990.

262. Liou GY, Storz P. Reactive oxygen species in cancer. *Free Radic Res* 2010 May; **44**(5)**:** 479-496.

263. de Sá Junior PL, Câmara DAD, Porcacchia AS, Fonseca PMM, Jorge SD, Araldi RP*, et al.* The Roles of ROS in Cancer Heterogeneity and Therapy. *Oxid Med Cell Longev* 2017 Oct 16; **2017:** 2467940.

264. Sabharwal SS, Schumacker PT. Mitochondrial ROS in cancer: initiators, amplifiers or an Achilles' heel? *Nat Rev Cancer* 2014 Nov; **14**(11)**:** 709-721.

265. Wallace DC. Mitochondria and cancer. *Nat Rev Cancer* 2012 Oct; **12**(10)**:** 685-698.

266. Fruehauf JP, Meyskens FL. Reactive oxygen species: a breath of life or death? *Clin Cancer Res* 2007 Feb 1; **13**(3)**:** 789-794.

267. Efrati E, Tocco G, Eritja R, Wilson SH, Goodman MF. "Action-at-a-distance" mutagenesis. 8-oxo-7, 8-dihydro-2'-deoxyguanosine causes base substitution errors at neighboring template sites when copied by DNA polymerase beta. *The Journal of biological chemistry* 1999 May 28; **274**(22)**:** 15920-15926.

268. Warburg O, Wind F, Negelein E. The Metabolism of Tumors in the Body. *The Journal of general physiology* 1927 Mar 7; **8**(6)**:** 519-530.

269. Marin D, Sabater B. The cancer Warburg effect may be a testable example of the minimum entropy production rate principle. *Phys Biol* 2017 Apr; **14**(2).

270. Jiang P, Du WJ, Wu MA. Regulation of the pentose phosphate pathway in cancer. *Protein Cell* 2014 Aug; **5**(8)**:** 592-602.

271. Kamarajugadda S, Cai Q, Chen H, Nayak S, Zhu J, He M*, et al.* Manganese superoxide dismutase promotes anoikis resistance and tumor metastasis. *Cell death & disease* 2013 Feb; **4:** e504.

272. Mandujano-Tinoco EA, Gallardo-Perez JC, Marin-Hernandez A, Moreno-Sanchez R, Rodriguez-Enriquez S. Anti-mitochondrial therapy in human breast cancer multi-cellular spheroids. *Bba-Mol Cell Res* 2013 Mar; **1833**(3)**:** 541-551.

273. Bonuccelli G, Whitaker-Menezes D, Castello-Cros R, Pavlides S, Pestell RG, Fatatis A*, et al.* The reverse Warburg effect Glycolysis inhibitors prevent the tumor promoting effects of

caveolin-1 deficient cancer associated fibroblasts. *Cell Cycle* 2010 May 15; **9**(10)**:** 1960-1971.

274. Pavlides S, Whitaker-Menezes D, Castello-Cros R, Flomenberg N, Witkiewicz AK, Frank PG*, et al.* The reverse Warburg effect Aerobic glycolysis in cancer associated fibroblasts and the tumor stroma. *Cell Cycle* 2009 Dec 1; **8**(23)**:** 3984-4001.

275. Samper E, Morgado L, Estrada JC, Bernad A, Hubbard A, Cadenas S*, et al.* Increase in mitochondrial biogenesis, oxidative stress, and glycolysis in murine lymphomas. *Free Radical Bio Med* 2009 Feb 1; **46**(3)**:** 387-396.

276. Skrtic M, Sriskanthadevan S, Jhas B, Gebbia M, Wang X, Wang Z*, et al.* Inhibition of Mitochondrial Translation as a Therapeutic Strategy for Human Acute Myeloid Leukemia. *Cancer Cell* 2011 Nov 15; **20**(5)**:** 674-688.

277. Lagadinou ED, Sach A, Callahan K, Rossi RM, Neering SJ, Minhajuddin M*, et al.* BCL-2 inhibition targets oxidative phosphorylation and selectively eradicates quiescent human leukemia stem cells. *Cell stem cell* 2013 Mar 7; **12**(3)**:** 329-341.

278. Yu M, Li RS, Zhang J. Repositioning of antibiotic levofloxacin as a mitochondrial biogenesis inhibitor to target breast cancer. *Biochem Bioph Res Co* 2016 Mar 18; **471**(4)**:** 639-645.

279. Fulda S, Galluzzi L, Kroemer G. Targeting mitochondria for cancer therapy. *Nat Rev Drug Discov* 2010 Jun; **9**(6)**:** 447-464.

280. Yun J, Mullarky E, Lu CY, Bosch KN, Kavalier A, Rivera K*, et al.* Vitamin C selectively kills KRAS and BRAF mutant colorectal cancer cells by targeting GAPDH. *Science* 2015 Dec 11; **350**(6266)**:** 1391-1396.

281. Andrzejewski S, Gravel SP, Pollak M, St-Pierre J. Metformin directly acts on mitochondria to alter cellular bioenergetics. *Cancer & metabolism* 2014; **2:** 12.

282. Xu Z, Yan Y, Li Z, Qian L, Gong Z. The Antibiotic Drug Tigecycline: A Focus on its Promising Anticancer Properties. *Frontiers in pharmacology* 2016; **7:** 473.

283. Livermore DM. Tigecycline: what is it, and where should it be used? *The Journal of antimicrobial chemotherapy* 2005 Oct; **56**(4)**:** 611-614.

284. Stein GE, Craig WA. Tigecycline: a critical analysis. *Clinical infectious diseases : an official publication of the Infectious Diseases Society of America* 2006 Aug 15; **43**(4)**:** 518-524.

285. Kaewpoowat Q, Ostrosky-Zeichner L. Tigecycline : a critical safety review. *Expert opinion on drug safety* 2015 Feb; **14**(2)**:** 335-342.

286. Sader HS, Castanheira M, Farrell DJ, Flamm RK, Mendes RE, Jones RN. Tigecycline antimicrobial activity tested against clinical bacteria from Latin American medical centres: results from SENTRY Antimicrobial Surveillance Program (2011-2014). *International journal of antimicrobial agents* 2016 Aug; **48**(2)**:** 144-150.

287. Rao GG, Ly NS, Diep J, Forrest A, Bulitta JB, Holden PN*, et al.* Combinatorial pharmacodynamics of polymyxin B and tigecycline against heteroresistant Acinetobacter baumannii. *International journal of antimicrobial agents* 2016 Sep; **48**(3)**:** 331-336.

288. Thaden JT, Pogue JM, Kaye KS. Role of newer and re-emerging older agents in the treatment of infections caused by carbapenem-resistant Enterobacteriaceae. *Virulence* 2017 May 19; **8**(4)**:** 403-416.

289. Bradford PA, Weaver-Sands DT, Petersen PJ. In vitro activity of tigecycline against isolates from patients enrolled in phase 3 clinical trials of treatment for complicated skin and skin-structure infections and complicated intra-abdominal infections. *Clinical infectious diseases : an official publication*

of the Infectious Diseases Society of America 2005 Sep 1; **41 Suppl 5:** S315-332.

290. Wyeth Pharmaceuticals Inc. Wyeth Pharmaceuticals Inc. Tygacil® [tigecycline] for injection for intravenous use. Full prescribing information. 2012 2018, April [cited; Available from: http://labeling.pfizer.com/showlabeling.aspx?id=491

291. Bucaneve G, Micozzi A, Picardi M, Ballanti S, Cascavilla N, Salutari P*, et al.* Results of a multicenter, controlled, randomized clinical trial evaluating the combination of piperacillin/tazobactam and tigecycline in high-risk hematologic patients with cancer with febrile neutropenia. *Journal of clinical oncology : official journal of the American Society of Clinical Oncology* 2014 May 10; **32**(14)**:** 1463-1471.

292. Lauf L, Ozsvar Z, Mitha I, Regoly-Merei J, Embil JM, Cooper A*, et al.* Phase 3 study comparing tigecycline and ertapenem in patients with diabetic foot infections with and without osteomyelitis. *Diagnostic microbiology and infectious disease* 2014 Apr; **78**(4)**:** 469-480.

293. Stein GE, Babinchak T. Tigecycline: an update. *Diagnostic microbiology and infectious disease* 2013 Apr; **75**(4)**:** 331-336.

294. Garrison MW, Neumiller JJ, Setter SM. Tigecycline: an investigational glycylcycline antimicrobial with activity against resistant gram-positive organisms. *Clinical therapeutics* 2005 Jan; **27**(1)**:** 12-22.

295. Zhanel GG, Homenuik K, Nichol K, Noreddin A, Vercaigne L, Embil J*, et al.* The glycylcyclines - A comparative review with the tetracyclines. *Drugs* 2004; **64**(1)**:** 63-88.

296. Bergeron J, Ammirati M, Danley D, James L, Norcia M, Retsema J*, et al.* Glycylcyclines bind to the high-affinity tetracycline ribosomal binding site and evade Tet(M)- and Tet(O)-mediated ribosomal protection. *Antimicrob Agents Ch* 1996 Sep; **40**(9)**:** 2226-2228.

297. Lamb R, Ozsvari B, Lisanti CL, Tanowitz HB, Howell A, Martinez-Outschoorn UE*, et al.* Antibiotics that target mitochondria effectively eradicate cancer stem cells, across multiple tumor types: Treating cancer like an infectious disease. *Oncotarget* 2015 Mar 10; **6**(7)**:** 4569-4584.

298. Zimorski V, Ku C, Martin WF, Gould SB. Endosymbiotic theory for organelle origins. *Curr Opin Microbiol* 2014 Dec; **22:** 38-48.

299. Esposti M, Chouaia B, Comandatore F, Crotti E, Sassera D, Lievens PMJ*, et al.* Evolution of Mitochondria Reconstructed from the Energy Metabolism of Living Bacteria. *Plos One* 2014 May 7; **9**(5).

300. Chandel NS, Schumacker PT. Cells depleted of mitochondrial DNA (rho(0)) yield insight into physiological mechanisms. *Febs Lett* 1999 Jul 9; **454**(3)**:** 173-176.

301. Vandecasteele SJ, Seneca S, Smet J, Reynders M, De Ceulaer J, Vanlander AV*, et al.* Tigecycline-induced inhibition of mitochondrial DNA translation may cause lethal mitochondrial dysfunction in humans. *Clinical microbiology and infection : the official publication of the European Society of Clinical Microbiology and Infectious Diseases* 2018 Apr; **24**(4)**:** 431 e431-431 e433.

302. Yang R, Yi L, Dong Z, Ouyang Q, Zhou J, Pang Y*, et al.* Tigecycline Inhibits Glioma Growth by Regulating miRNA-199b-5p-HES1-AKT Pathway. *Mol Cancer Ther* 2016 Mar; **15**(3)**:** 421-429.

303. Zhong XX, Zhao EH, Tang CL, Zhang WB, Tan J, Dong Z*, et al.* Antibiotic drug tigecycline reduces neuroblastoma cells proliferation by inhibiting Akt activation in vitro and in vivo. *Tumor Biol* 2016 Jun; **37**(6)**:** 7615-7623.

304. Tang CL, Yang LQ, Jiang XL, Xu C, Wang M, Wang QR*, et al.* Antibiotic drug tigecycline inhibited cell proliferation and induced autophagy in gastric cancer cells. *Biochem Bioph Res Co* 2014 Mar 28; **446**(1)**:** 105-112.

305. Jia XF, Gu ZF, Chen WM, Jiao JB. Tigecycline targets nonsmall cell lung cancer through inhibition of mitochondrial function. *Fund Clin Pharmacol* 2016 Aug; **30**(4)**:** 297-306.

306. Hu HR, Dong Z, Tan P, Zhang YL, Liu LC, Yang LQ*, et al.* Antibiotic drug tigecycline inhibits melanoma progression and metastasis in a p21(CIP1/Waf1)-dependent manner. *Oncotarget* 2016 Jan 19; **7**(3)**:** 3171-3185.

307. Ren A, Qiu Y, Cui H, Fu G. Tigecycline exerts an antitumoral effect in oral squamous cell carcinoma. *Oral Dis* 2015 Jul; **21**(5)**:** 558-564.

308. Tan J, Song MJ, Zhou M, Hu YR. Antibiotic tigecycline enhances cisplatin activity against human hepatocellular carcinoma through inducing mitochondrial dysfunction and oxidative damage. *Biochem Bioph Res Co* 2017 Jan 29; **483**(1)**:** 17-23.

309. Wang B, Ao JS, Yu D, Rao T, Ruan Y, Yao XB. Inhibition of mitochondrial translation effectively sensitizes renal cell carcinoma to chemotherapy. *Biochem Bioph Res Co* 2017 Aug 26; **490**(3)**:** 767-773.

310. Li H, Jiao S, Li X, Banu H, Hamal S, Wang XR. Therapeutic effects of antibiotic drug tigecycline against cervical squamous cell carcinoma by inhibiting Wnt/beta-catenin signaling. *Biochem Bioph Res Co* 2015 Nov 6; **467**(1)**:** 14-20.

311. Jones RA, Robinson TJ, Liu JC, Shrestha M, Voisin V, Ju YJ*, et al.* RB1 deficiency in triple-negative breast cancer induces rnitochondrial protein translation. *J Clin Invest* 2016 Oct; **126**(10)**:** 3739-3757.

312. Kuntz EM, Baquero P, Michie AM, Dunn K, Tardito S, Holyoake TL*, et al.* Targeting mitochondrial oxidative phosphorylation eradicates therapy-resistant chronic myeloid leukemia stem cells. *Nat Med* 2017 Oct; **23**(10)**:** 1234-1240.

313. Reed GA, Schiller GJ, Kambhampati S, Tallman MS, Douer D, Minden MD*, et al.* A Phase 1 study of intravenous infusions of tigecycline in patients with acute myeloid leukemia. *Cancer medicine* 2016 Nov; **5**(11)**:** 3031-3040.

CHAPTER II

ETNK1 mutations induce a mutator phenotype that can be reverted with phosphoethanolamine

Diletta Fontana[1], Mario Mauri[1], Rossella Renso[1], Mattia Docci[1], Ilaria Crespiatico[1], Lisa Marie Røst[2], Antonio Niro[1], Deborah D'Aliberti[1], Luca Massimino[1], Mayla Bertagna[1], Giovanni Zambrotta[1], Mario Bossi[1], Stefania Citterio[3], Barbara Crescenzi[4], Francesca Fanelli[5], Valeria Cassina[1], Roberta Corti[1], Domenico Salerno[1], Luca Nardo[1], Francesco Mantegazza[1], Cristina Mecucci[4], Guido Cavaletti[1], Per Bruheim[2], Delphine Rea[6], Steen Larsen[7,8], Carlo Gambacorti-Passerini[1,9]†, Rocco Piazza[1,9]†*

[1] Department of Medicine and Surgery, University of Milano - Bicocca, Monza, Italy.

[2] Department of Biotechnology and Food Science, Norwegian University of Science and Technology, Trondheim, Norway.

[3] Department of Biotechnology and Biosciences, University of Milano - Bicocca, Milano, Italy.

[4] Centro Ricerche Emato-Oncologiche, University of Perugia, Perugia, Italy.

[5] Department of Life Sciences, University of Modena and Reggio Emilia, Modena, Italy.
[6] Service d'Hématologie adulte, Hôpital Saint-Louis, Paris, France.
[7] X-lab, Center for Healthy Aging, Department of Biomedical Sciences, University of Copenhagen, Copenhagen, Denmark.
[8] Clinical Research Centre, Medical University of Bialystok, Bialystok, Poland.
[9] Hematology and Clinical Research Unit, San Gerardo Hospital, Monza, Italy.

†Joint Senior Authors

*Correspondence to: rocco.piazza@unimib.it

[Submitted]

Abstract

Recurrent somatic mutations in ETNK1 (Ethanolamine-Kinase-1) were identified in several myeloid malignancies and are responsible for a reduced enzymatic activity. Here we demonstrate in cell lines and in primary leukemic cells that mutated ETNK1 causes a significant increase in mitochondrial activity, ROS production, Histone H2AX phosphorylation and a higher mutation rate compared to WT. Phosphoethanolamine, the metabolic product of ETNK1, negatively controls mitochondrial activity through direct competition with succinate at mitochondrial complex II. Hence, reduced intracellular phosphoethanolamine causes mitochondria hyperactivation, ROS production and DNA damage. Also, clonal hierarchy reconstruction experiments show that ETNK1 mutations invariably occur very early during neoplastic transformation. Finally, treatment with phosphoethanolamine is able to restore a normal phenotype.

Introduction

ETNK1 kinase is responsible for the phosphorylation of Ethanolamine (Et) to Phosphoethanolamine (P-Et). P-Et plays a critical role in the Kennedy pathway, representing the main metabolic route by which mammalian cells synthetize the two most abundant phospholipids of the cell membrane: phosphatidylethanolamine (PE) and

phosphatidylcholine (PC). Specifically, P-Et synthesis represents the first metabolic step required for PE anabolism (1).

PE plays a major role in defining cell membrane architecture (2). It is believed to cause lateral pressure and to introduce curvature stress, therefore influencing folding and activity of several membrane proteins (3). Its presence is critical at the end of the cytokinesis, where cells lacking PE are unable to complete the cell division process (4). Finally, PE is required for optimal activity of the mitochondrial respiratory complexes and ubiquinone function (5).

By using next-generation sequencing techniques, we and other identified recurrent missense somatic mutations occurring on ETNK1 in about 13% of patients affected by atypical chronic myeloid leukemia (aCML) (6), in 3-14% of chronic myelomonocytic leukemia (CMML) (6, 7) and in 20% of Systemic Mastocytosis (SM) patients with eosinophilia (7). Recently, somatic ETNK1 mutations were also described in diffuse large B-cell lymphomas (DLBCL) (8), supporting the notion that these mutations are not restricted to myeloid disorders. These mutations, encoding for H243Y, N244S/T/K, and G245V/A substitutions, cluster in a very narrow region of ETNK1 catalytic domain and cause an impairment in ETNK1 enzymatic activity leading to a significant decrease in the intracellular concentration of P-Et (6).

Here we investigated the specific role of ETNK1 mutations: by using cellular CRISPR/Cas9 models as well as patients' samples we showed that ETNK1 mutations are responsible for mitochondria hyperactivation owing to a direct competition between P-Et and succinate for mitochondrial complex II succinate dehydrogenase

(SDH), leading to increased ROS production and to the induction of a mutator phenotype.

Results

ETNK1 mutations do not affect cell membrane lipid composition

To study the biological effect of ETNK1 mutations we generated CRISPR/Cas9 models of mutated (ETNK1-N244S) and knock-out (ETNK1-KO) ETNK1 (Suppl. Table 1). From studies done on bacteria (4, 9), an adequate PE concentration in cell membranes is thought to be required for proper cell division, as PE modulates the curvature and rigidity (10, 11) of the cell membrane. Hence, we hypothesized that a reduced ETNK1 enzymatic activity, leading to a decrease in intracellular P-Et concentration (6), could result in a similarly reduced intracellular PE, as P-Et is the primary building block for the synthesis of PE in the Kennedy pathway (1).

To test this hypothesis, we initially characterized the cell membrane lipidome profile of 293-WT and genome-edited 293-ETNK1-N244S cells (named from now on as ETNK1-N244S). Globally, we analyzed a total of 21 lipid families (Suppl. Fig. 1A), comprising a total of 217 different PE species characterized by different fatty acids length and different double-bonds composition. Differential lipidome profile analysis failed to reveal significant changes in the absolute or relative

cell-membrane PE concentration as well as in the concentration of related phospholipids, such as PC and phosphatidylserine (PS), therefore suggesting the presence of compensatory mechanisms able to vicariate the decreased intracellular P-Et concentration. Similarly, no difference was detected in fatty acid composition (Suppl. Fig. 1B) or in PE double-bonds and fatty acid length (Suppl. Fig. 2).

Decreased enzymatic activities are often compensated through the upregulation of side pathways. Whole-transcriptome differential expression analysis (Suppl. Fig. 3A,B) between ETNK1-WT and ETNK1-N244S lines revealed the presence of only 119 differentially expressed genes (FDR < 0.1; Suppl. Table 2), suggesting a very limited role of ETNK1 variants in modulating gene expression. Of them 104 were upregulated and 15 downregulated. None of the differentially expressed genes were ascribable to ontologies related to lipid biosynthesis pathways, however a trend towards a decreased expression of PTDSS1 (-0.4 Log2 fold-change) and PTDSS2 (-0.3 Log2 fold-change), the two main effectors of PS synthesis from PE and PC, could be noted (Suppl. Fig. 3C), which suggests the activation of regulatory mechanisms compensating the reduced PE production.

In line with these findings, analysis of cell membrane rigidity by mean of atomic-force indentation assays (Suppl. Fig 4A-D) failed to reveal substantial differences among ETNK1-WT, ETNK1-N244S and homozygous ETNK1 knock-out (ETNK1-KO) cells.

Taken globally these data indicated that human cells are able to vicariate ETNK1 activity, at least for PE synthesis, therefore ruling-out a critical role for cell membrane PE in the oncogenesis mediated by ETNK1 mutations. This was not completely unexpected, given the

critical role of PE phospholipids for cell survival and taking into account the important cross-talk between the PE, PC and PS branches of the Kennedy pathway.

ETNK1 mutations increase mitochondria activity

As the presence of a physiological PE concentration in mitochondria membranes is reported to be critical for the oxidative phosphorylation pathway (12, 13), we investigated mitochondria respiratory chain activity. Analyses done on target cells by using MitoTracker Red and Green to assess mitochondria potential and mass showed an absolute increase of green signal (Fig. 1A; 1.38 and 1.33 fold increase in ETNK1-N244S and ETNK1-KO compared to ETNK1-WT; $p<0.0001$ and $p=0.023$, respectively) and in red-to-green ratio in both mutated and knock-out ETNK1 lines (Fig. 1B; 1.87 and 2.48 fold increase in ETNK1-N244S and ETNK1-KO compared to ETNK1-WT; $p=0.0001$ and $p<0.0001$, respectively), hence suggesting an association between inhibition of ETNK1 activity and increased mitochondrial polarization and mass.

Transmission electron microscopy applied to WT, mutated and knock-out ETNK1 cells confirmed these findings, showing that in WT cells mitochondria are characterized by a round-shaped morphology with higher electron density compared to both ETNK1-N244S and ETNK1-KO. Conversely, mutated lines showed a bigger and polymorphic shape with regions of low electron density in which the mitochondria crests were clearly defined, thus suggesting an increased

activity (14, 15) (Fig. 1C-F; 1.72 and 2.02 fold increase in ETNK1-N244S and ETNK1-KO compared to ETNK1-WT; $p<0.0001$ for both N244S and KO compared to WT).

Given the importance of mitochondrial PE for the oxidative phosphorylation pathway (12, 13), we initially hypothesized that the alteration of mitochondria membrane potential in presence of mutated or knock-out ETNK1 could be due to alteration in the mitochondrial membranes composition and to a reduced PE fraction. To test this hypothesis we generated a whole-lipidome mass-spectrometry profile of purified mitochondria from WT and mutated lines. Again, no significant difference in PE composition could be found (Suppl. Fig. 5; N244S/WT PE ratio = 1.08; $p=0.61$).

Phosphoethanolamine restores a normal mitochondrial activity

Recently, Gohil and colleagues demonstrated that treatment with meclizine, a known inhibitor of phosphoethanolamine cytidylyltransferase 2 (PCYT2), the second step in the Kennedy pathway downstream to ETNK1, led to a potent inhibition of mitochondria respiration (16) and accumulation of P-Et. Similarly, Ferreira and colleagues showed that supplementation of MCF-7 cells with millimolar concentration of P-Et caused an abrupt decrease in mitochondria membrane potential (17). Owing to these preliminary evidences, we turned our attention to P-Et, investigating a potential role for P-Et (or lack thereof) in the regulation of mitochondria

activity. Hence, we repeated MitoTracker Red/Green experiments in presence/absence of P-Et (1mM). In our previous work we showed that ETNK1 somatic mutations impair ETNK1 catalytic activity, therefore resulting in a decrease in P-Et intracellular concentration. Hence we hypothesized that the decreased P-Et concentration in ETNK1-mutated cells could be responsible for the increased mitochondrial activity. In line with this hypothesis, MitoTracker experiments in cells treated with 1mM P-Et showed a complete restoration of the normal membrane potential in both mutated and knock-out ETNK1 models (Fig. 1G,H; 1.56 and 2.21 fold decrease in ETNK1-N244S and ETNK1-KO compared to ETNK1-WT; $p=0.0008$ and $p<0.0001$, respectively); conversely, no effect was detected in ETNK1-WT, where treatment with P-Et did not alter mitochondrial activity level (Fig. 1G,H; 1.06 fold decrease; $p>0.05$). Taken globally, these data suggested a direct role for P-Et downregulation in modulating mitochondria membrane potential.

To assess if the apparent increase in mitochondria activity in ETNK1-mutated lines was accompanied by an increased cell respiration rate, we measured oxygen consumption rate (reported as O2 pmol/(s*106 cells)) and concentration (nmol/ml) in ETNK1-WT and KO lines (Fig. 2A). In accordance with MitoTracker experiments showing an increased mitochondrial respiratory activity in mutated lines, the oxygen consumption rate resulted strongly increased in ETNK1-KO lines compared to WT (Fig. 2A). Similarly, the oxygen concentration curve showed a much faster decrease in ETNK1-KO than in WT over the entire course of the experiment, indicating that the cellular respiration rate is markedly increased in ETNK1-KO cells (Fig. 2A).

Treatment with 100μM, 1mM and 2mM P-Et (Fig. 2A: first, second and third P-Et arrow) caused in all cases a rapid decrease of the respiration rate, therefore suggesting a role for P-Et as a negative regulator of mitochondria respiration.

ETNK1 mutations are responsible for increased mitochondrial ROS production and can be reverted back to a normal level by treatment with phosphoethanolamine or tigecycline

A large fraction of the total intracellular ROS are generated during the process of oxidative phosphorylation in the inner mitochondrial membrane. Hence, oxidative phosphorylation and generation of ROS are tightly connected processes. To investigate if the increased mitochondrial membrane potential in ETNK1-mutated lines could be also associated with an abnormal production of ROS, we assessed their intracellular level by using the CellROX Green Reagent fluorogenic dye. CellROX dye is weakly fluorescent while in a reduced state; however it exhibits a bright green fluorescence upon oxidation by ROS, therefore allowing us to estimate the levels of oxidative stress in live cells. As expected, we detected a significant increase in ROS production in mutated and knock-out ETNK1 lines compared to WT ones (Fig. 2B; 2.05 and 2.38 fold increase; $p<0.0001$). To assess if the production of ROS was modulated by the intracellular P-Et content, we re-evaluated ROS levels after

supplementation of target cells with 1mM P-Et. Notably, treatment with P-Et completely restored the normal ROS production (Fig. 2C; 2.14 and 1.79 fold decrease in treated ETNK1-N244S and ETNK1-KO lines compared to untreated; p=0.0001 and p=0.0002, respectively), therefore indicating a role for P-Et as a potent regulator of mitochondria activity and generation of ROS.

Given the direct connection of mitochondrial oxidative phosphorylation activity and ROS production, we hypothesized that the synthesis of ROS could be controlled by reducing the activity of mitochondria machinery. Tigecycline is an antibiotic used to treat a number of bacterial infections (18). Its mechanism of action relies on the inhibition of bacterial protein synthesis. Because of the similarity of mitochondrial and bacterial ribosomes, tigecycline also inhibits the synthesis of mitochondrial proteins required for the oxidative phosphorylation machinery (19). To assess if tigecycline could dampen mitochondrial ROS production in the context of ETNK1-mutated cells, we treated ETNK1 lines with 2.5 and 10μM tigecycline for 24 hours: ROS production was assessed by mean of CellROX assay (Fig. 2B,D). In line with the known tigecycline ability in modulating mitochondria oxidative phosphorylation, treatment in ETNK1-N244S and KO lines almost completely restored the normal ROS levels (Fig. 2D; 1.33 and 1.32 fold decrease in ETNK1-N244S and ETNK1-KO treated with 2.5μM tigecycline compared to untreated; p=0.0237 and p=0.0214, respectively; 1.57 and 1.78 fold decrease in 10μM tigecycline treated ETNK1-N244S and ETNK1-KO compared to untreated; p=0.0040 and p=0.0010, respectively), while virtually no effect could be detected in WT controls (Fig. 2D; 1.03 and

1.13 fold decrease in ETNK1-WT treated with 2.5 and 10μM tigecycline; $p>0.05$).

As glycolysis and mitochondrial respiration are tightly coupled processes, we sought to investigate if the alteration in mitochondrial activity was associated with changes in the glycolytic profile of ETNK1-N244S cells. Whole-transcriptome profile was used to analyze the expression level of all glycolytic enzymes, while targeted mass spectrometric metabolic profiling and nuclear magnetic resonance (NMR) was applied to quantify glycolytic intermediates, and glucose consumption and lactate excretion, respectively (Suppl. Fig. 6; suppl. Table 3). These analyses did not reveal significant changes at neither gene or metabolite level, suggesting that altered glycolytic function does not play a major role in the ETNK1-driven leukemogenesis.

ETNK1 mutations cause accumulation of 8-Oxoguanine DNA lesions and induction of a mutator phenotype that can be reverted with phosphoethanolamine or tigecycline treatment

The role of ROS as mutagenic agents is well-documented as they are known to play a major role in the onset and clonal evolution of many cancers (20). Hundreds of different oxidative DNA modifications have already been identified in eukaryotic genomes; in particular guanine is extremely vulnerable to ROS damage, due to its low redox

potential (21). The main product of ROS-mediated guanine oxidation is the 7,8-dihydro-8-oxo-2′-deoxyguanosine (oxoG; Fig. 3A). If not repaired by the physiologic DNA repair mechanisms, such as the oxoG-Glycosidases, oxoG can pair with adenine, causing G->T transversions (Fig. 3B). Hence, oxoG can be used as a biomarker of ROS-mediated genomic DNA damage. To leverage this information and to assess if ETNK1 mutations could cause accumulation of DNA lesions we generated ChIP-Seq data for ETNK1-N244S lines using an antibody raised against the oxoG and we compared oxoG signal against the wild-type 293 line. Analysis of the oxoG signal at whole-genome level using custom bioinformatic tools (details can be found in the methods section) revealed a significant increase in oxoG in ETNK1-N244S (Fig. 3C; p= 0.018; Wilcoxon signed-rank test). As the accumulation of intracellular ROS was accompanied by a significant increase of oxoG lesions in the nucleus of ETNK1-mutated cells, we sought to investigate if these lesions were driving the onset of a mutator phenotype, therefore overcoming the physiologic DNA repair mechanisms of the target cells. Hence we performed 6-thioguanine (6TG) resistance assays in our cell models: in line with ChIP-Seq data, 6TG assays demonstrated a significant increase in the number of resistant colonies in mutated and knock-out ETNK1 lines when compared to the reference (Fig. 3D; Suppl. Table 4; 5.4 and 4.9 fold increase compared to the WT line in ETNK1-N244S and KO, respectively; p=0.0001 for ETNK1-N244S and p<0.0001 for ETNK1-KO). As the increase in ROS production and in oxoG gDNA content suggested a direct relationship between increased mitochondrial oxidative phosphorylation and DNA damage, we hypothesized that

this damage could be antagonized by treating cells with either P-Et or tigecycline. To test this hypothesis we performed new 6TG resistance assays in cells pre-treated with 1mM P-Et or 2.5μM tigecycline. In support of our hypothesis, treatment with both compounds caused an almost complete reversion of the mutant phenotype back to the normal level in mutated and knock-out lines (Fig. 3D; Suppl. Table 5; P-Et treatment: 0.86 and 1.19 fold compared to the WT line for ETNK1-N244S and KO, respectively; tigecycline treatment: 2.28 and 1.4 fold compared to the WT), indicating that the presence of a mutator phenotype is fully dependent on mitochondria increased activity and can be controlled by physiological or pharmacological modulators of oxidative phosphorylation.

Mutant ETNK1 leads to DNA double-strand breaks

Under normal conditions, human DNA is subjected to a constant process of oxidative damage mediated by ROS that are generated in large part as a byproduct of mitochondria oxidative phosphorylation (22). It is estimated that in a single cell cycle almost 5000 single-stranded DNA breaks can occur as a result of ROS production. Approximately 1% of these DNA breaks is converted into double strand breaks (DSBs), mainly during DNA replication, while the remaining 99% is repaired (22, 23). As ETNK1+ clonal disorders, such as aCML, are typically characterized by chromosome instability and clonal evolution, we sought to investigate if the ROS-mediated genotoxic insult operating in ETNK1-mutated lines could be also

associated with an increase in DNA DSBs. To achieve this goal we analyzed the level of phosphorylated histone H2AX (□H2AX), a well-known marker of DNA DSBs (24), by confocal microscopy. Comparison of ETNK1-N244S and ETNK1-WT lines revealed a sharp increase in the number of □H2AX foci (Fig. 4A-C; 2.52 fold increase; $p<0.0001$) in the former. Similar results were achieved in presence of ETNK1-KO (Fig. 4A,C; 2.51 fold increase; $p=0.0046$), indicating that suppression of ETNK1 activity and the ensuing decrease in P-Et intracellular concentration are followed by an increase in DNA DSBs. To test for a causative role of the ETNK1-dependent mitochondrial machinery in the onset of the chromosome instability phenotype, we repeated the same experiments in presence of 1mM P-Et or 2.5μM tigecycline: both treatments were able to restore the rate of DNA DSBs back to a normal level (Fig. 4A,C; 1.94 and 2.71 fold decrease in P-Et treated ETNK1-N244S and ETNK1-KO compared to untreated; $p=0.0001$ and $p=0.0035$, respectively; 1.95 and 2.45 fold decrease in tigecycline treated ETNK1-N244S and ETNK1-KO compared to untreated; $p=0.0004$ and $p=0.0068$, respectively), therefore supporting the hypothesis of a direct involvement of the ETNK1-P-Et-Mitochondria axis in the induction of the double stranded DNA damage. Anti-□H2AX western blots on ETNK1-WT and ETNK1-KO lysates confirmed the same finding (Fig. 4D,E).

To assess if the presence of ETNK1 somatic mutations could similarly associate with increased DNA damage in patients' samples, we analyzed by anti-□H2AX western blots ficoll-purified bone marrow mononuclear cell lysates of aCML patients, either positive (4) or

negative (4) for ETNK1 mutations, whose mutation landscape had been characterized by mean of paired exome-sequencing (Suppl. Tables 6-15). In line with the results generated in CRISPR/Cas9 cell-line models, the ex vivo analysis confirmed a strong activation of the □H2AX signal which was restricted to the entire group of the ETNK1-mutated samples (Fig. 4F,G; 2.70 fold increase; p=0.0037). In an ETNK1+ aCML patient whom bone marrow cells where available we tested □H2AX signal by western blot in absence and in presence of 1mM P-Et (Fig. 4H): as shown with ETNK1+ cell lines, ex vivo experiments with patient cells confirmed the reduction of □H2AX signal in presence of the drug.

Subclonal architecture of ETNK1+ leukemias indicates that ETNK1 mutations are early events

Taken globally these data indicate that ETNK1 mutations are mainly responsible for the induction of a mutator phenotype, which, in turn, can promote the development of new mutations and chromosomal instability, therefore accelerating the process of clonal evolution. For this process to be effective however, variants responsible for the induction of the mutator phenotype must arise early in the process of neoplastic transformation (25, 26), allowing further mutations to accumulate and hence increasing the global fitness of the mutated subclone. Hence we hypothesized that ETNK1 mutations should be a very early event in the history of the ETNK1+ leukemia. To test this hypothesis we grew in semisolid methylcellulose medium ficoll-

purified bone marrow cells taken from 4 ETNK1+ aCML patients whose mutational landscape had been previously characterized by paired exome sequencing (Suppl. Tables 6-15). On average 100 colonies were obtained from each sample. Genomic DNA was extracted from each colony and used as a template for targeted, barcoded ultradeep sequencing covering all the known mutations present in the sample and characterized by oncogenic potential as evaluated by OncoScore (27). Identification of all the variants present in each colony allowed us to reconstruct, in large part, the mutation hierarchy of the leukemic clones (Fig. 5A-D). In all the cases under analysis, ETNK1 mutation was identified as the first event, either alone (two cases. Fig. 5A,B) or in combination with NRAS-G12D (1 case. Fig. 5C) or CBL-C384Y (1 case. Fig. 5D), indicating that ETNK1 mutations represent very early events in the clonal history of aCML.

Phosphoethanolamine directly modulates mitochondrial complex II activity

Although the data from mitochondria activity and ROS production were clearly pointing to a precise role for P-Et as a modulator of mitochondria activity, to our knowledge no known pathway was able to explain this connection from a mechanistic point of view. To dissect the precise mechanism by which P-Et intracellular levels are able to control mitochondria activity, we isolated the oxidative phosphorylation complexes I to IV (Suppl. Fig 7) from WT cells by

mean of immunoprecipitation from lysed mitochondria (complexes I, II and IV) or purified mitochondria (complex III). Subsequently we measured the activity of each complex in absence/presence of increasing P-Et concentrations. This approach failed to show any effect for P-Et in complexes I, III and IV (Fig. 5E,G,H) but revealed a profound dose-dependent decrease in redox activity for mitochondrial complex II (Fig. 5F; P-Et 10μM: 1.39 fold decrease; $p>0.05$; P-Et 20μM: 5.67 fold decrease; $p=0.0011$; P-Et 50μM: 10.93 fold decrease; $p=0.0002$), hence indicating that P-Et controls mitochondria potential through direct inhibition of complex II.

Mitochondrial complex II, also known as succinate dehydrogenase (SDH), is both a central component of the mitochondria oxidative phosphorylation chain and of the tricarboxylic acid cycle (TCA) cycle, therefore representing a bridge between these two critical cellular processes. Together with complex I and complex III, complex II represents the top mitochondrial ROS factory in terms of maximal capacity (28). Although ROS generation through SDH is a complex and still non completely understood phenomenon, it is known that increased ROS production may occur in presence of high intracellular succinate concentration, causing complex II to increment the rate of ubiquinone reduction and promoting reverse electron transfer to Complex I (29). In this scenario, P-Et could physiologically act like a brake, keeping ROS production from complex II at bay by negatively modulating SDH activity.

To gain insight into the specific mechanism by which P-Et could repress complex II, we analyzed its activity in competition assays in presence of both P-Et and increasing concentration of succinate, the

molecular substrate of SDH. As already shown in previous analyses (Fig. 5F), treatment with 20μM P-Et alone caused a significant decrease in complex II activity (Fig. 5I). Subsequent supplementation of succinate was able to restore the normal SDH activity starting from 50μM (Fig. 5I), while lower dosages were unable to restore it, hence suggesting that P-Et acts as a competitive inhibitor of succinate for SDH activity.

In line with these data, automatic docking of P-Et and SDH suggests that P-Et can occupy the succinate binding site in an energetically favorable conformation, also mimicking succinate in some relevant interactions with SDH (Fig. 5J). In the predicted docking mode, the phosphate group of P-Et interacts with H354 and R399 like one of the two carboxylates of succinate, whereas the protonated amino-group interacts with FAD and approaches T254 similarly to the other carboxylate of succinate (Fig. 5J). These results strengthen our in vitro evidence that P-Et may act as a competitive inhibitor of SDH.

Discussion

Owing to the introduction of Next Generation Sequencing technologies, the identification of somatic mutations present in human cancer cells has become, relatively speaking, trivial. However, the plain identification of these mutations has a very limited practical impact if it is not accompanied by wet-lab studies dedicated to the dissection of the functional effects of each mutation. Unfortunately, these studies proved to be very complex: SF3B1 mutation was

discovered in 2011 (30) and, despite the vast progresses in the field (31, 32), the characterization of its functional role as a splicing mutation is yet to be completed. Similarly, it took us 4 years since our original identification of SETBP1 somatic mutations (33) to define a role for this protein as an epigenetic transcriptional regulator (34). Despite their intrinsic complexity, these studies are invaluable not only to gain further insight into the specific prooncogenic mechanisms at work with each variant, but also to dissect the functional relationships among different mutations and, most importantly, in order to convert this information into effective treatments for patients.

ETNK1 somatic mutations were identified for the first time by our group in aCML and chronic myelomonocytic leukemia (6) and by Lasho and colleagues in Systemic Mastocytosis (7) and, more recently, in DLBCL (8). In our first work we showed that ETNK1 mutations caused a decreased ETNK1 enzymatic activity, hence translating into a reduced intracellular P-Et concentration. However, at that time the functional role of the impaired ETNK1 activity was completely unclear. In this work we focused on the events occurring downstream of the impaired ETNK1 activity, trying to track-down the specific molecular mechanisms explaining why ETNK1 mutations are oncogenic.

As we know, cancer cells are in direct competition with each other for limited resources. At subclonal level, the existence of a strong selective pressure translates into the accumulation of new somatic mutations causing an increase in the overall ‘fitness’ of the competing subclones. This process can occur through at least two different mechanisms: the first one is the acquisition of mutations directly

improving the overall fitness. Variants like these translate into an immediate benefit for the mutated subclone, which in turn can e.g. proliferate faster, have a more efficient metabolic profile or can be protected from pro-apoptotic signals. The second mechanism does not affect the fitness of the target subclone directly; instead it increases the chances for the target cell to incorporate new mutations through the induction of a mutator phenotype. While this mechanism does not lead to an immediate benefit for the target subclone in terms of increased fitness, it allows the cells bearing these mutations to accumulate new mutations at an increased pace, hence gaining momentum over time.

Conclusions

Here we showed that ETNK1 mutations operate through this second mechanism owing to their ability in modulating mitochondria activity and ROS production. Taking into account the well-known ability of aCML to undergo clonal evolution towards a very aggressive, blastic phase, the risk of clonal evolution should be avoided at all costs. Although preliminary, our data suggest that treatment with P-Et, the metabolite whose production is reduced by ETNK1 mutations, 1) allows to quickly and efficiently decrease mitochondria hyperactivation; 2) normalizes ROS production; 3) reduces the accumulation of new mutations at levels comparable to ETNK1-WT cells, even though the exact mechanism by which this small, polar molecule is imported into the cells is at present unknown. Similarly,

treatment with the antibiotic tigecycline, a drug that is routinely used to treat microbial infections, leads to very similar results. Tigecycline is a well-known inhibitor of mitochondria activity, owing to its ability in blocking mitochondria protein synthesis and to selectively induce cell death in several leukemia cell lines (18-21). Also, combination of tigecycline with the standard chemotherapy regimen for acute myeloid leukemia led to a synergistic toxicity against the leukemic cells (22). The evidence that two molecules, P-Et and tigecycline, completely unrelated from a chemical point of view but functionally converging at mitochondrial level, are indeed able to suppress the ETNK1-driven mutator phenotype strongly supports the notion that mitochondria are the center of this ETNK1-based prooncogenic machinery.

Further studies will be required to assess if treatment with tigecycline or P-Et are able to reduce the risk of progression of ETNK1+ leukemias.

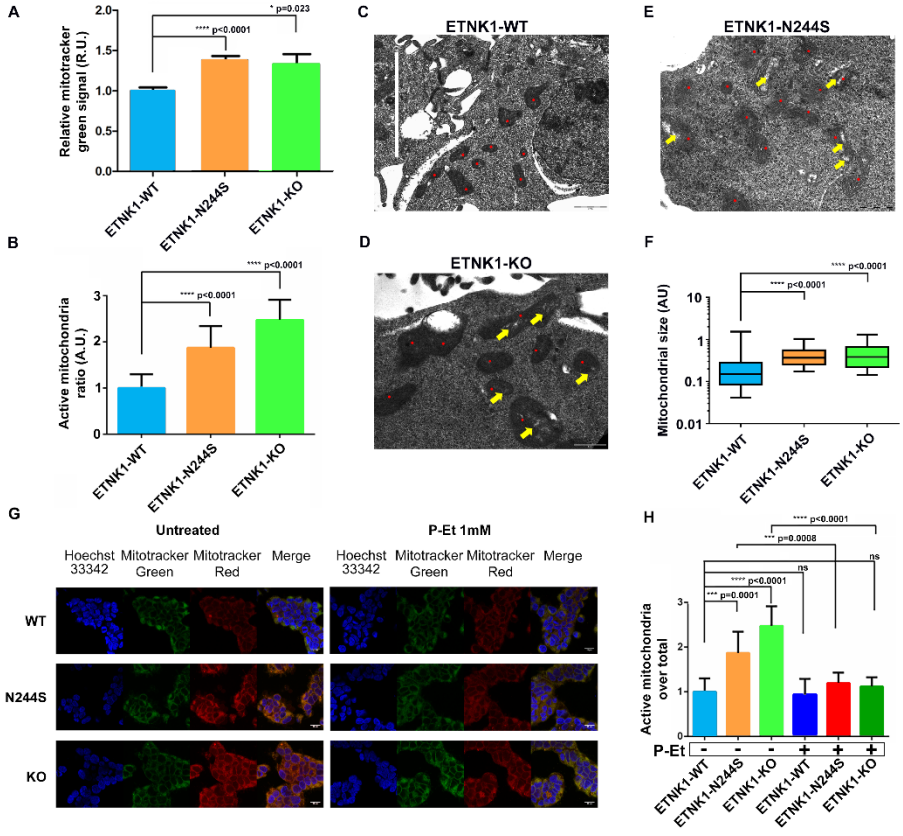

Fig. 1: mitochondria morphology and activity. **A**) Histograms representing the mitotracker green analysis of ETNK1-WT, N244S and KO cell lines. Values represent relative units normalized on the ETNK1-WT signal. The error bars represent the standard deviation of the mean (n=3). **B**) Histograms showing the mitotracker red-to-green signal ratio as assessed on ETNK1-WT, N244S and KO cell lines normalized on ETNK1-WT. Statistical analyses were performed using t-test on three replicates. Error bars represent the standard deviation of the mean. **C-E**) Electron microscopy scans relative to ETNK1-WT (C), N244S (D) and KO (E) cell lines. Red dots highlight the position of individual mitochondria. Yellow arrows point to low electron

density areas. **F**) Quantification of mitochondria size in ETNK1-WT, N244S and KO cell lines as assessed by electron microscopy. The boxplots delimit the interquartile range; the whiskers extend from 5th to 95th percentile. **G**) Confocal microscopy of mitotracker red/green signal in ETNK1-WT, N244S and KO cell lines in absence (left) and presence (right) of 1mM phosphoethanolamine. **H**) Histograms showing the mitotracker red-to-green signal ratio of ETNK1-WT, N244S and KO cell lines normalized on ETNK1-WT in absence and in presence of 1mM phosphoethanolamine. Statistical analyses were performed using t-test (n=3). Error bars represent the standard deviation of the mean.

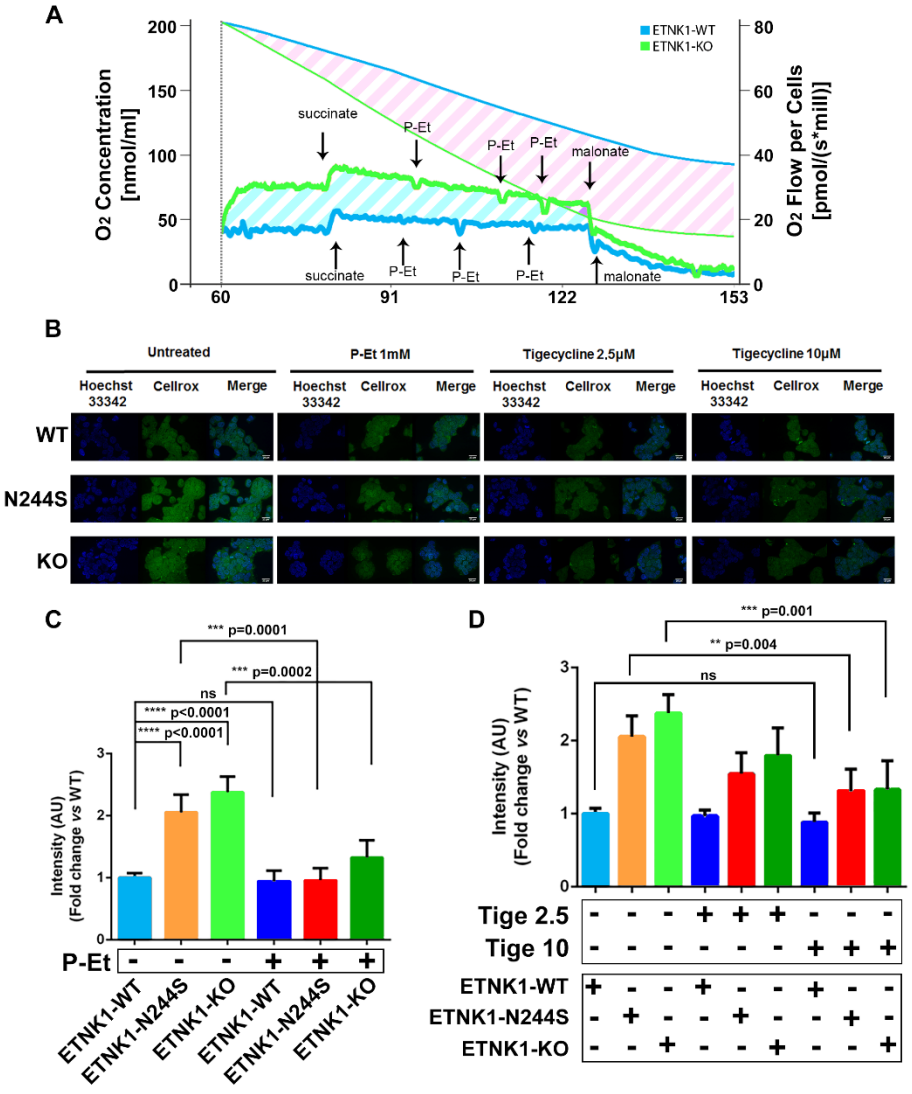

Fig. 2: mitochondria respiration and ROS production. **A**) O_2 consumption rate (pmol/(s*10^6 cells)) and O_2 concentration (nmol/ml) in ETNK1-WT and KO lines. The thick blue and green lines represent the oxygen consumption rate of ETNK1-WT and KO cells, respectively; the thin blue and green lines show the oxygen concentration in ETNK1-WT and KO oxygraph chambers,

respectively. The diagonal cyan and pink stripes highlight, respectively, the difference in oxygen consumption rate and oxygen concentration of ETNK1-WT and KO cells. **B**) Intracellular reactive oxygen species as assessed by confocal microscopy using the Cellrox reagent. ROS analysis was performed in ETNK1-WT, N244S and KO lines in absence and presence of phosphoethanolamine 1mM, tigecycline 2.5µM and tigecycline 10µM. **C**) ROS quantification in ETNK1-WT, N244S and KO lines in absence and presence of 1mM phosphoethanolamine. Error bars represent the standard deviation of the mean (n=3). Statistical analyses were performed using t-test (n=3). **D**) ROS quantification in ETNK1-WT, N244S and KO lines in absence and presence of 2.5µM and 10µM tigecycline. Error bars represent the standard deviation of the mean. Statistical analyses were performed using the t-test (n=3).

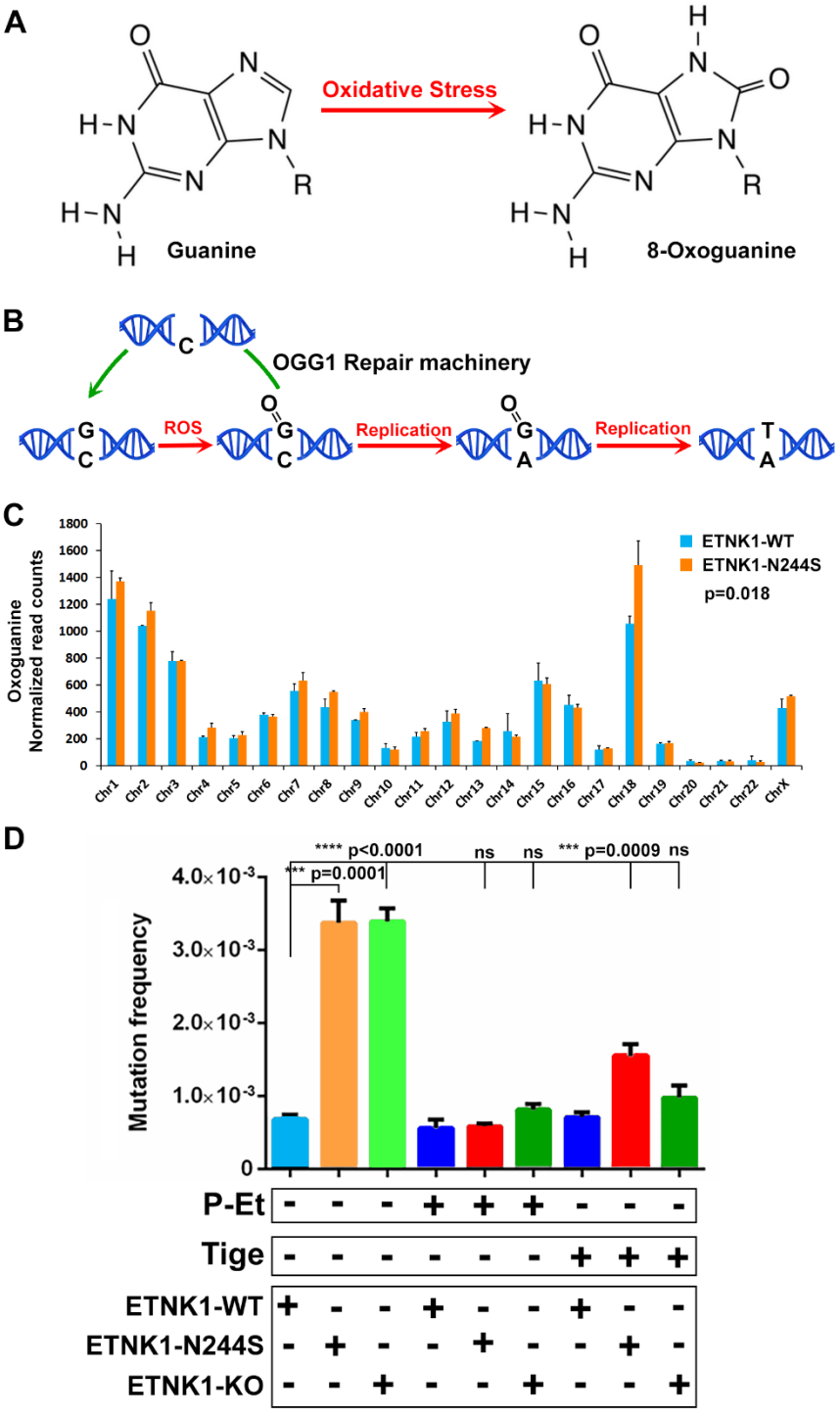
A
Oxidative Stress
Guanine
8-Oxoguanine
B
OGG1 Repair machinery
ROS
Replication
Replication
C
Oxoguanine
Normalized read counts
ETNK1-WT
ETNK1-N244S
p=0.018
Chr1
Chr2
Chr3
Chr4
Chr5
Chr6
Chr7
Chr8
Chr9
Chr10
Chr11
Chr12
Chr13
Chr14
Chr15
Chr16
Chr17
Chr18
Chr19
Chr20
Chr21
Chr22
ChrX
D
Mutation frequency
**** p<0.0001
*** p=0.0001
ns
ns
*** p=0.0009
ns
P-Et
Tige
ETNK1-WT
ETNK1-N244S
ETNK1-KO

Fig. 3: oxoguanine analysis and 6-thioguanine resistance. **A**) Diagram showing the chemical reaction responsible for the generation of oxoguanine from guanine after exposure of gDNA to reactive oxygen species. **B**) Scheme of the oxoguanine-mediated DNA damage. In presence of the modified base the gDNA may undergo two different destinies: either the base is excised, owing to the recruitment of the oxoguanine DNA glycosylase 1 (OGG1) repair machinery before the onset of a new replication cycle, or it will cause the misincorporation of an adenine in the complementary strand, eventually leading to a G:C to T:A transversion. **C**) Per-chromosome quantification of oxoguanine binned read counts in ETNK1-WT and N244S lines following total read counts normalization. The error bars represent the standard deviation of the mean (n=2). Statistical analysis was performed using a Wilcoxon matched-pairs signed rank test. **D**) Mutation frequency assessed by 6-thioguanine assays in ETNK1-WT, N244S and KO lines in absence or presence of 1mM phosphoethanolamine or 2.5µM tigecycline. The error bars represent the standard deviation of the mean (n=3). Statistical analyses were performed using the t-test.

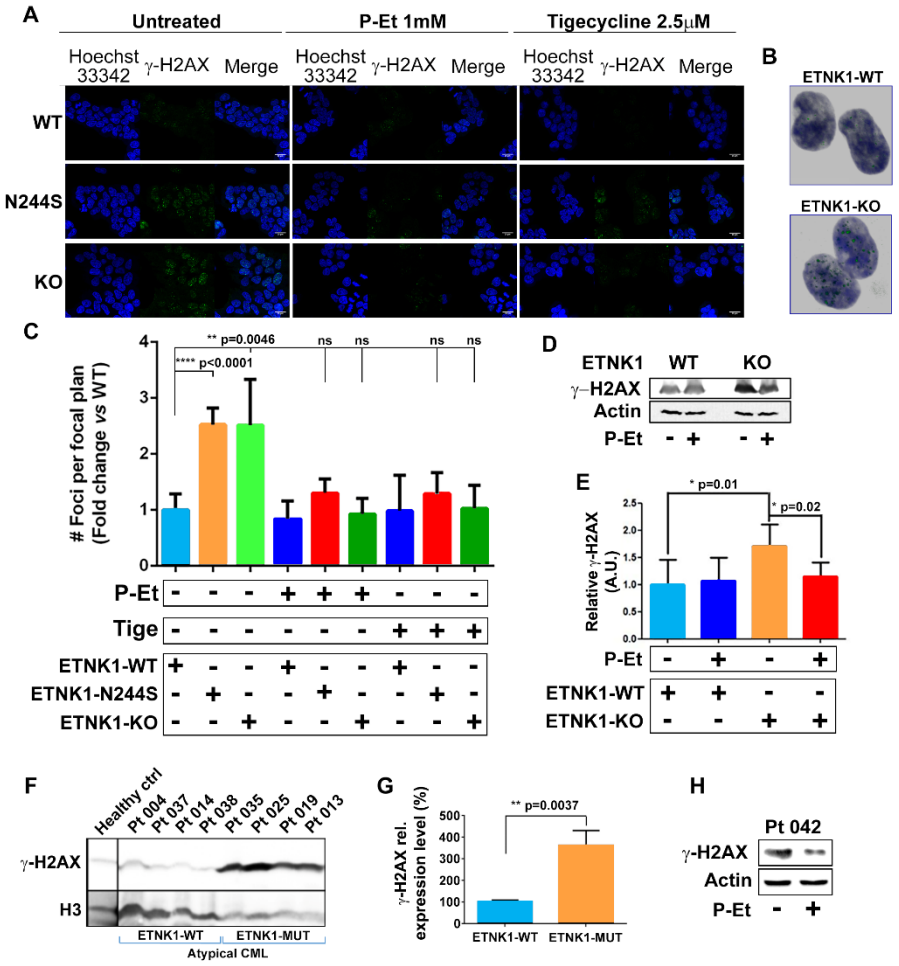

Fig. 4: double-strand DNA damage. **A**) confocal microscopy analysis of γH2AX foci in ETNK1-WT, N244S and KO lines in absence or presence of 1mM phosphoethanolamine or 2.5µM tigecycline. **B**) Detail of γH2AX foci in individual ETNK1-WT and ETNK1-KO cells. **C**) γH2AX signal quantification in ETNK1-WT, N244S and KO lines in absence or presence of 1mM phosphoethanolamine or 2.5µM tigecycline. The error bars represent the standard deviation of the mean (n=3). Statistical analyses were performed using t-test (n=3). **D**) Anti γH2AX western blot analysis on ETNK1-WT and ETNK1-KO

lysates in absence and presence of 1mM phosphoethanolamine. Gel loading was normalized using actin. **E**) Densitometric analysis of the western blot shown in panel D. **F**) Anti γH2AX western blot analysis on ETNK1-WT (left; 4 cases) and ETNK1-mutated (right; 4 cases) aCML patient samples. Gel loading was normalized using total H3. **G**) Densitometric analysis of the western blot shown in panel F. The two bars correspond to the mean, H3-normalized anti γH2AX signal of ETNK1-WT and ETNK1-mutated aCML patients, respectively; the error bars represent the standard deviation of the mean (n=4). Statistical analysis was performed using the t-test. **H**) Anti γH2AX western blot analysis on cell lysates from an ETNK1-mutated aCML bone marrow sample treated/non-treated with 1mM phosphoethanolamine for 24 hours.

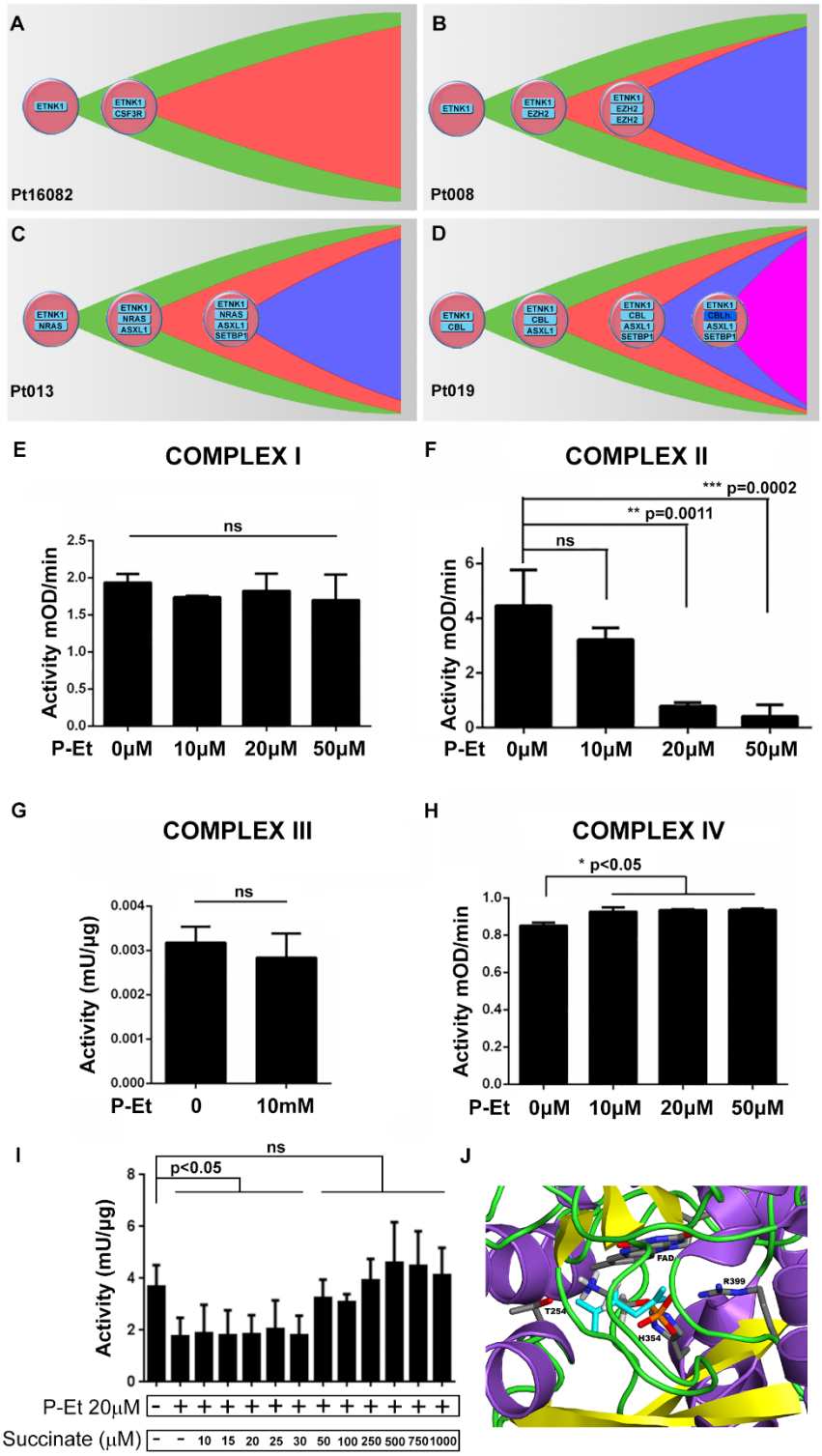
A
ETNK1
ETNK1
CSF3R
Pt16082
B
ETNK1
ETNK1
EZH2
ETNK1
EZH2
EZH2
Pt008
C
ETNK1
NRAS
ETNK1
NRAS
ASXL1
ETNK1
NRAS
ASXL1
SETBP1
Pt013
D
ETNK1
CBL
ETNK1
CBL
ASXL1
ETNK1
CBL
ASXL1
SETBP1
ETNK1
CBLB
ASXL1
SETBP1
Pt019
E
COMPLEX I
ns
Activity mOD/min
2.5
2.0
1.5
1.0
0.5
0.0
P-Et 0μM 10μM 20μM 50μM
F
COMPLEX II
*** p=0.0002
** p=0.0011
ns
Activity mOD/min
6
4
2
0
P-Et 0μM 10μM 20μM 50μM
G
COMPLEX III
ns
Activity (mU/μg)
0.004
0.003
0.002
0.001
0.000
P-Et 0 10mM
H
COMPLEX IV
* p<0.05
Activity mOD/min
1.0
0.8
0.6
0.4
0.2
0.0
P-Et 0μM 10μM 20μM 50μM
I
ns
p<0.05
Activity (mU/μg)
8
6
4
2
0
P-Et 20μM - + + + + + + + + + + +
Succinate (μM) - - 10 15 20 25 30 50 100 250 500 750 1000
J
FAD
R399
T254
H354

Fig. 5: clonal architecture of ETNK1+ patients and mitochondria complexes activity. **A-D**) Schematic representation of the clonal architecture of 4 aCML patients whose bone marrow mononuclear cells were grown in semisolid medium and underwent targeted resequencing based on previously identified somatic mutations. Variants reported on the left represent earlier clones. CBLh indicates a homozygous, somatic CBL mutation. **E-H**) Analysis of the activity of mitochondria complexes I to IV in presence of increasing concentrations of phosphoethanolamine. The analysis of complexes I, II and IV was performed on mitochondria lysates, while the analysis of complex III was performed on intact isolated mitochondria. Error bars represent the standard deviation of the mean (n=3). Statistical analyses were performed using the t-test. **I)** The activity of mitochondria complex II was assessed in absence and in presence of 20µM phosphoethanolamine in combination with increasing concentrations of succinate. Error bars represent the standard deviation of the mean (n=2). Statistical analyses were performed using the t-test. **J**) One of the best docking poses of P-Et onto the crystal structure of SDH (PDB: 1NEN) is shown. P-Et is represented in sticks colored by atom type. The protein is represented in cartoons colored according to secondary structure, i.e. helices, strands, and loops are respectively violet, yellow, and green. FAD and selected amino acid side chains in the catalytic site are represented in sticks colored by atom type. Succinate from the 1NEN complex is also shown in cyan sticks. Hydrogen atoms are shown only on P-Et.

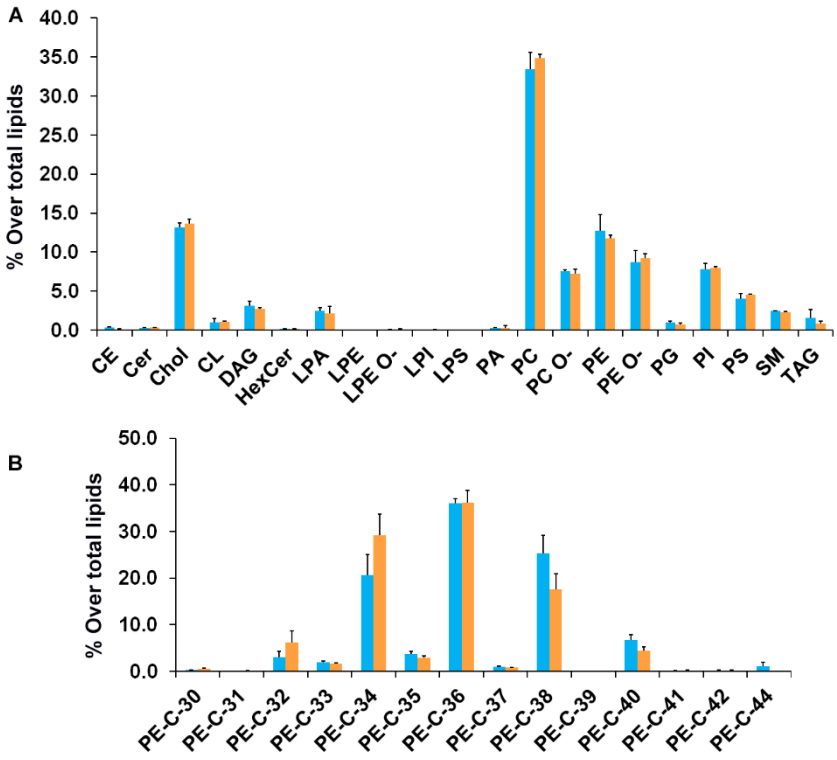

Suppl. Fig. 1: Cell membrane analysis. **A**) Relative cell membrane lipids content expressed as percent of the total lipids. Blue bars represent the ETNK1-WT line, the orange ones represent the ETNK1-N244S. The error bars represent the standard deviation of the mean. CE=Cholesterol esters; CER=Ceramide; CHOL=Cholesterol; CL=Cardiolipin; DAG=Diacylglycerol; HexCer=Hexosylceramide; LPA=lyso-Phosphatidate; LPE=lyso-Phosphatidylethanolamine; LPE(O-)=lyso-Phosphatidylethanolamine (-ether); LPI=lyso-Phosphatidylinositol; LPS=lyso-Phosphatidylserine; PA=Phosphatidate; PC= Phosphatidylcholine; PC(O-)=Phosphatidylcholine (-ether); PE=Phosphatidylethanolamine; PE(O-

)=Phosphatidylethanolamine (-ether); PG=Phosphatidylglycerol; PI=Phosphatidylinositol; PS=Phosphatidylserine; SM=Sphingomyelin; TAG=Triacylglycerol. **B**) Phosphatidylethanolamine carbon length profile, analyzed from C30 to C44, expressed as percent of the total lipids. Blue bars represent the ETNK1-WT line, the orange ones represent the ETNK1-N244S. The error bars represent the standard deviation of the mean.

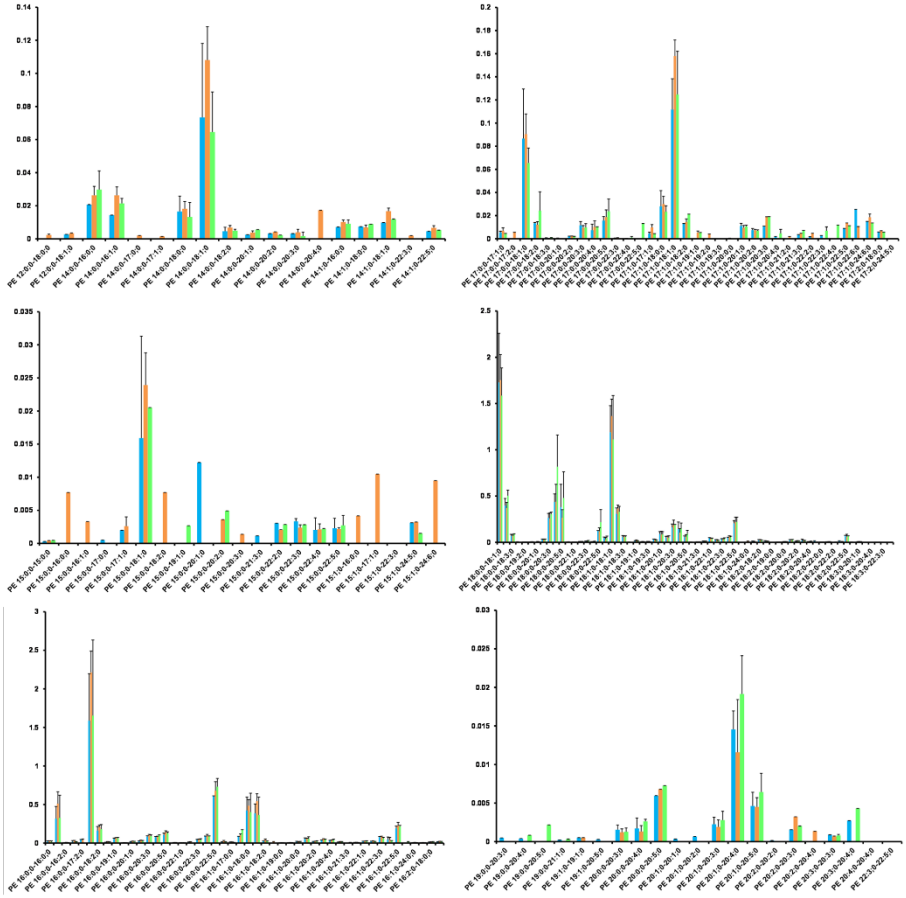

Suppl. Fig. 2: Cell membrane phosphatidylethanolamine content. Phosphatidylethanolamine carbon length profile, analyzed from C12 to C24, expressed as percent of the total lipids. Lipid species are annotated according to their molecular composition as: ‘lipid name’ followed by <Sum of the carbon atoms in the hydrocarbon moiety – fatty acid #1>:<sum of the double bonds in the hydrocarbon moiety – fatty acid #1>;<sum of hydroxyl groups - fatty acid #1>-<Sum of the carbon atoms in the hydrocarbon moiety – fatty acid #2>:<sum of the double bonds in the hydrocarbon moiety – fatty acid #2>;<sum of

hydroxyl groups - fatty acid #2>. Blue bars represent the ETNK1-WT line, the orange ones represent the ETNK1-N244S. The error bars represent the standard deviation of the mean.

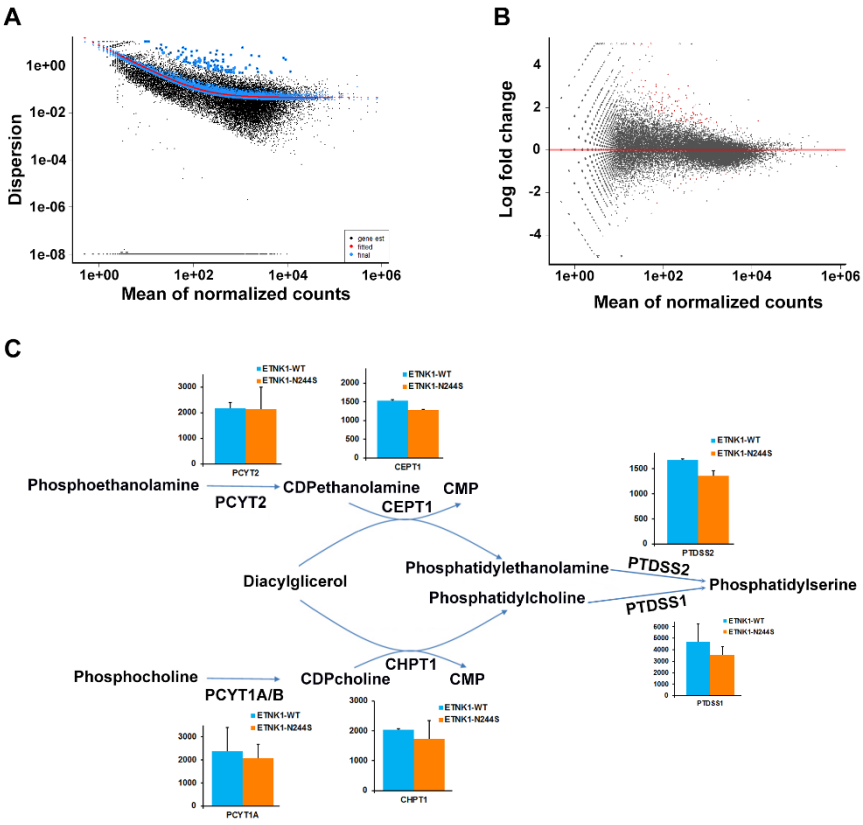

Suppl. Fig. 3: Whole-transcriptome differential expression analysis. **A**) The black points represent the dispersion estimates for the entire gene set as obtained by taking into account the information from each gene separately. The red line represents the fitted trend, which shows the dependence of the dispersion on the mean. The blue points represent the final estimate that is subsequently used in the statistical tests. The blue circles highlight the dispersion outliers. **B**) MA-plot showing the log2 gene expression fold changes of ETNK1-N244S line vs WT (y axis) over the mean of the normalized read counts. Individual dots represent genes; black dots show genes whose expression is not statistically different in ETNK1-N244S cells and in

the WT controls. Red dots represent differentially expressed genes. **C**) Pathways for the synthesis of phosphatidylserine through phosphoethanolamine and phosphocholine. The histograms represent the expression levels of enzymes assessed by RNA-seq analysis; the error bars represent the standard deviation of the mean. PCYT2=Ethanolamine-phosphate cytidylyltransferase 2; CEPT1=Choline/Ethanolamine Phosphotransferase 1; PTDSS2=Phosphatidylserine Synthase 2; PCYT1A/B=Choline-phosphate cytidylyltransferase A/B; CHPT1=Choline-phosphotransferase 1; PTDSS1= Phosphatidylserine Synthase 1.

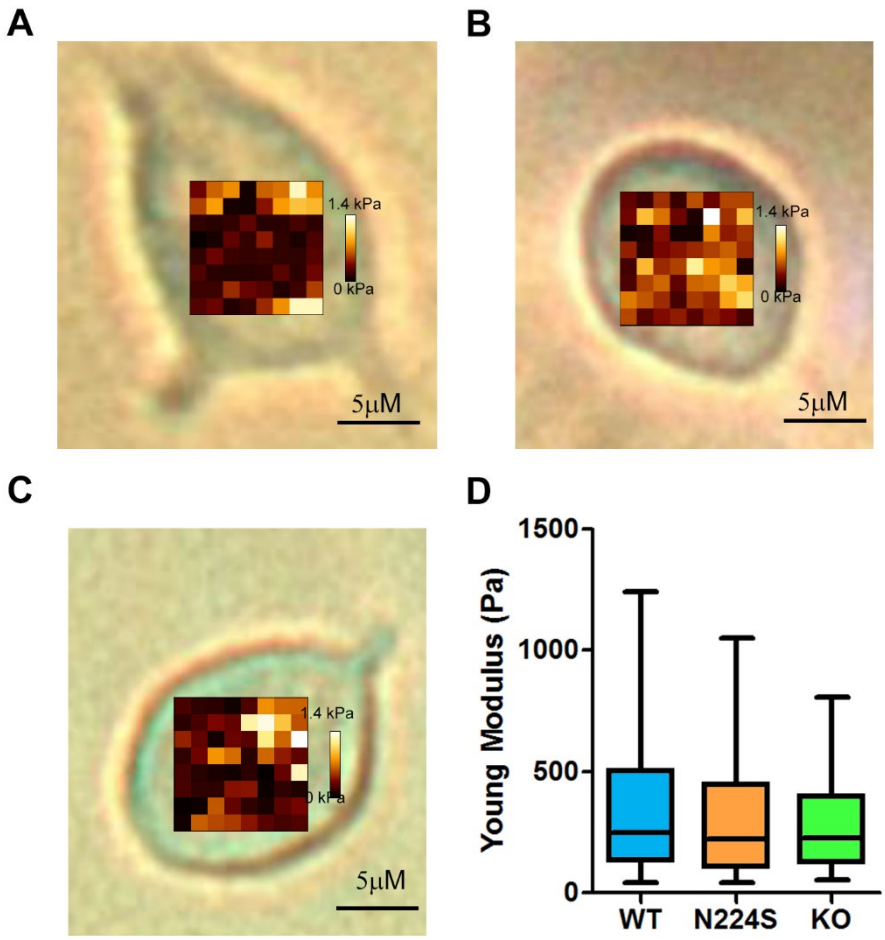

Suppl. Fig. 4: **A-C**) Exemplificative atomic force microscopy force maps (8x8 pixels grid) of ETNK1-WT (A), ETNK1-N244S (B) and ETNK1-KO (C) cells. Pixel color code is scaled between 0 (black) and 1.4 kiloPascal (white). **D**) Young's modulus of elasticity calculated for ETNK1-WT (blue), N244S (orange) and KO (green) lines. Boxes represent the interquartile range; whiskers delimit the 5th and 95th percentile range.

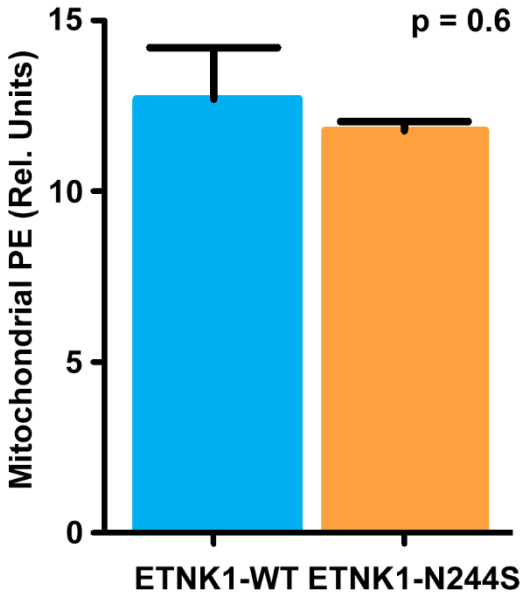

Suppl. Fig. 5: Mitochondrial PE content. The bars represent the mitochondrial membrane content of PE. Blue bar represents the ETNK1-WT line, the orange one represents ETNK1-N244S. The error bars represent the standard deviation of the mean.

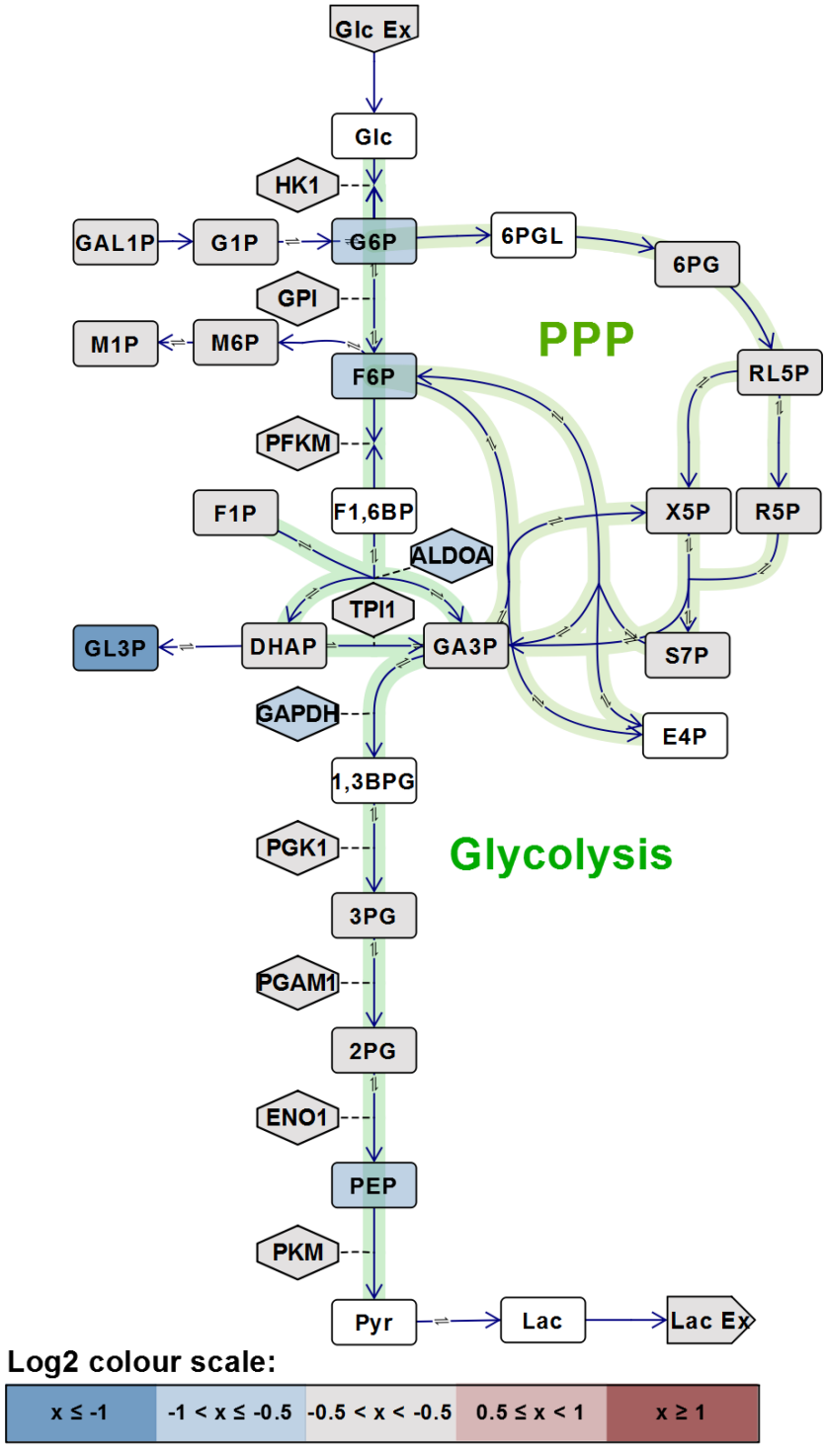
Glc Ex
Glc
HK1
GAL1P
G1P
G6P
6PGL
6PG
GPI
M1P
M6P
PPP
F6P
RL5P
PFKM
F1P
F1,6BP
X5P
R5P
ALDOA
TPI1
GL3P
DHAP
GA3P
S7P
GAPDH
E4P
1,3BPG
PGK1
Glycolysis
3PG
PGAM1
2PG
ENO1
PEP
PKM
Pyr
Lac
Lac Ex
Log2 colour scale:
x ≤ -1
-1 < x ≤ -0.5
-0.5 < x < -0.5
0.5 ≤ x < 1
x ≥ 1

Suppl. Fig. 6: Glycolysis. Simplified schematic overview of glycolysis and the pentose phosphate pathway (PPP), showing metabolite levels and enzyme expression levels in ETNK1-N244S cell lines relative to ETNK1-WT cell lines. Data is in log2-space. Rectangular boxes represent metabolite levels as measured by capIC-MS/MS, arrow-shaped boxes represent consumption or excretion /cell/48h as measured by NMR, and diamond shaped boxes represent enzyme expression levels as measured by RNA-seq analysis. Metabolites in white color were not quantified.G1-/M1P, GA3P/DHAP, 2-/3PG and R-/RL-/X5P could not be chromatographically separated, and is presented together. For abbreviations, see supplementary table 3.

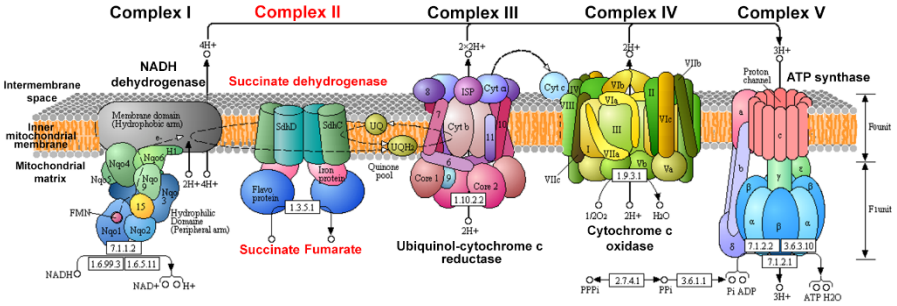

Suppl. Fig. 7: Schematic representation of the five mitochondria respiratory complexes. Complex II (in red), also known as succinate dehydrogenase, is responsible for the oxidation of succinate to fumarate.

NAME	SEQUENCE
gRNA	TATTCATGCACACAATGGC
single-stranded DNA oligonucleotide	TGATACTTAAGTTTTTCTTTTTATGC GGTTTTGTTTTAAACAGGCTAATAG CTCGTCAGCTTGCTAAAATCCATGC TATTCATGCACACAGTGGCTGGATC CCCAAATCTAATCTTTGGCTAAAGA TGAAAGTATTTCTCTCTCATTCCCA CAGGATTTGCAGATGAAGACATTA ATAA
ETNK_P19_1_FOR	aaaCATCAAGAATCTTTGTCAGGAG
ETNK_P19_2_FOR	aatCATCAAGAATCTTTGTCAGGAG
ETNK_P19_3_FOR	aacCATCAAGAATCTTTGTCAGGAG
ETNK_P19_4_FOR	aagCATCAAGAATCTTTGTCAGGAG
ETNK_P19_5_FOR	agcCATCAAGAATCTTTGTCAGGAG
ETNK_P19_6_FOR	actCATCAAGAATCTTTGTCAGGAG
ETNK_P19_7_FOR	accCATCAAGAATCTTTGTCAGGAG
ETNK_P19_8_FOR	acgCATCAAGAATCTTTGTCAGGAG
ETNK_P19_9_FOR	ataCATCAAGAATCTTTGTCAGGAG
ETNK_P19_10_FOR	aggCATCAAGAATCTTTGTCAGGAG
ETNK_P19_11_FOR	atcCATCAAGAATCTTTGTCAGGAG
ETNK_P19_12_FOR	agtCATCAAGAATCTTTGTCAGGAG
ETNK1_P19_REV	CAAATCCTGTGGGAATGAGAGAG

Suppl. Table 1: Oligonucleotides list. The gRNA and the ssODN sequences used for CRISPR/Cas9 genome editing, together with the primers used for sequencing are reported.

Genes	ETNK1-N244S_2	ETNK1-N244S_3	ETNK1-WT_1	ETNK1-WT_2	baseMean	log2FoldChange	lfcSE	stat	pvalue	padj
AC000123.3	38,3575	104,3214	315,6346	222	170,0784	-1,91305	0,499357	-3,83103	0,000128	0,034967
AC139769.1	69,64914	102,3531	0,965244	5	44,49186	4,860707	0,879141	5,528929	3,22E-08	6,68E-05
ADCYAP1R1	237,2108	324,7741	114,864	101	194,4622	1,380358	0,399911	3,451666	0,000557	0,088022
AGAP2	802,4792	436,9688	246,1371	181	416,6463	1,536569	0,391458	3,925241	8,66E-05	0,027119
AL109615.3	159,4864	118,0997	36,67925	39	88,31634	1,874947	0,50497	3,712987	0,000205	0,049245
AL139407.1	22,20697	21,65161	181,4658	63	72,08109	-2,47932	0,63327	-3,9151	9,04E-05	0,027297
ANKRD36	328,0575	504,8762	1272,191	738	710,7812	-1,27102	0,373708	-3,4011	0,000671	0,096735
ANKRD36C	267,4931	346,4257	1023,158	551	547,0192	-1,35849	0,378621	-3,588	0,000333	0,064278
ATP2B3	248,3143	172,2287	50,19266	57	131,9339	1,972159	0,452351	4,359798	0,000013	0,00617
BEX5	100,9408	23,61994	7,721948	8	35,07067	2,98554	0,867026	3,443426	0,000574	0,089149
C16orf89	250,3331	95,46391	49,22742	38	108,2561	1,986253	0,552143	3,597349	0,000321	0,064253
C1RL	877,1754	721,3923	194,0139	188	495,1454	2,065	0,328124	6,293352	3,11E-10	1,72E-06
C1RL-AS1	36,33868	200,7695	7,721948	28	68,20752	2,733531	0,788346	3,467425	0,000525	0,087149
CCKBR	102,9596	162,3871	29,92255	26	80,3173	2,246212	0,541009	4,151895	0,000033	0,013675
CD24	1219,365	676,1207	313,7041	455	666,0474	1,30216	0,376116	3,462121	0,000536	0,087163
CHP2	126,176	59,04984	3,860974	25	53,5217	2,685844	0,775177	3,464815	0,000531	0,087149
CNN2	3453,184	2840,297	1540,529	1653	2371,753	0,978707	0,287467	3,404589	0,000663	0,096735
CRABP1	847,9025	435,0005	57,91461	100	360,2044	3,022979	0,431622	7,003766	2,49E-12	4,13E-08
CRABP2	6096,823	3951,419	1587,826	1645	3320,267	1,636065	0,311685	5,249106	1,53E-07	0,000181
CREB3L1	169,5805	136,7988	27,99206	34	92,09284	2,305631	0,503311	4,580925	4,63E-06	0,002844
CTAG2	3,028223	123,0205	1,930487	1	32,2448	5,422743	1,364651	3,973721	7,08E-05	0,023016

CTF1	85,79966	30,50909	2,89573	9	32,05112	3,293686	0,89648	3,674018	0,000239	0,055787
DGKH	1572,657	2496,824	5893,777	4144	3526,815	-1,3025	0,332873	-3,91291	9,12E-05	0,027297
DNAH17	164,5335	85,62227	430,4986	318	249,6636	-1,58181	0,422519	-3,74377	0,000181	0,044225
DOC2A	2093,512	1362,083	607,1382	584	1161,683	1,536533	0,324002	4,74235	2,11E-06	0,001402
DTX1	145,3547	72,82814	24,13109	11	63,32849	2,632033	0,646827	4,069148	4,72E-05	0,017395
EEF1A2	23516,17	15992,67	4528,922	10675	13678,19	1,377749	0,388457	3,546721	0,00039	0,071106
ENO2	6872,048	5640,244	2710,404	3326	4637,174	1,051599	0,289941	3,626936	0,000287	0,063311
FBLN5	2164,17	1297,128	788,6039	483	1183,226	1,444476	0,365033	3,957111	7,59E-05	0,024201
FRMPD3	306,86	313,9483	121,6207	121	215,8572	1,355448	0,374017	3,624027	0,00029	0,063311
FXYD6	1021,521	439,9213	323,3566	124	477,1996	1,707363	0,481371	3,546878	0,00039	0,071106
GABRA5	3,028223	150,5771	3,860974	3	40,11657	4,483954	1,176578	3,811012	0,000138	0,036443
GALNT8	59,55506	111,2105	10,61768	20	50,34582	2,481948	0,677794	3,661803	0,00025	0,057704
GPRASP1	435,0548	702,6931	58,87985	147	335,9069	2,467404	0,453156	5,444937	5,18E-08	9,46E-05
GPX3	1509,065	1764,606	295,3645	885	1113,509	1,471925	0,429754	3,425039	0,000615	0,091965
GUCY1A2	216,0133	231,2786	652,5046	503	400,6991	-1,36929	0,341512	-4,00949	6,08E-05	0,020601
HES2	96,90315	89,55893	22,2006	21	57,41567	2,109531	0,587055	3,593411	0,000326	0,064278
HLA-B	9014,012	6027,021	3615,802	3725	5595,459	1,034886	0,304047	3,403705	0,000665	0,096735
HTRA3	412,8478	376,9348	100,3853	124	253,542	1,815785	0,370054	4,906808	9,26E-07	0,000731
IGFBP4	199,8627	114,163	29,92255	34	94,48708	2,296569	0,523872	4,383837	1,17E-05	0,005862
IGSF21	123,1477	171,2445	38,60974	33	91,50051	2,03928	0,505057	4,037723	0,000054	0,01905
INPP5D	884,2412	580,6568	310,8084	121	474,1766	1,761738	0,438552	4,017171	5,89E-05	0,020356
ITGB4	609,6823	374,9665	240,3456	122	336,7486	1,441623	0,422896	3,408932	0,000652	0,096598

KCNK6	379,5373	299,1859	86,87191	50	203,8988	2,308855	0,425369	5,427889	5,7E-08	9,46E-05
KRT17	648,0398	323,79	85,90667	211	317,1841	1,711221	0,474541	3,606058	0,000311	0,064253
LAMC2	286,6718	218,4844	45,36644	67	154,3807	2,169265	0,440626	4,923147	8,52E-07	0,000731
LAMC3	830,7426	649,5483	181,4658	186	461,9392	2,010171	0,335038	5,999824	1,98E-09	8,19E-06
LINC01446	60,56447	23,61994	0,965244	0	21,28741	6,422478	1,698658	3,780914	0,000156	0,040501
LRRC4B	292,7283	186,9912	100,3853	43	155,7762	1,741004	0,494845	3,518283	0,000434	0,076308
MDK	4218,315	5439,475	2077,204	1748	3370,748	1,336141	0,294643	4,534782	5,77E-06	0,003416
MMP2	1160,819	453,6996	285,7121	225	531,3077	1,660278	0,428064	3,87857	0,000105	0,030053
MT1F	64,6021	49,2082	9,652435	8	32,86568	2,687705	0,768257	3,498444	0,000468	0,080034
MYCBP2	2378,165	4060,661	6579,1	7474	5122,981	-1,12598	0,325864	-3,45538	0,00055	0,087654
NCKAP1L	477,4499	311,98	113,8987	90	248,3322	1,952463	0,397753	4,908731	9,17E-07	0,000731
NDRG4	2211,612	1781,337	927,599	730	1412,637	1,268259	0,306126	4,142936	3,43E-05	0,013874
NECTIN3	148,3829	95,46391	32,81828	34	77,66628	1,867497	0,537527	3,474241	0,000512	0,085844
NECTIN4	335,1234	375,9507	160,2304	114	246,3261	1,374224	0,379837	3,617933	0,000297	0,063341
NOS1	292,7283	325,7583	52,12315	74	186,1524	2,294741	0,411173	5,580966	2,39E-08	5,67E-05
NOVA2	1348,569	1147,535	529,9187	651	919,2557	1,079837	0,30833	3,502218	0,000461	0,079731
NSG1	759,0747	750,9172	265,442	347	530,6084	1,302102	0,326971	3,982319	6,82E-05	0,022643
OXER1	117,0913	109,2422	14,47865	38	69,70304	2,110903	0,600256	3,516673	0,000437	0,076308
PCLO	790,3663	1242,015	2232,608	2120	1596,247	-1,09863	0,320767	-3,42502	0,000615	0,091965
PGF	768,1593	1222,332	411,1937	331	683,1712	1,423206	0,347976	4,08995	4,31E-05	0,016267
PGM5	463,3182	212,5794	119,6902	40	208,897	2,080264	0,531984	3,910392	9,21E-05	0,027297
PIANP	966,0032	783,3946	288,6078	266	576,0014	1,657202	0,321674	5,151809	2,58E-07	0,000285

PROM1	306,86	248,0093	81,08045	71	176,7374	1,86696	0,406168	4,596524	4,3E-06	0,002741
PRSS8	113,0537	172,2287	43,43596	29	89,42958	1,976862	0,524821	3,766737	0,000165	0,042211
PTGIS	92,86552	50,19237	5,791461	9	39,46234	3,275574	0,767131	4,269903	1,96E-05	0,008768
QPRT	2484,153	1972,265	901,5374	875	1558,239	1,326784	0,295439	4,490891	7,09E-06	0,003922
RAB25	180,684	144,6721	34,74877	61	105,2762	1,765727	0,49657	3,555849	0,000377	0,070226
RAC2	486,5346	443,858	123,5512	225	319,7359	1,417003	0,390458	3,62908	0,000284	0,063311
RAMP1	394,6784	495,0345	170,8481	130	297,6403	1,564041	0,367219	4,259146	2,05E-05	0,008958
RASGRF1	142,3265	100,3847	32,81828	37	78,13238	1,797654	0,52925	3,39661	0,000682	0,096735
RFLNA	154,4394	88,57477	21,23536	9	68,31238	3,003454	0,632924	4,745364	2,08E-06	0,001402
RIN3	826,705	474,3671	107,142	315	430,8035	1,624368	0,472022	3,441301	0,000579	0,089149
RINL	461,2994	919,2092	277,0249	275	483,1334	1,322514	0,386163	3,424754	0,000615	0,091965
S100A16	109,016	199,7853	35,71401	34	94,62884	2,147321	0,52481	4,091617	4,28E-05	0,016267
SCARF2	174,6275	260,8035	53,08839	26	128,6299	2,459397	0,500898	4,909978	9,11E-07	0,000731
SCN4B	598,5788	642,6591	255,7895	188	421,2569	1,483552	0,34228	4,33432	1,46E-05	0,006738
SERPINB1	710,6231	758,7905	277,0249	346	523,1096	1,238069	0,324546	3,814768	0,000136	0,036443
SEZ6L2	1651,391	1168,203	414,0895	583	954,1708	1,499807	0,335154	4,474983	7,64E-06	0,004089
SFRP5	370,4527	431,0639	114,864	147	265,8451	1,614315	0,369492	4,369008	1,25E-05	0,00609
SLC15A1	203,9004	127,9413	35,71401	16	95,88893	2,679439	0,55623	4,817144	1,46E-06	0,001094
SLC22A17	1790,689	816,8562	583,0071	369	889,8882	1,453432	0,403683	3,60043	0,000318	0,064253
SLC2A3	891,3071	836,5395	226,8322	453	601,9197	1,346071	0,37635	3,576645	0,000348	0,066362
SLC7A3	958,9374	453,6996	199,8054	214	456,6106	1,771297	0,399497	4,43382	9,26E-06	0,004799
SLIT1	1248,637	857,2069	480,6913	372	739,6339	1,304109	0,3373	3,866314	0,00011	0,031067

SMG1	3939,719	6903,911	13967,07	10704	8878,676	-1,18596	0,335548	-3,5344	0,000409	0,073695
SPINT1	437,0736	311,98	99,42008	170	254,6184	1,475696	0,409886	3,600262	0,000318	0,064253
SSPN	135,2606	110,2264	14,47865	14	68,49142	3,107427	0,582686	5,332939	9,66E-08	0,000125
STRA6	377,5185	409,4122	181,4658	129	274,3491	1,341431	0,370862	3,617059	0,000298	0,063341
STX1B	365,4056	385,7923	110,0378	37	224,5589	2,351557	0,479128	4,907992	9,2E-07	0,000731
SULT1C4	346,2269	432,048	34,74877	71	221,0059	2,881325	0,438114	6,576651	4,81E-11	3,99E-07
SYT17	587,4753	415,3172	226,8322	142	342,9062	1,442469	0,385054	3,746142	0,00018	0,044225
TGFB1I1	532,9673	374,9665	157,3347	203	317,0671	1,333402	0,371354	3,590646	0,00033	0,064278
THBS4	629,8705	469,4463	140,9255	41	320,3106	2,593865	0,486662	5,329912	9,83E-08	0,000125
TMEFF2	58,54565	119,0839	11,58292	22	52,80311	2,405353	0,673314	3,572411	0,000354	0,066678
TMEM130	174,6275	124,0047	57,91461	24	95,13671	1,864379	0,54929	3,394162	0,000688	0,096777
TMEM178B	979,1255	1152,456	2206,547	2316	1663,532	-1,08517	0,288976	-3,75523	0,000173	0,04353
TMEM35A	52,4892	89,55893	10,61768	4	39,16645	3,276524	0,783772	4,180455	2,91E-05	0,012375
TMEM59L	1408,124	713,5189	361,0011	286	692,161	1,713132	0,379402	4,515344	6,32E-06	0,003616
TMSB15A	270,5213	124,0047	48,26217	60	125,697	1,865685	0,505958	3,687426	0,000227	0,053685
TNK1	157,4676	52,1607	0	0	52,40708	9,179497	1,598241	5,743499	9,27E-09	2,56E-05
TNNT1	2070,295	928,0667	531,8492	659	1047,303	1,332182	0,387193	3,440616	0,00058	0,089149
TRIM47	490,5722	878,8585	192,0835	285	461,6285	1,521643	0,390148	3,900166	9,61E-05	0,027976
TSPAN11	288,6906	182,0704	55,01888	28	138,445	2,501775	0,494054	5,063767	4,11E-07	0,000426
TUNAR	293,7377	191,912	61,77558	88	158,8563	1,697532	0,443316	3,829167	0,000129	0,034967
UBE2L6	1127,508	636,7541	250,9633	146	540,3065	2,151482	0,397895	5,407158	6,4E-08	9,66E-05
USF3	496,6286	667,2632	1332,036	1490	996,482	-1,27766	0,311959	-4,0956	4,21E-05	0,016267

WFDC2	292,7283	141,7196	21,23536	49	126,1708	2,630512	0,546997	4,809005	1,52E-06	0,001094
ZNF121	1826,019	1372,909	3942,054	3022	2540,745	-1,1224	0,30713	-3,65446	0,000258	0,058566
ZNF32	1036,662	826,6978	381,2712	388	658,1577	1,276307	0,315883	4,040442	5,34E-05	0,01905
ZNF43	70,65854	254,8985	12,54817	46	96,0263	2,47756	0,685566	3,613887	0,000302	0,063341
ZNF483	65,61151	62,00234	262,5462	138	132,04	-1,65063	0,477168	-3,45922	0,000542	0,087253
ZNF501	122,1383	42,31905	12,54817	18	48,75139	2,429142	0,717874	3,383801	0,000715	0,099659
ZNF681	145,3547	325,7583	7,721948	32	127,7087	3,572049	0,614224	5,815548	6,04E-09	2,01E-05
ZNF714	769,1687	645,6116	1556,938	1382	1088,43	-1,05479	0,299932	-3,51677	0,000437	0,076308
ZNF808	25,23519	47,23987	3,860974	2	19,58401	3,624795	1,067099	3,39687	0,000682	0,096735
ZNF83	10,09408	99,40057	1,930487	6	29,35628	3,792656	1,08954	3,48097	0,0005	0,08457

Suppl. Table 2: RNA-Seq data. The list of the 119 differentially expressed genes (FDR<0.1) between ETNK1-WT and ETNK1-N244S cell lines are reported.

2PG	2-Phosphoglycerate
3PG	3-Phosphoglycerate
6PG	6-phosphogluconate
ALDOA	Aldolase A
DHAP	Dihydroxyacetone phosphate
ENO1	Enolase 1
Ex Glc	Extracellular glucose
Ex Lac	Extracellular lactate
F1P	Fructose 1-phosphate
F6P	Fructose 6-phosphate
G1P	Glucose 1-phosphate
G6P	Glucose 6-phosphate
GA3P	Glyceraldehyde 3-phosphate
GAL1P	Galactose 1-phosphate
GAPDH	Glyceraldehyde 3-phosphate dehydrogenase
GL3P	Glycerol 3-phosphate
GPI	Glucose-6-phosphate isomerase
HK1	Hexokinase-1
M1P	Mannose 1-phosphate
M6P	Mannose 6-phosphate
PEP	Phosphoenolpyruvate
PFKM	Phosphofructokinase
PGAM1	Phosphoglycerate mutase
PGK1	Phosphoglycerate kinase 1
PKM	Pyruvate kinase
R5P	Ribose 5-phosphate
RL5P	Ribulose 5-phosphate
S7P	Sedoheptulose 7-phosphate
TPI1	Triosephosphate isomerase
X5P	Xylulose-5-phosphate

Suppl. Table 3: Abbreviations used in supplementary figure 6.

	number of colonies		- 6-TG		+ 6-TG	
	- 6-TG	+ 6-TG	mean	SD	mean	SD
ETNK1-WT	100 78 112	64 59 74	96,67	17,24	65,67	7,64
ETNK1-N244S	120 108 123	363 387 432	117,00	7,94	394,00	35,03
ETNK1-KO	120 126 127	430 424 411	124,33	3,79	421,67	9,71

Suppl. Table 4: 6-thioguanine assay. The number of ETNK1-WT, ETNK1-N244S, and ETNK1-KO colonies grown in presence/absence of 6-thioguanine in three different experiments are listed, together with the mean and standard deviation.

	number of colonies		number of colonies		number of colonies	
	untreated		+ P-Et 1mM		+ Tygecycline 2.5µM	
	- 6-TG	+ 6-TG	- 6-TG	+ 6-TG	- 6-TG	+ 6-TG
ETNK1-WT	100	64	70	43	60	45
	78	59	64	41	69	52
	112	74	98	42	64	41
ETNK1-N244S	120	363	90	50	111	154
	108	387	92	53	87	136
	123	432	76	48	108	184
ETNK1-KO	120	430	125	106	137	133
	126	424	120	88	127	146
	127	411	113	99	145	120

untreated				+ P-Et 1mM				+ Tygecycline 2.5µM			
- 6-TG		+ 6-TG		- 6-TG		+ 6-TG		- 6-TG		+ 6-TG	
mean	SD	mean	SD	mean	SD	mean	SD	mean	SD	mean	SD
96,67	17,24	65,67	7,64	77,33	18,15	42,00	1,00	64,33	4,51	46,00	5,57
117,00	7,94	394,00	35,03	86,00	8,72	50,33	2,52	102,00	13,08	158,00	24,25
124,33	3,79	421,67	9,71	119,33	6,03	97,67	9,07	136,33	9,02	133,00	13,00

Suppl. Table 5: 6-thioguanine assay after P-Et or tigecycline treatment. The number of ETNK1-WT, ETNK1-N244S, and ETNK1-KO colonies grown in presence/absence of 6-thioguanine in three different experiments after exposure to P-Et 1mM or tigecycline 2.5µM for 15 days are listed, together with the mean and standard deviation.

Suppl. Tables 6-15: Somatic variants identified by matched exome sequencing in atypical Chronic Myeloid Leukemia patients 004, 037, 014, 038, 035, 025, 019, 013 and 042.

These tables are available upon request (diletta.fontana@unimib.it)

References and Notes

1. Kennedy EP, Weiss SB. The function of cytidine coenzymes in the biosynthesis of phospholipides. *The Journal of biological chemistry* 1956 Sep; **222**(1)**:** 193-214.

2. Dawaliby R, Trubbia C, Delporte C, Noyon C, Ruysschaert JM, Van Antwerpen P*, et al.* Phosphatidylethanolamine Is a Key Regulator of Membrane Fluidity in Eukaryotic Cells. *The Journal of biological chemistry* 2016 Feb 12; **291**(7)**:** 3658-3667.

3. Birner R, Burgermeister M, Schneiter R, Daum G. Roles of phosphatidylethanolamine and of its several biosynthetic pathways in Saccharomyces cerevisiae. *Mol Biol Cell* 2001 Apr; **12**(4)**:** 997-1007.

4. Mileykovskaya E, Dowhan W. Role of membrane lipids in bacterial division-site selection. *Curr Opin Microbiol* 2005 Apr; **8**(2)**:** 135-142.

5. Steenbergen R, Nanowski TS, Beigneux A, Kulinski A, Young SG, Vance JE. Disruption of the phosphatidylserine decarboxylase gene in mice causes embryonic lethality and mitochondrial defects. *The Journal of biological chemistry* 2005 Dec 2; **280**(48)**:** 40032-40040.

6. Gambacorti-Passerini CB, Donadoni C, Parmiani A, Pirola A, Redaelli S, Signore G*, et al.* Recurrent ETNK1 mutations in atypical chronic myeloid leukemia. *Blood* 2015 Jan 15; **125**(3)**:** 499-503.

7. Lasho TL, Finke CM, Zblewski D, Patnaik M, Ketterling RP, Chen D*, et al.* Novel recurrent mutations in ethanolamine kinase 1 (ETNK1) gene in systemic mastocytosis with

eosinophilia and chronic myelomonocytic leukemia. *Blood Cancer J* 2015 Jan 23; **5:** e275.

8. Zhou XA, Louissaint A, Jr., Wenzel A, Yang J, Martinez-Escala ME, Moy AP*, et al.* Genomic Analyses Identify Recurrent Alterations in Immune Evasion Genes in Diffuse Large B-Cell Lymphoma, Leg Type. *The Journal of investigative dermatology* 2018 Nov; **138**(11)**:** 2365-2376.

9. Signorell A, Gluenz E, Rettig J, Schneider A, Shaw MK, Gull K*, et al.* Perturbation of phosphatidylethanolamine synthesis affects mitochondrial morphology and cell-cycle progression in procyclic-form Trypanosoma brucei. *Molecular microbiology* 2009 May; **72**(4)**:** 1068-1079.

10. Dill KA, Stigter D. Lateral interactions among phosphatidylcholine and phosphatidylethanolamine head groups in phospholipid monolayers and bilayers. *Biochemistry* 1988 May 3; **27**(9)**:** 3446-3453.

11. van den Brink-van der Laan E, Killian JA, de Kruijff B. Nonbilayer lipids affect peripheral and integral membrane proteins via changes in the lateral pressure profile. *Biochimica et biophysica acta* 2004 Nov 3; **1666**(1-2)**:** 275-288.

12. Tasseva G, Bai HD, Davidescu M, Haromy A, Michelakis E, Vance JE. Phosphatidylethanolamine deficiency in Mammalian mitochondria impairs oxidative phosphorylation and alters mitochondrial morphology. *The Journal of biological chemistry* 2013 Feb 8; **288**(6)**:** 4158-4173.

13. Vance JE. Phospholipid synthesis and transport in mammalian cells. *Traffic* 2015 Jan; **16**(1)**:** 1-18.

14. Redpath CJ, Bou Khalil M, Drozdzal G, Radisic M, McBride HM. Mitochondrial hyperfusion during oxidative stress is coupled to a dysregulation in calcium handling within a C2C12 cell model. *PloS one* 2013; **8**(7)**:** e69165.

15. Torri Tarelli F, Bossi M, Fesce R, Greengard P, Valtorta F. Synapsin I partially dissociates from synaptic vesicles during exocytosis induced by electrical stimulation. *Neuron* 1992 Dec; **9**(6)**:** 1143-1153.

16. Gohil VM, Zhu L, Baker CD, Cracan V, Yaseen A, Jain M*, et al.* Meclizine inhibits mitochondrial respiration through direct targeting of cytosolic phosphoethanolamine metabolism. *The Journal of biological chemistry* 2013 Dec 6; **288**(49)**:** 35387-35395.

17. Ferreira AK, Meneguelo R, Pereira A, Filho OM, Chierice GO, Maria DA. Synthetic phosphoethanolamine induces cell cycle arrest and apoptosis in human breast cancer MCF-7 cells through the mitochondrial pathway. *Biomedicine & pharmacotherapy = Biomedecine & pharmacotherapie* 2013 Jul; **67**(6)**:** 481-487.

18. Rose WE, Rybak MJ. Tigecycline: first of a new class of antimicrobial agents. *Pharmacotherapy* 2006 Aug; **26**(8)**:** 1099-1110.

19. Norberg E, Lako A, Chen PH, Stanley IA, Zhou F, Ficarro SB*, et al.* Differential contribution of the mitochondrial translation pathway to the survival of diffuse large B-cell lymphoma subsets. *Cell death and differentiation* 2017 Feb; **24**(2)**:** 251-262.

20. Sabharwal SS, Schumacker PT. Mitochondrial ROS in cancer: initiators, amplifiers or an Achilles' heel? *Nat Rev Cancer* 2014 Nov; **14**(11)**:** 709-721.

21. David SS, O'Shea VL, Kundu S. Base-excision repair of oxidative DNA damage. *Nature* 2007 Jun 21; **447**(7147)**:** 941-950.

22. Vilenchik MM, Knudson AG. Endogenous DNA double-strand breaks: production, fidelity of repair, and induction of cancer. *Proceedings of the National Academy of Sciences of the United States of America* 2003 Oct 28; **100**(22)**:** 12871-12876.

23. Takahashi A, Ohnishi T. Does gammaH2AX foci formation depend on the presence of DNA double strand breaks? *Cancer letters* 2005 Nov 18; **229**(2)**:** 171-179.

24. Sharma A, Singh K, Almasan A. Histone H2AX phosphorylation: a marker for DNA damage. *Methods in molecular biology (Clifton, NJ)* 2012; **920:** 613-626.

25. Ferrando AA, Lopez-Otin C. Clonal evolution in leukemia. *Nature medicine* 2017 Oct 6; **23**(10)**:** 1135-1145.

26. Hirsch P, Zhang Y, Tang R, Joulin V, Boutroux H, Pronier E*, et al.* Genetic hierarchy and temporal variegation in the clonal history of acute myeloid leukaemia. *Nature communications* 2016 Aug 18; **7:** 12475.

27. Piazza R, Ramazzotti D, Spinelli R, Pirola A, De Sano L, Ferrari P*, et al.* OncoScore: a novel, Internet-based tool to assess the oncogenic potential of genes. *Scientific reports* 2017 Apr 7; **7:** 46290.

28. Brand MD. Mitochondrial generation of superoxide and hydrogen peroxide as the source of mitochondrial redox signaling. *Free radical biology & medicine* 2016 Nov; **100:** 14-31.

29. Chouchani ET, Pell VR, Gaude E, Aksentijevic D, Sundier SY, Robb EL*, et al.* Ischaemic accumulation of succinate controls reperfusion injury through mitochondrial ROS. *Nature* 2014 Nov 20; **515**(7527)**:** 431-435.

30. Papaemmanuil E, Cazzola M, Boultwood J, Malcovati L, Vyas P, Bowen D*, et al.* Somatic SF3B1 mutation in myelodysplasia

with ring sideroblasts. *N Engl J Med* 2011 Oct 13; **365**(15)**:** 1384-1395.

31. Dolatshad H, Pellagatti A, Fernandez-Mercado M, Yip BH, Malcovati L, Attwood M*, et al.* Disruption of SF3B1 results in deregulated expression and splicing of key genes and pathways in myelodysplastic syndrome hematopoietic stem and progenitor cells. *Leukemia* 2015 May; **29**(5)**:** 1092-1103.

32. Shiozawa Y, Malcovati L, Galli A, Sato-Otsubo A, Kataoka K, Sato Y*, et al.* Aberrant splicing and defective mRNA production induced by somatic spliceosome mutations in myelodysplasia. *Nature communications* 2018 Sep 7; **9**(1)**:** 3649.

33. Piazza R, Valletta S, Winkelmann N, Redaelli S, Spinelli R, Pirola A*, et al.* Recurrent SETBP1 mutations in atypical chronic myeloid leukemia. *Nat Genet* 2013 Jan; **45**(1)**:** 18-24.

34. Piazza R, Magistroni V, Redaelli S, Mauri M, Massimino L, Sessa A*, et al.* SETBP1 induces transcription of a network of development genes by acting as an epigenetic hub. *Nature communications* 2018 Jun 6; **9**(1)**:** 2192.

Materials and Methods

Chemicals

Phosphoethanolamine (P-Et) (Sigma) and 6-Thioguanine (6-TG) (Sigma) were dissolved in DMEM at 1M and 1.5mM concentration, respectively, aliquoted and stored at -20°C. Succinate (Sigma) and tigecycline (Tigacil®;Pfizer) were dissolved in ddH_2O at 500mM and 5mM, respectively, aliquoted and stored at -80°C.

Cell lines

Human embryonic kidney (HEK) cell line 293 was purchased from Thermo Fisher Scientific. Cells were cultured in DMEM (Lonza) medium supplemented with 10% FBS (Euroclone), 2mM L-glutamine (Euroclone), 100U/mL penicillin (Euroclone), 100µg/mL streptomycin (Euroclone), 20mM HEPES (Euroclone), and incubated in a humidified atmosphere at 37°C with 5% CO_2. Cells were routinely screened for mycoplasma contamination (GATC Biotech AG). Cell number and viability were assessed by Trypan Blue (Sigma) count every 48 or 72 hours.

ETNK1-WT, ETNK1-N244S, and ETNK1-KO clones were obtained as described in Ran et al. (1) with minor modifications, by cotransfecting 293 cells with pCas9_WT_GFP vector (derived from the Addgene vector pCas9D10A_GFP; please see Site-directed mutagenesis), pSG-U6-gRNA vector (GenScript) encoding for the following gRNA sequence: TATTCATGCACACAATGGC, and with a single-stranded DNA oligonucleotide (ssODN) purchased by IDT

Integrated DNA Technology. The ssODN sequence is: TGATACTTAAGTTTTTCTTTTTATGCGGTTTTGTTTTAAACAG GCTAATAGCTCGTCAGCTTGCTAAAATCCATGCTATTCATGC ACACAGTGGCTGGATCCCCAAATCTAATCTTTGGCTAAAGA TGAAAGTATTTCTCTCTCATTCCCACAGGATTTGCAGATGAA GACATTAATAA

Briefly, 240.000 cells were resuspended in 24µl transfection solution supplied in the Amaxa SF cell line 4D-Nucleofector X kit S (Lonza), and transferred in a tube containing 250ng pCas9_WT_GFP plasmid, 250ng pSG-U6-gRNA plasmid, and 1µl ssODN template (10µM). Then, the resuspended cells were transferred to a nucleocuvette strip chamber and electroporated by using the Amaxa nucleofector, with CM-130 Nucleofector 4D program. After 48 hours, GFP^+ cells were sorted and expanded. Then, single-cell sorting was performed on a FACSAria (BD Biosciences) flow cytometer. Individual clones were splitted, and one part was lysed in 20µL of the following buffer: 10mM Tris-HCl, 50mM NaCl, 6.25mM $MgCl_2$, 0.045% NP40, and 0.45% Tween-20 at pH 7.6. After adding 1µL of 20µg/mL proteinase K, the lysate was incubated at 56°C for 1 hour and at 95°C for 15 minutes. Subsequently, the sample was polymerase chain reaction-amplified using FastStart™ High Fidelity PCR System and specific primers which are listed below:

- ETNK_P19_1_FOR:
  5’ – aaaCATCAAGAATCTTTGTCAGGAG – 3’
- ETNK_P19_2_FOR:
  5’ – aatCATCAAGAATCTTTGTCAGGAG – 3’
- ETNK_P19_3_FOR:

5’ – aacCATCAAGAATCTTTGTCAGGAG – 3’

- ETNK_P19_4_FOR:
  5’ – aagCATCAAGAATCTTTGTCAGGAG – 3’
- ETNK_P19_5_FOR:
  5’ – agcCATCAAGAATCTTTGTCAGGAG – 3’
- ETNK_P19_6_FOR:
  5’ – actCATCAAGAATCTTTGTCAGGAG – 3’
- ETNK_P19_7_FOR:
  5’ – accCATCAAGAATCTTTGTCAGGAG – 3’
- ETNK_P19_8_FOR:
  5’ – acgCATCAAGAATCTTTGTCAGGAG – 3’
- ETNK_P19_9_FOR:
  5’ – ataCATCAAGAATCTTTGTCAGGAG – 3’
- ETNK_P19_10_FOR:
  5’ – aggCATCAAGAATCTTTGTCAGGAG – 3’
- ETNK_P19_11_FOR:
  5’ – atcCATCAAGAATCTTTGTCAGGAG – 3’
- ETNK_P19_12_FOR:
  5’ – agtCATCAAGAATCTTTGTCAGGAG – 3’
- ETNK1_P19_REV:
  5’ – CAAATCCTGTGGGAATGAGAGAG – 3’

The purity of PCR fragments was checked by agarose gel electrophoresis. Single bands were purified on column using the QIAquick PCR Purification Kit (Qiagen). Purified PCR products were pooled and used for library preparation and deep-sequencing (Galseq

SRL). Molecular barcodes were used to deindex the individual amplicons.

Deep-sequencing

Amplicon libraries were generated starting from 500ng PCR product purified on agarose gel.

PCR product was end-repaired and adenylated at 3' ends before ligation of Truseq DNA Adapter Indices and then amplified with 6-cycles PCR. Libraries were subsequently sequenced on Illumina HiSeq instrument with paired-end reads 150bp long. Paired fastq were initially deindexed using a custom, home-made tool and subsequently aligned to the reference human genome (hg38) using BWA (2). Bam alignment files were generated from sam using Samtools (3). Variant calls were performed using CEQer2 (4).

Site-directed mutagenesis and competent cells transformation

The pCas9D10A_GFP plasmid (a gift from Kiran Musunuru, Addgene plasmid # 44720) was used as a template for *in vitro* site-directed mutagenesis. Plasmid coding for substitution at position D10A, named pCas9_WT_GFP was generated. Site-directed mutagenesis was conducted using QuikChange II XL Site-Directed Mutagenesis Kit (Stratagene, La Jolla, CA) according to manufacturer's instructions. For site-directed mutagenesis the following oligonucleotide sequences were used:

- Cas9_WT_FW: 5’ – GAAGTACTCCATTGGGCTCGATATCGGCACAAACAG CGTCG – 3’
- Cas9_WT_REV: 5’ – CGACGCTGTTTGTGCCGATATCGAGCCCAATGGAGTA CTTC – 3’

After the digestion with DpnI restriction enzyme (Roche) for at least 1 hour at 37°C, 2µl of DpnI-treated PCR product were used for transformation of TOP10 competent cells (Life Technology) by heat shock according to manufacturer’s instructions. Transformed cells were plated on Luria-Bertani (LB)-ampicillin (50µg/mL) agar plates and incubated overnight at 37°C. Bacterial colonies picked from plates were grown overnight at 37° in LB with 50µg/mL ampicillin (Euroclone). Plasmids were recovered from 10 clones using Zyppy plasmid Miniprep Kit (Zymo Research), and the presence of the A10D substitution was confirmed by standard sequencing (GATC Biotech AG), using the following primer:

- Cas9_seq_rev: 5’ – GCAGGTAGCAGATCCGATTC – 3’

Clones carrying the desired mutation were amplified and plasmid was extracted using NucleoBond Xtra Maxi EF (Macherey-Nagel) and verified again by Sanger sequencing (GATC Biotech AG).

Electron Microscopy

Samples were treated for 10 minutes with 0.12M sodium phosphate buffer (twice). Then, specimens were fixed for 1 hour at room

temperature with a mixture of 2% glutaraldehyde, 4% formaldehyde (freshly prepared from paraformaldehyde) in 0.12M sodium phosphate buffer (pH 7.4). Following the fixation, samples were washed two times in sodium phosphate buffer (0.12M) for 10 minutes. Small pellet blocks are post fixed for 1 hour at 20 °C with 1% osmium tetroxide in sodium cacodylate buffer (0.12M). Subsequently, specimens were dehydrated for 10 minutes with ascending concentration series of ethanol (50%, 70%, 96% and 100%). After a further incubation with ethanol 100%, cells were treated twice for 10 minutes with propylene oxide. Specimens were left overnight in 50% propylene oxide and 50% epon 812 under a vented hood. The following day, flat was embedded in pure fresh resin (epon 812). Silver gray sections were cut on an Ultracut microtome (Reichert-Jung), double stained with uranyl acetate and lead citrate, and examined in a PHILIPS CM10 electron microscope.

Single cell force spectroscopy (SCFS)

Prior to experiments, cells were cultured on poly-D-lysine functionalized glass in culture medium, in the CO_2 incubator for at least 2 hours, then washed very carefully two times with phosphate-buffered saline solution (pH 7.4). All SCFS measurements were carried out using standard atomic force microscopy (Nanowizard II, JPK, Berlin, Germany) working in force spectroscopy mode. To prevent significant changes in morphology or biochemistry of living cells outside the incubator, each sample was measured within 3 hours. During that time, at least two force maps (8×8 pixels grid, scan size of $8 \times 8 \mu m^2$) in the center of the cells were recorded. The force set

point was set at 0.5nN and the approach and retract speeds were kept at 2μm/s. For a given cell line type at least 25 living cells were measured. The cantilevers (MLCT- A, Nominal Constant 0.07N/m, Bruker Corporation, Santa Barbara, CA) were calibrated before the SCFS measurements both in air and in PBS solution using Thermal Noise method. The force-displacement curves between contact and 200-nm deformation depth have been analyzed, and the softer the sample the larger the deformation recorded. The evaluation of cells elastic properties, described quantitatively through the Young's modulus, was obtained by force curves analysis with the Hertz-Sneddon contact mechanics for a paraboloidal tip (5, 6).

Immunofluorescence analysis

150.000 cells were seeded on coverslips previously treated with poly-D-lysine (Sigma) at 0.1mg/ml concentration. After adhesion, cells were treated with P-Et 1mM or tigecycline 2.5μM for 24 hours, depending upon experimental conditions.

Mitochondrial activity

Mitotracker assay was performed for 30 minutes in culture condition with 50nM MitoTracker Red CMX (Thermo Fisher Scientific), 50nM MitoTracker Green (Thermo Fisher Scientific), and Hoechst 33342 (Thermo Fisher Scientific). Then, cells were washed in PBS and glass coverslips were mounted on glass slides with a 90% (v/v) glycerol/PBS solution.

Mitochondrial ROS production

Cells were incubated for 30 minutes in culture condition with 5µM CellROX® Green Reagent (Thermo Fisher Scientific), fixed for 15 minutes at room temperature in 4% (w/v) paraformaldehyde in 0.12M sodium phosphate buffer, pH 7.4 (Sigma), incubated 10 minutes with Hoechst 33342 (Thermo Fisher Scientific), washed with PBS, and left in PBS overnight at 4 °C. Then glass coverslips were mounted on glass slides with a 90% (v/v) glycerol/PBS solution.

γ-H2AX detection

Cells seeded on glass coverslips were washed twice with PBS and fixed for 15 minutes at room temperature in 4% paraformaldehyde in 0.12M sodium phosphate buffer, pH 7.4, then left in PBS overnight at 4 °C. Cells were incubated for 2 hours at room temperature with Phospho-Histone H2A.X (Ser139) (Cell Signaling Technology) primary antibody (1:100 dilution in GDB buffer [0.02M sodium phosphate buffer, pH 7.4, containing 0.45M NaCl, 0.2% (w/v) bovine gelatin]), followed by staining with Alexa 488-conjugated secondary antibody (1:100 dilution in GDB buffer) (Thermo Fisher Scientific) for 1 hour. After two washes with PBS and staining with Hoechst 33342 (Thermo Fisher Scientific), coverslips were mounted on glass slides with a 90% (v/v) glycerol/PBS solution. For 3D reconstruction of the whole cell volume, a Z-stack of 35 sequential optical planes was acquired and the obtained images were merged using the rendering tool of Zen 2009 software (Carl Zeiss) using manual thresholding.

Confocal images acquisition

Images were acquired using Zeiss LSM 710 confocal laser-scanning microscope (Zeiss) using a 63x, 1.4 N/A oil-immersion objective, applying an additional hardware zoom were required. Laser intensities and acquisition parameters were held constant throughout each experiment.

Mitochondrial respiration

Mitochondrial respiratory capacity was measured in intact cells using high-resolution respirometry (Oxygraph-2k, Oroboros Instruments, Innsbruck, Austria), in 2ml glass chambers with stirrer speed 750rpm. Data were recorded with DatLab 6 software. Correction for instrumental background and air calibration was performed according to the manufacturer's instructions. All respiratory measurements were carried out in the MiR05 buffer (0.5mM EGTA, 3mM MgCl2 6H2O, 60mM K-Lactobionate, 20mM Taurine, 10mM KH2PO4, 20mM HEPES, 110mM Sucrose and 1g/l BSA (fatty acid free) adjusted to pH 7.1 with 5M KOH at 37°C) at normoxia at 37°C.

The protocol used to measure mitochondrial respiratory capacity was as follows: initially samples were left to stabilize at a routine respiration state. Then two different protocols were performed. O_2 flow was measured after sequentially addiction of succinate (final concentration of 250μM), P-Et (titrated at final concentrations of 100μM, 1mM, and 2mM), and malonate (1mM); or after sequentially addiction of P-Et (titrated at final concentrations of 100μM, 1mM, and 2mM), succinate (250μM) and malonate (1mM).

Since it is known that succinate is not able to enter intact cells, the succinate prodrug NV189 was used (7).

Cells preparation and mitochondria isolation for lipidomics

Cells were collected and washed twice in D-PBS without Mg^{++} and Ca^{++}, to reach concentration of 1500 cells/µl, in 1ml, stored at -80°C, and shipped to Lipotype GmbH.

Mitochondria were isolated using Mitochondria Isolation Kit for Cultured Cells (Thermo Fisher Scientific), Option B with dounce homogenization, according to manufacturer's instructions. Briefly, 20 million of cells harvested, resuspended in 800µl Reagent A supplied, and transferred to pre-chilled dounce tissue grinder. After 80 strokes Reagent C was added, and sample was centrifuged at 700×*g* for 10 minutes at 4°C. The surpernatant was further centrifuged at 3000×*g* for 15 minutes at 4°C and the mitochondria pellet was resuspended in PBS to reach the final concentration of 0.35mg/ml, stored at -80°C, and shipped to Lipotype GmbH.

Lipid extraction for mass spectrometry lipidomics

Mass spectrometry-based lipid analysis was performed by Lipotype GmbH (Dresden, Germany) as described (8). Lipids were extracted using a two-step chloroform/methanol procedure (9). Samples were spiked with internal lipid standard mixture containing: cardiolipin 16:1/15:0/15:0/15:0 (CL), ceramide 18:1;2/17:0 (Cer), diacylglycerol 17:0/17:0 (DAG), hexosylceramide 18:1;2/12:0 (HexCer), lyso-phosphatidate 17:0 (LPA), lyso-phosphatidylcholine 12:0 (LPC), lyso-

phosphatidylethanolamine 17:1 (LPE), lyso-phosphatidylglycerol 17:1 (LPG), lyso-phosphatidylinositol 17:1 (LPI), lyso-phosphatidylserine 17:1 (LPS), phosphatidate 17:0/17:0 (PA), phosphatidylcholine 17:0/17:0 (PC), phosphatidylethanolamine 17:0/17:0 (PE), phosphatidylglycerol 17:0/17:0 (PG), phosphatidylinositol 16:0/16:0 (PI), phosphatidylserine 17:0/17:0 (PS), cholesterol ester 20:0 (CE), sphingomyelin 18:1;2/12:0;0 (SM), triacylglycerol 17:0/17:0/17:0 (TAG) and cholesterol D6 (Chol). After extraction, the organic phase was transferred to an infusion plate and dried in a speed vacuum concentrator. 1st step dry extract was re-suspended in 7.5mM ammonium acetate in chloroform/methanol/propanol (1:2:4, V:V:V) and 2nd step dry extract in 33% ethanol solution of methylamine in chloroform/methanol (0.003:5:1; V:V:V). All liquid handling steps were performed using Hamilton Robotics STARlet robotic platform with the Anti Droplet Control feature for organic solvents pipetting.

Mass spectrometry data acquisition

Samples were analyzed by direct infusion on a QExactive mass spectrometer (Thermo Fisher Scientific) equipped with a TriVersa NanoMate ion source (Advion Biosciences). Samples were analyzed in both positive and negative ion modes with a resolution of Rm/z=200=280000 for MS and Rm/z=200=17500 for MSMS experiments, in a single acquisition. MSMS was triggered by an inclusion list encompassing corresponding MS mass ranges scanned in 1 Da increments (10). Both MS and MSMS data were combined to monitor CE, DAG and TAG ions as ammonium adducts; PC, PC O-, as acetate adducts; and CL, PA, PE, PE O-, PG, PI and PS as

deprotonated anions. MS only was used to monitor LPA, LPE, LPE O-, LPI and LPS as deprotonated anions; Cer, HexCer, SM, LPC and LPC O- as acetate adduct and cholesterol as ammonium adduct of an acetylated derivative (11).

Data analysis and post-processing

Data were analyzed with in-house developed lipid identification software based on LipidXplorer (12, 13). Data post-processing and normalization were performed using an in-house developed data management system. Only lipid identifications with a signal-to-noise ratio >5, and a signal intensity 5-fold higher than in corresponding blank samples were considered for further data analysis.

Targeted mass spectrometric metabolic profiling and quantification of extracellular metabolites

Cells were seeded ($6*10^6$ cells/dish) and incubated for 48 hours to reach 70% confluency. Four technical replicates were washed and sampled as described in (14), transferred directly to liquid nitrogen after mechanical detachment, and extracted and concentrated as described in (15). Intracellular phosphorylated metabolite pools were quantified by capillary ion chromatography (capIC)-MS/MS as described in (14), with the modifications and isotope dilution strategy described in (16). Absolute quantification was performed in MassLynx 4.1 from a standard series calculated by least squares regression with 1/x weighting. Measured concentrations were normalized to sampled cell numbers to obtain metabolite pool sizes (mole/cell).

Extracellular glucose and lactate in culture supernatants were quantified by recording 1D proton nuclear magnetic resonance (NMR) spectra and applying electronic reference to access in vivo concentrations (ERETIC2, Topspin 3.5, Bruker) as described in (17). Consumption/production was normalized to the average number of live cells within the interval to obtain consumption/excretion /cell/48h.

ChIP-seq analysis of 8-oxoguanine distribution

5 million cells were harvested and DNA was extracted using PureLink Genomic DNA kit according to the standard protocol (Thermo Fisher Scientific). 7µg of DNA in a final volume of 150µl were sonicated with a Bioruptor sonicator system (Diagenode), gel purified with QIAquick PCR Purification Kit (Qiagen), and subsequently immunoprecipitated with Anti-8-Oxoguanine Antibody, clone 483.15 (Millipore-Merck) and Pierce Protein A/G Magnetic Beads (Thermo Fisher Scientific). After immunoprecipitation, DNA was purified and libraries were prepared for sequencing following the Illumina ChIP-Seq protocol (TrueSeq ChIP library prep kit IP-202-1012) with an Illumina HiSeq4000 in paired-end mode (Galseq, Monza, Italy).

Oxoguanine Analysis

Paired Fastq files were initially mapped to the reference human genome (hg38) using BWA (2). Bam were generated from sam alignment files using Samtools (3). Subsequently, sorted, indexed Bam files were processed by a custom home-made tool (OxoGuanineProfiler). Briefly, individual Bam files were filtered for

reads with mapping quality ≥ 20. Reads mapping to mitochondria chromosome were similarly discarded. The remaining reads were binned according to their first-base position in the reference genome, using 10000-bases bin size. All the bins were subsequently normalized for the total number of filtered reads. Bins containing less than 10 hits were discarded. Finally, the total number of normalized hits per individual chromosome was calculated for two independent experiments and the mean value calculated. The final statistical analysis was performed by OxoGuanineProfiler on mean values using a Wilcoxon signed-rank test, with threshold p-value set at 0.05.

6-TG assay

Cells were cultured in presence of P-Et 1mM and tigecycline 2.5µM for 15 days, refreshed every 2 days. Then 1 million of cell was plated and exposed to 15µM of 6-TG for 15 days. In parallel, as control, 1500 cells was plates for 15 days. Colonies were counted and the induced mutant frequency was calculated as following:

$$\frac{total\ number\ of\ 6-TG\ resistant\ colonies}{1000000} \Big/ \frac{total\ number\ of\ untreated\ colonies}{1500}$$

Patients

Diagnosis of aCML and related diseases was performed according to the World Health Organization 2008 and 2016 classification. All patients provided written informed consent, which was approved by the institutional ethics committee. This study was conducted in accordance with the Declaration of Helsinki. Sample collection and

processing and exome sequencing were performed as already described (18).

Interphase-FISH

Interphase FISH was performed on genome-edited and WT 293 lines as previously described (19). Genomic probe for ETNK1 gene (RP11-268P4/12p12.1 - UCSC Genome Browser Feb. 2009, GRCh37/hg19 Assembly: 22,707,126-22,881,094), was labeled with spectrum orange (Vysis, IL, USA) and combined with green alpha satellite centromeric probe of chromosome 12 (Vysis, Abbott Laboratories, Illinois USA; Cytocell Ltd, Cambridge, UK).

The ploidy was estimated on the mean signal numbers of centromeric probes. Nuclei with a target/centromeric probe ratio of ≥ 3:1 were defined as amplified, and those with a probe ratio of > 1:1 but <3:1 were classified as relative copy gain. Nuclei with a probe ratio 1:1 but more than two copies of each probe were defined as polisomy. Analyses were carried out on 200 nuclei/experiment.

MethoCult™ colonies assay

Peripheral blood or bone marrow cells were seeded in methylcellulose-based medium Methocult H4034 (StemCell Technologies), according to manufacturer's instructions. 20000 BM-derived cells or 1000000 PB-derived cells were plated in 6-well dishes. After 2 weeks of incubation at 37°C, 5% CO2, individual colonies were picked, washed with 200µL PBS, and lysed in 20µL of the following buffer: 10mM Tris-HCl, 50mM NaCl, 6.25mM MgCl2, 0.045% NP40, and 0.45% Tween-20 at pH 7.6. On average 100

colonies per sample were isolated. After adding 1µL of 20µg/mL proteinase K, the lysate was incubated at 56°C for 1 hour and at 95°C for 15 minutes. Subsequently, the sample was polymerase chain reaction-amplified using dedicated primers. Known driver mutations already identified by whole-exome sequencing were individually tested by Sanger sequencing (GATC Biotech AG) in each clone.

Clonal architecture analysis

The sequence of each methylcellulose colony was analyzed in order to generate the clonal architecture of the corresponding sample. Briefly, a generic mutation A was considered to be an earlier event compared to mutation B if A was identified in more than one clone in absence of mutation B.

RNA-sequencing

Five million cells were lysed in TRIzol (Thermo Fisher Scientific) and total RNA was extracted according to manufacturer's instructions. 4µg of RNA (concentration 400ng/µl) were used for library preparation (Galseq, Monza, Italy).

Western blot and antibodies

5 million cells were seeded in absence or presence of P-Et for 24 hours. Then cells were harvested, washed once in PBS at 4°C, and resuspended in 100µL Laemmli buffer supplemented with 10% β-mercaptoethanol (Sigma). Lysates were denatured at 99°C for 20 min and then used for electrophoresis. Equal volumes (30µL) were loaded on 12% sodium dodecyl sulfate polyacrylamide gel electrophoresis

(SDS-PAGE), transferred to nitrocellulose membrane Hybond ECL (GE Healthcare Life Science), and incubated overnight at 4°C with primary antibody (1:1000 dilution in bovine serum albumin [BSA] 2.5%, Roche). Secondary horseradish peroxidase-conjugated anti-rabbit antibodies (1:2000) was incubated for 1 hour at room temperature and then bands were visualized by chemiluminescence ECL (Thermo Scientific) as recommended by the manufacturer. Phospho-Histone H2AX (Ser139), anti-H3, anti-actin and anti-rabbit antibodies were purchased from Cell Signaling Technology, Abcam, Sigma, and Bio-Rad, respectively.

Mitochondrial complexes I, II, and IV activity

180 million of cells were harvested, and resuspended first in NKM buffer (1mM Tris-HCl, pH 7.4, 0.13M NaCl, 5mM KCl, 7.5mM $MgCl_2$), and later in homogenization buffer (10mM Tris-HCl, 10mM KCl, 0.15mM $MgCl_2$, 1mM AEBSF, 1mM DTT). Cells were transferred to a pre-chilled glass homogenizer, incubated for 10 minutes on ice, and homogenized. The homogenate was transferred into a conical centrifuge tube containing 2M sucrose solution, and centrifuged at 1200×*g* for 5 minutes. This treatment was repeated twice. Mitochondria were collected by centrifugation at 7,000×*g* for 10 minutes and resuspended in mitochondrial suspension buffer (10mM Tris-HCl, pH 6.7, 0.15mM $MgCl_2$, 0.25mM sucrose, 1mM AEBSF). Mitochondria were lysed on ice for 30 minutes with the supplied 10X Detergent solution, and centrifuged at 4°C at 12,000×*g*. Surnatant was collected and used for the measurement of mitochondrial activity according to manufacturer's instructions. The

following kits (Abcam) were used: Complex I Enzyme Activity Microplate Assay Kit (Colorimetric) (ab109721), Complex II Enzyme Activity Microplate Assay Kit (ab109908), and Complex IV Human Enzyme Activity Microplate Assay Kit (ab109909).

Mitochondrial complex III activity

Mitochondria were extracted as described above and resuspended mitochondrial suspension buffer without being lysed. Complex III was measured by using Mitochondrial Complex III Activity Assay Kit (BioVision), according to manufacturer's instructions.

Software and data analysis

Validation of the CRISPR/Cas9 mutations was performed by ultradeep-sequencing, as already described. Chromatograms were visualized using Chromas 2 (Technelysium). Statistical analysis and graphs were analyzed using GraphPad Prism6 (GraphPad Software, Inc.). Confocal microscopy fields were analyzed using specific homemade-designed macro with ImageJ (https://imagej.nih.gov/ij/) software. Mitochondrial activity quantification was performed measuring the integrated density (ID) of red over green signal ratio, after proper manual thresholding; ROS production was analyzed measuring the ID in nuclear compartment; for yH2AX assay number of foci was detected after manual thresholding and with the precast "analyzed particle" plug-in of ImageJ. All the data obtained derived from at least ten fields per experimental condition (at least 200 cells each). Western blot bands were visualized using ChemiDoc™ XRS+ (Bio-Rad).

Docking

The structure of P-Et was optimized by the PM3 Hamiltonian in the MOPAC16 package v17.349L (HTTP://OpenMOPAC.net (2016)) and docked into the catalytic site of E. Coli SDH (PDB: 1NEN (20)) by the glide software (21). For P-Et, the PM3 charges were used for docking. Prior to docking, the SDH structure was processed by the Maestro software (https://www.schrodinger.com/maestro) to add all hydrogens according to the predicted pKa of amino acids. Before fixing the docking setup, a number of conditions were probed. Shown results refer to docking in the presence of the FAD co-factor upon removal of all water molecules. According to the Glide setup, the protein is rigid whereas the ligand is fully flexible. The five best docking poses were saved, showing the first one.

References and Notes

1. Ran FA, Hsu PD, Wright J, Agarwala V, Scott DA, Zhang F. Genome engineering using the CRISPR-Cas9 system. *Nature protocols* 2013 Nov; **8**(11)**:** 2281-2308.

2. Li H, Durbin R. Fast and accurate short read alignment with Burrows-Wheeler transform. *Bioinformatics (Oxford, England)* 2009 Jul 15; **25**(14)**:** 1754-1760.

3. Li H, Handsaker B, Wysoker A, Fennell T, Ruan J, Homer N*, et al.* The Sequence Alignment/Map format and SAMtools. *Bioinformatics* 2009; **25**(16)**:** 2078-2079.

4. Piazza R, Magistroni V, Pirola A, Redaelli S, Spinelli R, Galbiati M*, et al.* CEQer: a graphical tool for copy number and

allelic imbalance detection from whole-exome sequencing data. *Plos One* 2013; **8**(10)**:** e74825.

5. Cao Y, Ma D, Raabe D. The use of flat punch indentation to determine the viscoelastic properties in the time and frequency domains of a soft layer bonded to a rigid substrate. *Acta biomaterialia* 2009 Jan; **5**(1)**:** 240-248.

6. Pogoda K, Jaczewska J, Wiltowska-Zuber J, Klymenko O, Zuber K, Fornal M*, et al.* Depth-sensing analysis of cytoskeleton organization based on AFM data. *European biophysics journal : EBJ* 2012 Jan; **41**(1)**:** 79-87.

7. Ehinger JK, Piel S, Ford R, Karlsson M, Sjovall F, Frostner EA*, et al.* Cell-permeable succinate prodrugs bypass mitochondrial complex I deficiency. *Nature communications* 2016 Aug 9; **7:** 12317.

8. Sampaio JL, Gerl MJ, Klose C, Ejsing CS, Beug H, Simons K*, et al.* Membrane lipidome of an epithelial cell line. *Proceedings of the National Academy of Sciences of the United States of America* 2011 Feb 1; **108**(5)**:** 1903-1907.

9. Ejsing CS, Sampaio JL, Surendranath V, Duchoslav E, Ekroos K, Klemm RW*, et al.* Global analysis of the yeast lipidome by quantitative shotgun mass spectrometry. *Proceedings of the National Academy of Sciences of the United States of America* 2009 Feb 17; **106**(7)**:** 2136-2141.

10. Surma MA, Herzog R, Vasilj A, Klose C, Christinat N, Morin-Rivron D*, et al.* An automated shotgun lipidomics platform for high throughput, comprehensive, and quantitative analysis of blood plasma intact lipids. *European journal of lipid science and technology : EJLST* 2015 Oct; **117**(10)**:** 1540-1549.

11. Liebisch G, Binder M, Schifferer R, Langmann T, Schulz B, Schmitz G. High throughput quantification of cholesterol and cholesteryl ester by electrospray ionization tandem mass spectrometry (ESI-MS/MS). *Biochimica et biophysica acta* 2006 Jan; **1761**(1)**:** 121-128.

12. Herzog R, Schwudke D, Schuhmann K, Sampaio JL, Bornstein SR, Schroeder M*, et al.* A novel informatics concept for high-throughput shotgun lipidomics based on the molecular fragmentation query language. *Genome biology* 2011; **12**(1)**:** R8.

13. Herzog R, Schuhmann K, Schwudke D, Sampaio JL, Bornstein SR, Schroeder M*, et al.* LipidXplorer: a software for consensual cross-platform lipidomics. *PloS one* 2012; **7**(1)**:** e29851.

14. Kvitvang HF, Kristiansen KA, Bruheim P. Assessment of capillary anion exchange ion chromatography tandem mass spectrometry for the quantitative profiling of the phosphometabolome and organic acids in biological extracts. *Journal of chromatography A* 2014 Nov 28; **1370:** 70-79.

15. Kvitvang HF, Bruheim P. Fast filtration sampling protocol for mammalian suspension cells tailored for phosphometabolome profiling by capillary ion chromatography - tandem mass spectrometry. *Journal of chromatography B, Analytical technologies in the biomedical and life sciences* 2015 Aug 15; **998-999:** 45-49.

16. Stafsnes MH, Rost LM, Bruheim P. Improved phosphometabolome profiling applying isotope dilution strategy and capillary ion chromatography-tandem mass spectrometry. *Journal of chromatography B, Analytical technologies in the biomedical and life sciences* 2018 Apr 15; **1083:** 278-283.

17. Sogaard CK, Blindheim A, Rost LM, Petrovic V, Nepal A, Bachke S*, et al.* "Two hits - one stone"; increased efficacy of cisplatin-based therapies by targeting PCNA's role in both DNA repair and cellular signaling. *Oncotarget* 2018 Aug 21; **9**(65)**:** 32448-32465.

18. Piazza R, Valletta S, Winkelmann N, Redaelli S, Spinelli R, Pirola A*, et al.* Recurrent SETBP1 mutations in atypical chronic myeloid leukemia. *Nat Genet* 2013 Jan; **45**(1)**:** 18-24.

19. Gorello P, La Starza R, Varasano E, Chiaretti S, Elia L, Pierini V*, et al.* Combined interphase fluorescence in situ hybridization elucidates the genetic heterogeneity of T-cell acute lymphoblastic leukemia in adults. *Haematologica* 2010 Jan; **95**(1)**:** 79-86.

20. Yankovskaya V, Horsefield R, Tornroth S, Luna-Chavez C, Miyoshi H, Leger C*, et al.* Architecture of succinate dehydrogenase and reactive oxygen species generation. *Science (New York, NY)* 2003 Jan 31; **299**(5607)**:** 700-704.

21. Friesner RA, Murphy RB, Repasky MP, Frye LL, Greenwood JR, Halgren TA*, et al.* Extra precision glide: docking and scoring incorporating a model of hydrophobic enclosure for protein-ligand complexes. *Journal of medicinal chemistry* 2006 Oct 19; **49**(21)**:** 6177-6196.

Acknowledgments

We kindly acknowledge the contributions of Michela Viltadi, Cristina Mastini and Silje Malene Olsen for technical help. We thank Sarah Piel and Eskil Elmer for providing succinate prodrug NV189.

Funding

This work was supported by Associazione Italiana Ricerca sul Cancro 2015 (IG-17727) to R.P., Associazione Italiana Ricerca sul Cancro 2017 (IG-20112) to C.G.P.

Author contributions

Diletta Fontana: Investigation, Methodology, Visualization, Writing – review & editing

Mario Mauri: Investigation, Methodology, Visualization

Rossella Renso: Investigation

Mattia Docci: Investigation

Ilaria Crespiatico: Investigation

Lisa Marie Røst: Investigation

Antonio Niro: Investigation

Deborah D'Aliberti: Investigation

Luca Massimino: Formal analysis

Mayla Bertagna: Investigation

Giovanni Zambrotta: Investigation

Mario Bossi: Investigation

Stefania Citterio: Resources

Barbara Crescenzi: Resources

Francesca Fanelli: Investigation, Formal analysis

Valeria Cassina: Investigation, Formal analysis

Roberta Corti: Investigation, Formal analysis

Domenico Salerno: Investigation, Formal analysis

Luca Nardo: Investigation, Formal analysis

Francesco Mantegazza: Supervision

Cristina Mecucci: Supervision

Guido Cavaletti: Supervision

Per Bruheim: Formal analysis, Supervision

Delphine Rea: Resources

Steen Larsen: Investigation, Formal analysis, Supervision

Carlo Gambacorti-Passerini: Conceptualization, Funding acquisition, Writing – review & editing, Supervision

Rocco Piazza: Conceptualization, Methodology, Funding acquisition, Writing – original draft Preparation, Supervision

CHAPTER III

Summary, conclusions and future perspectives

1. SUMMARY

During the three years of PhD course, my activity has been mainly focused on the study of atypical chronic myeloid leukemia (aCML) *BCR-ABL1*-negative. According to the 2016 revision of WHO, this disease is a clonal disorder belonging to the myelodysplastic/myeloproliferative (MDS/MPN) syndromes (1). Until 2012, the molecular lesions responsible for the onset of this leukemia remained largely unknown, first of all for the absence of a pathognomonic alteration, but also for the lacking of a recurrent mutational pattern. Then, by applying Next Generation Sequencing (NGS) techniques, our group firstly identified recurrent somatic mutations occurring in *SETBP1* and *ETNK1* genes (2, 3). In particular, about 13% of aCML cases carry somatic mutations in *ETNK1* gene, encoding for H243Y, N244S, and G245V substitutions (3). *ETNK1* mutations attracted our attention for several reasons. Mutations occurring in this gene had never been associated before with cancers, except a single report in which the amplification of the loci where *ETNK1* is located was described in human testicular seminomas (4).

Then, despite *ETNK1* mutations were sought in a large set of leukemias, solid tumors, and cell lines (3), they were found only in aCML (3), chronic myelomonocytic leukemia (a disorder belonging to the MDS/MPN syndromes) (3, 5), and in another myeloid neoplasia such as the systemic mastocytosis (5), suggesting that they can be specifically associated with a group of strictly related diseases. Moreover, the recurrent somatic, missense and heterozygous point mutations occurred in the same highly conserved hotspot of the *ETNK1* kinase domain, as they could play a crucial functional role (3, 5). In our previous work (3), preliminary data showed that, in both *ETNK1*-positive aCML primary samples and TF1 cells transduced with mutated *ETNK1*, the mutations led to an impairment of ETNK1 enzymatic activity, responsible for a 5.2-fold reduction in the intracellular phosphoethanolamine (P-Et) level ($p<0.05$).

On this background, my PhD project that aimed to characterize the role of mutated *ETNK1* in the etiopathogenesis of aCML, took place. To dissect the functional role of *ETNK1* mutations I created a new isogenic CRISPR/Cas9 cellular model in which *ETNK1* N244S mutation was present as heterozygous variant, reflecting the patients' situation, and an *ETNK1* KO cell line, useful for exacerbating the mutation effects. First, since P-Et is the precursor for the biosynthesis of phosphatidylethanolamine (PE) (6) that is the major component of the cellular membrane, its stiffness was measured by applying atomic force microscopy tests. However, limited differences in the membrane rigidity were noticed. Additionally, a subsequent mass spectrometry-based lipid analysis confirmed that no difference in membrane phospholipids content was present, suggesting that further

mechanisms of compensation for the PE biosynthesis might be present. At this point, other effects of the reduction of P-Et were taken in account. I investigated the functional role of P-Et modulation by using several approaches, showing that it causes (i) change in mitochondrial morphology, (ii) increased mitochondrial potential, (iii) increased ROS production, and (iv) increased gDNA mutation rate. The latter point is very interesting, since it is known that aCML is characterized by genetic instability and presence of several mutations. This finding was confirmed analyzing the presence of γH2AX protein in mutated *ETNK1* patients' samples *versus* samples derived from aCML patients carrying WT *ETNK1*. Furthermore, the administration of P-Et to the mutated and KO cells was able to restore the basal mitochondrial activity, ROS and mutation frequency levels, confirming that the effects on mitochondria were due to an impairment in the P-Et content. The following step was the identification of the mitochondrial complex II as the responsible of the increased activity, leading us to hypothesize that P-Et might compete with succinate for the same binding site. In order to verify this idea and to better understand the molecular mechanism by which an impairment in the P-Et level modulates the mitochondrial activity, I personally contributed to establish new international collaborations with the groups of Professor Per Bruheim at the Norwegian University of Science and Technology in Trondheim, and Professor Steen Larsen at the University of Copenhagen. During the last year of PhD, I moved to Prof. Larsen laboratories, and this allowed me to prove that a direct competition between P-Et and succinate for complex II succinate

dehydrogenase enzyme was present. This functional role of P-Et has been further confirmed with a computational modeling.

2. CONCLUSIONS

The present PhD project shed light on the molecular mechanisms underlying the pathogenesis of ETNK1 mutations in aCML. The activities I carried out during these years allowed me to broaden my knowledge in both the molecular medicine and the hematology fields.

All the data presented in this thesis suggest that the impairment of *ETNK1* function and the consequent reduction in the P-Et content cause an increase in mitochondrial activity due to a reduced competition between P-Et and succinate for complex II. This increased mitochondrial activity is responsible for the enhanced ROS production, which leads to accumulation of DNA mutations. These findings are interesting as the parallel analysis of aCML subclonal architecture indicates *ETNK1* mutations as a very early event in the history of the disease. This suggests that *ETNK1* mutations could contribute to the onset of aCML through the activation of a mutant phenotype, which in turn would accelerate the accumulation of further oncogenic mutations. Furthermore, the ability of P-Et to restore the basal mitochondrial activity, as well as ATP and ROS levels, in both *ETNK1* mutated and KO cell lines, besides slow down the accumulation of further mutations in both cell lines and patients'

samples, suggests possible future therapeutic options for the treatment of patients affected by aCML ETNK1-positive. Moreover, the property of tigecycline to inhibit the mitochondrial protein synthesis suppressing the mitochondrial respiration could indicate a new therapeutic strategy.

In conclusion, this work has been made possible thanks to an already established national and international network among hematologic units, and an active integration between clinicians and the research laboratory. Moreover, the research work I carried out during my PhD course hinges the translational research principles: from the bench to the bedside. In the specific instance, the starting point was the “bedside”, beginning from the collection of samples from patients affected by a disease with an unknown pathogenic cause, moving toward the “bench” where the molecular mechanism and its functional role have been dissected, analyzed and understood, and with the wish to go back to the “bedside” suggesting possible therapeutic options.

3. FUTURE PERSPECTIVES

In the present PhD work, the functional role of *ETNK1* mutations in the onset of aCML is reported. In order to perform the experiments, the human embryonic kidney (HEK) cell line 293 was used. These cells are adherent ones, and they easily allowed the execution of microscopy experiments. However, one of the major limitations of this model is that the cells used are not of hematological

derivation. In order to validate the results obtained until now on the 293 cell line, I set up a new *ETNK1* KO cellular model based on the hematological U937 cell line. Since the experiments are still ongoing, we chose not to present them in this thesis. Our future plan will be to generate a murine model in order to test the efficacy of P-Et in slowing the accumulation of mutations. Animals will be injected subcutaneously with a suspension of *ETNK1* KO U937 cells, and treated with P-Et. After the treatment, tumor cells will be excised and the mutation frequency rate will be evaluated and compared to untreated mice.

Regarding the analysis of the clonal evolution and the hierarchical reconstruction, one of the biggest limiting factors is represented by the small number of patients affected by aCML, which is known to be a rare disease. Furthermore, among then, the percentage of *ETNK1*-mutated cases is reported to be around 13%. In order to reach a sufficiently large samples cohort able to give a solid statistical significance, our center is still collecting aCML samples.

Additionally, our purpose will be to analyze the mutational profile of patients and to correlate the data obtained with the available clinical information, in order to obtain useful prognostic information for the follow-up. Finally I will try to use this newly obtained information to build a pathogenesis-informed, personalized treatment modality for aCML patients.

References

1. Arber DA, Orazi A, Hasserjian R, Thiele J, Borowitz MJ, Le Beau MM*, et al.* The 2016 revision to the World Health Organization classification of myeloid neoplasms and acute leukemia. *Blood* 2016 May 19; **127**(20)**:** 2391-2405.

2. Piazza R, Valletta S, Winkelmann N, Redaelli S, Spinelli R, Pirola A*, et al.* Recurrent SETBP1 mutations in atypical chronic myeloid leukemia. *Nat Genet* 2013 Jan; **45**(1)**:** 18-24.

3. Gambacorti-Passerini CB, Donadoni C, Parmiani A, Pirola A, Redaelli S, Signore G*, et al.* Recurrent ETNK1 mutations in atypical chronic myeloid leukemia. *Blood* 2015 Jan 15; **125**(3)**:** 499-503.

4. Zafarana G, Gillis AJM, van Gurp RJHLM, Olsson PG, Elstrodt F, Stoop H*, et al.* Coamplification of DAD-R, SOX5, and EKI1 in human testicular seminomas, with specific overexpression of DAD-R, correlates with reduced levels of apoptosis and earlier clinical manifestation. *Cancer Res* 2002 Mar 15; **62**(6)**:** 1822-1831.

5. Lasho TL, Finke CM, Zblewski D, Patnaik M, Ketterling RP, Chen D*, et al.* Novel recurrent mutations in ethanolamine kinase 1 (ETNK1) gene in systemic mastocytosis with eosinophilia and chronic myelomonocytic leukemia. *Blood Cancer J* 2015 Jan 23; **5:** e275.

6. Kennedy EP, Weiss SB. The function of cytidine coenzymes in the biosynthesis of phospholipides. *The Journal of biological chemistry* 1956 Sep; **222**(1)**:** 193-214.

Publications

1. Diletta Fontana, Mario Mauri, Rossella Renso, Mattia Docci, Ilaria Crespiatico, Lisa Marie Røst, Antonio Niro, Deborah D'Aliberti, Luca Massimino, Mayla Bertagna, Giovanni Zambrotta, Mario Bossi, Stefania Citterio, Barbara Crescenzi, Francesca Fanelli, Valeria Cassina, Roberta Corti, Domenico Salerno, Luca Nardo, Francesco Mantegazza, Cristina Mecucci, Guido Cavaletti, Per Bruheim, Delphine Rea, Steen Larsen, Carlo Gambacorti-Passerini, Rocco Piazza. ETNK1 mutations induce a mutator phenotype that can be reverted with phosphoethanolamine. [submitted]

2. M. Mauri, E. Elli, D. D'Aliberti, I. Crespiatico, M. Nava, L. Massimino, G. G. Sharma, D. Fontana, S. Redaelli, S. Pelucchi, A. Piperno, C. Gambacorti-Passerini, R. Piazza. Paired exome sequencing reveals absence of clonal mutations in JAK2-negative and CALR-negative polycythemia patients. [submitted]

3. V. Magistroni, C. Mezzatesta, N. Sharma, W. Parker, A. Schreiber, D. Yeung, A. Pirola, M. Mauri, S. Redaelli, P. Wang, L. Massimino, P. Khandelwal, S. Citterio, D. Fontana, M. Viltadi, J. Boultwood, A. Morotti, G. Saglio, D.W. Kim, S. Branford, C. Gambacorti-Passerini, R. Piazza. De novo UBE2A mutations are recurrently acquired during CML progression and interfere with myeloid differentiation pathways. [under review]

4. Mah S., Park JH., Jung HY., Ahn K., Choi S., Tae HS., Jung KH., Rho JK., Lee JC., Passerini CG., Fontana D., Hong SS. and Hong S. Correction to Identification of 4-Phenoxyquinoline Based Inhibitors for L1196M Mutant of Anaplastic Lymphoma Kinase by Structure-Based Design. J Med Chem. 2018 Mar 8;61(5):2131. doi: 10.1021/acs.jmedchem.8b00212. Epub 2018 Feb 22.

5. Piazza R., Cecchetti C., Pirola A., Donandoni C., Fontana D., Mezzatesta C., Magistroni V., Bianchi B., Borin L., Fumagalli M. and Gambacorti-Passerini C. RNA-Seq is a valuable complement of conventional diagnostic tools in newly diagnosed AML patients. Am J Hematol. 2015 Oct 6. doi: 10.1002/ajh.24210.

6. Fontana D., Ceccon M., Gambacorti-Passerini C. and Mologni L. Activity of second-generation ALK inhibitors against crizotinib-resistant mutants in an NPM-ALK model compared to EML4-ALK. Cancer Med. 2015 Jul;4(7):953-65. doi:10.1002/cam4.413.

7. Ceccon M., Mologni L., Giudici G., Piazza R., Pirola A., Fontana D. and Gambacorti-Passerini C. Treatment efficacy and resistance mechanisms using the second-generation ALK inhibitor AP26113 in human NPM-ALK-positive anaplastic large cell lymphoma. Mol Cancer Res. 2015 Apr;13(4):775-83. doi: 10.1158/1541-7786.MCR-14-0157.

8. Gambacorti-Passerini CB., Donadoni C., Parmiani A., Pirola A., Redaelli S., Signore G., Piazza V., Malcovati L., Fontana D., Spinelli R., Magistroni V., Gaipa G., Peronaci M., Morotti A., Panuzzo C., Saglio G., Usala E., Kim DW., Rea D., Zervakis K., Viniou N., Symeonidis A., Becker H., Boultwood J., Campiotti L., Carrabba M., Elli E., Bignell GR., Papaemmanuil E., Campbell PJ., Cazzola M. and Piazza R. Recurrent ETNK1 mutations in atypical chronic myeloid leukemia. Blood. 2015 Jan 15;125(3):499-503. doi: 10.1182/blood-2014-06-579466. Epub 2014 Oct 24.

Congress Communications

1. D. Fontana, M. Mauri, A. Niro, L. Massimino, M. Bertagna, G. Zambrotta, M. Bossi, S. Citterio, B. Crescenzi, G. Signore, V. Piazza, C. Mecucci, G. Cavaletti, D. Rea, C. Gambacorti-Passerini, R. Piazza. ETNK1 mutations increase mitochondrial activity and promote DNA damage through ROS production. XV Congresso Nazionale SIES (Società Italiana Di Ematologia Sperimentale), Rimini, Italy, October 18-20, 2018

2. Diletta Fontana, Mario Mauri, Antonio Niro, Luca Massimino, Mayla Bertagna, Giovanni Zambrotta, Mario Bossi, Stefania Citterio, Barbara Crescenzi, Giovanni Signore, Vincenzo

Piazza, Cristina Mecucci, Guido Cavaletti, Delphine Rea, Carlo Gambacorti-Passerini, Rocco Piazza. ETNK1 mutations promote ROS production and DNA damage through increased mitochondrial activity [abstract]. In: Proceedings of the American Association for Cancer Research Annual Meeting 2018; 2018 Apr 14-18; Chicago, IL. Philadelphia (PA): AACR; Cancer Res 2018;78(13 Suppl):Abstract nr 3385.

3. D. Fontana, M. Mauri, A. Niro, L. Massimino, M. Bertagna, G. Zambrotta, M. Bossi, S. Citterio, B. Crescenzi, G. Signore, V. Piazza, F. Fanelli, C. Mecucci, G. Cavaletti, D. Rea, C. Gambacorti-Passerini, R. Piazza. ETNK1 mutations increase mitochondrial activity and promote DNA damage through ROS production. National Ph.D. Meeting, Salerno, Italy, March 22-24, 2018.

4. D. Fontana, M. Bertagna, M. Mauri, M. Bossi, S. Citterio, B. Crescenzi, G. Signore, V. Piazza, C. Mecucci, G. Cavaletti, C. Gambacorti-Passerini, and R. Piazza. Role of somatic ETNK1 mutation in the mitochondrial activity. Mitochondrial Physiology - From Organelle to Organism., Copenhagen, Denmark, August 21-25, 2017.

5. Francesca Farina, Monica Ceccon, Silvia Mori, Luisa Verga, Lorenza Maria Borin, Luca Mologni, Diletta Fontana, Geeta Geeta, Rocco Piazza, Carlo Gambacorti-Passerini. Long-term efficacy and safety of crizotinib in relapsed ALK positive lymphoma patients: clinical and biological correlates. European Hematology Association, 22nd Congress, 2017, Madrid, Spain, June 22-25, 2017.

6. Antonio Niro, Rocco Piazza, Gabriele Merati, Alessandra Pirola, Carla Donadoni, Diletta Fontana, Sara Redaelli, Caterina Mezzatesta, Rossella Renso, Francesca Farina, Delphine Rea and Carlo Gambacorti-Passerini. ETNK1 is an early event and SETBP1 a late event in atypical Chronic Myeloid Leukemia. 57th American Society of Hematology (ASH) – 2015 Dec 5-8; Orlando, FL. *Blood* 2015;126(23):3652; published ahead of print December 4, 2015.

7. A. Niro, R. Piazza, G. Merati, A. Pirola, C. Donadoni, D. Fontana,

S. Redaelli, C. Mezzatesta, R. Renso, C. Cecchetti, D. Rea, C. Gambacorti-Passerini. Clonal evolution analysis identifies ETNK1 as an early event and SETBP1 as a late event in atypical Chronic Myeloid Leukemia. 45° Congress of the Italian Society of Hematology (SIE), Firenze, Italy, October 4-7, 2015. Haematologica 2015;100(s3):45.

8. Luca Mologni, Monica Ceccon, Diletta Fontana, Alessandra Pirola, Rocco Piazza, Carlo Gambacorti-Passerini. Drug-resistant NPM/ALK mutants show different sensitivity to second generation tyrosine kinase inhibitors. [abstract]. In: Proceedings of the 106th Annual Meeting of the American Association for Cancer Research; 2015 Apr 18-22; Philadelphia, PA. Philadelphia (PA): AACR; Cancer Res 2015;75(15 Suppl):Abstract nr 3583. doi:10.1158/1538-7445.AM2015-3583.

9. Carla Donadoni, Rocco Piazza, Diletta Fontana, Andrea Parmiani, Alessandra Pirola, Sara Redaelli, Giovanni Signore, Vincenzo Piazza, Luca Malcovati, Roberta Spinelli, Vera Magistroni, Giuseppe Gaipa, Marco Peronaci, Alessandro Morotti, Cristina Panuzzo, Giuseppe Saglio, Elena Maria Elli, Emilio Usala, Dong-Wook Kim, Delphine Rea, Konstantinos Zervakis, Nora-Athina Viniou, Argiris Symeonidis, Heiko Becker, Jacqueline Boultwood, Leonardo Campiotti, Matteo G Carrabba, Graham R Bignell, Elli Papaemmanuil, Peter J Campbell, Mario Cazzola, Carlo Gambacorti-Passerini. Evidence of ETNK1 somatic variants in atypical Chronic Myeloid Leukemia. 56th American Society of Hematology (ASH) – 2014 Dec 6-9; San Francisco, CA. Blood 2014;124(21):2212; published ahead of print December 5, 2014.

10. Monica Ceccon, Luca Mologni, Giovanni Giudici, Rocco Piazza, Alessandra Pirola, Diletta Fontana, Carlo Gambacorti-Passerini. Mechanisms of resistance to the second-generation ALK inhibitor AP26113 in human NPM-ALK-positive anaplastic large cell lymphoma cells. [abstract]. In: Proceedings of the 105th Annual Meeting of the American Association for Cancer Research; 2014 Apr 5-9; San Diego, CA. Philadelphia (PA): AACR; Cancer Res 2014;74(19 Suppl):Abstract nr 3719. doi:10.1158/1538-7445.AM2014-3719